University of Strathclyde

Department of Electronic and Electrical Engineering

# The Performance of Visible Light Communication Systems in the Presence of Sunlight Irradiance

Mahmoud Hassan Shaaban Mansour Beshr

A Thesis presented in fulfilment of the requirements for the Degree of Doctor of Philosophy

December 2014

# Declaration

This Thesis is the result of the author's original research. It has been composed by the author and has not been previously submitted for examination which has led to the award of a degree.



Signed: *Mahmoud Beshr* Date: 26th November 2014

# Acknowledgements

All praise to Allah for guiding me through the PhD's lengthy and stressful journey.

My deep, sincere thanks and prayers go out to my beloved father for all his teaching, support and invaluable advice throughout my life. His prayers were what sustained me thus far. I owe my special sisters my profound gratitude for their unstinting support.

I would like to take this opportunity to extend my deepest gratitude to my supervisor, Professor Ivan Andonovic. He has a huge enthusiasm for research and has deeply inspired me with his fathomless knowledge in many areas. I fully appreciate his support and encouragement, especially during writing up. This research would have not reached its final form without the invaluable advice and enormous support offered by him. Also heartfelt thanks to Prof Moustafa Hussein and Dr Craig Michie for constructive suggestions and discussions.

I would also like to express my thanks to the Arab Academy for Science and Technology for the financial support.

I would like to thank the Academic and Research Computer Hosting Industry and Enterprise located in the West of Scotland (ARCHIE-WeSt) for access to the high performance computer facility and their support in solving many operations problems.

Finally, I am greatly indebted to my friends and work colleagues who have made the journey much easier.

# Abstract

Visible Light Communication has the potential to provide a licence free solution to implementing high data rate wireless communication within indoor environments. Although VLC systems offer many attractive features, a number of deployment barriers remain such as the impact of sunlight irradiance on performance, line-of-sight connections, uplink issues and the 'illumination on' operational mode.

The research investigates the design of VLC systems in the presence of sunlight irradiance. The foundation of the investigation is a sunlight irradiance model that generates hourly levels of natural light intensity over the year for different locations. System behaviour over different metrological conditions and extended to consider the effect of cloud coverage, is analysed for a range of the most common surfaces found in indoor environments using Matlab and Monte Carlo simulations. The evaluation of system performance considers both Line-of-Sight and Non-Line-of-Sight components (up to the fifth reflection) at a range of data rates. A comparative analysis of system performance with reported results assuming noise owing to sunlight follows Gaussian statistics is conducted.

Optimum placement of LED sources is investigated. System performance characterisation is conducted for different room sizes and as a function of distance from sources of sunlight such as windows and doors. Optimum LED layout maximises the SNR, fulfils the illumination constraint as governed IEC standards and minimises the variation of the SNR across the room. The design guidelines are applicable to any room size, LED specification, wall reflectivity, location and illumination level. An approach to managing the 'illumination on' scenario is developed. Operational performance as a function of the number of energised LEDs and LED panel layout for different room sizes, surface reflectivity, different operating conditions and applications is evaluated.

In summary, the research provides an in depth analysis of VLC system performance in the presence of sunlight irradiance, the results forming the foundation for future system designs and applications.

# Table of Contents

# List of Figures

# List of Tables

# List of mathematical symbols

| Symbol | Definition |
|---|---|
| $W$ | Radiant emmitance. |
| $A_R$ | Photosensitive area. |
| $A$ | The surface. |
| $d_A$ | The surface element. |
| R | The distance between the receiver and reflectance surface |
| $\gamma$ | The angle between the incident ray from surface *A* and the perpendicular on the receiver surface. |
| FOV | Receiver Field-of-View (FOV). |
| $P_R$ | Received optical power. |
| $P_S$ | Optical power for the source illuminating the room. |
| $P_{min}$ | The minimum power required by the receiver. |
| ρ | The reflection coefficient. |
| $R_O$ | The transmitter radiant intensity. |
| $\emptyset$ | LED viewing angle. |
| $A_{eff}$ | The effective signal detection area of the detector. |
| $\Psi$ | The angle of incidence with respect to receiver axis. |
| $T_s(\Psi)$ | The signal transmission of the filter |
| $g(\Psi)$ | The concentrator gain. |
| $\Psi_c$ | The concentrator FOV (semi angle). |
| n | Refractive index. |
| m | The order m is related to the transmitter semi angle at half power $\emptyset_{1/2}$. |
| h | The vertical distance between LED location and Receiver location. |
| K | Boltzmann's constant. |
| T | Absolute temperature (in Kelvin). |

| | |
|---|---|
| $\Gamma$ | FET channel noise factor. |
| k | FET $1/f$ noise coefficients. |
| a | FET $1/f$ noise coefficients. |
| $I_D$ | FET drain current. |
| $g_m$ | FET trans-conductance. |
| Cd | Detector capacitance. |
| $R_b$ | Bit rate. |
| $h(0)_{LOS,Gen,Lamb}$ | Channel DC gain for Line-of-Sight components. |
| $d_{sr}$ | The horizontal distance between the illumination LED and the photodiode. |
| $\sigma_{total}$ | Total variance. |
| $\sigma_{shot}$ | Shot noise variance. |
| $\sigma_{thermal}$ | Thermal noise variance. |
| $d_0$ | The distance between transmitter and receiver |
| $\theta_o$ | The incidence angle. |
| $R_b$ | Data rate. |
| q | Electron charge. |
| R | Receiver Responsivity. |
| $R_F$ | Feedback resistance. |
| $\mathcal{A}$ref | The area of the reflecting element. |
| m | The mode number of a radiation lobe. |
| $y_{room}$ | $y-$ axis of the room. |
| $X_{room}$ | $x-$ xis of the room. |
| $c$ | Speed of light. |
| $\Gamma_n^{(k)}$ | i the power of the reflected ray after $k$- reflections from the $n$th LED. |
| $\bar{\rho}_{n,k}$ | The average reflectance. |
| $N_{LED}$ | The total number of LEDs. |
| $T_o$ | Mean excess delay. |
| $T_{rms}$ | RMS delay spread |

| | |
|---|---|
| $E_h$ | The horizontal illuminance at a point. |
| $R_{distance}$ | The distance to the illuminated surface. |
| $I_o$ | The maximum luminous intensity. |
| H | The monthly average global radiation on a horizontal surface |
| Ho | The monthly average daily radiation |
| S | The daily sunshine hours |
| $S_0$ | The maximum possible monthly average daily sunshine hours |
| $a_{solar}$ | Solar constant |
| $b_{solar}$ | Solar Constant |
| $I_{SC}$ | The solar constant |
| $\varphi_{latiude}$ | The latitude of the location under consideration |
| $n_{day}$ | The day of the year |
| $\delta$ | The declination angle. |
| $I_b$ | The hourly beam radiation |
| $I_d$ | The hourly diffuse radiation |
| CF | The Cloud Factor |
| $\theta$ | The solar zenith angle |
| $\eta$ | Standard Meridian for the local time zone in degrees |
| $\Psi_{longitude}$ | The local longitude in degrees east or west |

# List of Abbreviations

| | |
|---|---|
| AH | Angle Hour |
| AST | Apparent Solar Time |
| BER | Bit Error Rate |
| BFSK | Binary Frequency Shift Keying |
| CF | Cloud Factor |
| CP | Cyclic Prefix |
| CPC | Compound Parabolic Concentrator |
| CRC | Cyclic Redundancy Check |
| CSK | Colour Shift Keying |
| DCO-OFDM | DC-biased Optical OFDM |
| DFE | Decision Feedback |
| DFE | Decision Feedback Equalization |
| DMT | Discrete Multi-Tone Modulation |
| DMT | Discrete Multi-Tone Modulation |
| DMT | Multi-Tone Modulation |
| DSL | Digital Subscriber Loop |
| FET | Field Effect Transistor |
| EMI | Electromagnetic Interference |

| | |
|---|---|
| FIR | Finite Impulse Response Equalizers |
| FOV | Field Of View |
| FSO | Free Space Optical |
| FTTP | Fibre-to-the-Premises |
| HB-LED | High Brightness LED |
| HBT | Half Bit Transmission |
| HWO | hybrid optical wireless |
| ICSA | Infrared Communication System Association |
| IEC | Information Exchange Centre |
| IEC | International Electro-technical Commission |
| IIN | Information Illuminating Node |
| IrDA | Infrared Data Association |
| ISI | Inter-Symbol Interference |
| ITS | Intelligent transport Systems |
| JEITA | Information Technology Industries Association |
| LAN | Local Area Network |
| LEDs | Light Emitting Diodes |
| LiFi | Light Fidelity |
| LMS | Least Mean Square |
| LMS | Least Mean Square |
| LOS | Line-Of-Sight |

| | |
|---|---|
| LST | Local Standard Time |
| LTE | Long Term Evolution |
| MEPPM | Multilevel Expurgated Pulse Position Modulation |
| MIMO | Multi-Input Multi-Output |
| MSD | Multi-Spot Diffusion |
| MT | Mobile Terminal |
| NEP | Noise Equivalent Power |
| NLOS | Non-Line-Of-Sight |
| NRZ | Non-Return-to-Zero |
| O-OFDM | Optical Orthogonal Frequency Division Multiplexing |
| OMEGA | Optical Gigabit Access Project |
| OOK | ON-OFF keying |
| OWC | Optical Wireless Communications |
| PAPR | Peak-to-Average Power Ratio |
| PCM | Pulse Code Modulation |
| PFM | Pulse Frequency Modulation |
| PLC | Power Line Communication |
| PLC | Power Line Communications |
| PLC | Power-Line-Carrier |
| PN | Pseudo-Noise |
| PPM | Pulse Position Modulation |

| | |
|---|---|
| QAM | Quadrature Amplitude Modulation |
| QPSK | Quadrate Phase Shift Keying |
| RF | Radio Frequency |
| RMS | Root Mean Square delay |
| Si pin-PD | Silicon P-type-insulator-n-type photodiode |
| SPD | Spectral Power Distribution |
| SPEA | Strength Pareto Evolutionary Algorithm |
| TDD | Time Division Duplexing |
| TDMA | Time Division Multiple Access |
| VICS | Vehicle Information and Communication System |
| VLC | Visible Light Communication |
| VLCC | Visible Light Communication Consortium |
| VPPM | Variable Pulse Position Modulation |
| W-LED | White LEDs |
| WDD | Wavelength Division Duplexing |
| WDM | Wavelength Division Multiplexing |
| Wi Fi | Wireless Fidelity |
| WWRF | Wireless World Research Forum |
| YB LEDs | Yellow-Phosphour/Blue LEDs |

# Chapter 1

# Introduction

## 1.1 Background

Wireless communication systems have experienced rapid development and deployment driven by the need to meet the continually growing demand for multimedia content delivered on the move. Wireless networks use a relatively limited and increasingly cluttered Radio Frequency (RF) segment of the electromagnetic spectrum to transmit and receive data. In addition to making the optimum use of the licensed spectrum, high data rate, highly available, energy efficient and environmental friendly operation are the main challenges for modern wireless systems [1-3].

The demand for spectrum is increasing at the rate 108% per annum whilst current network solutions achieve a modest 12% growth in spectrum use per year [2, 4]. Figure 1.1 captures the gulf between traffic demand for mobile services and the growth in network capacity. Overlaying this trend is the relatively recent requirement to deploy systems at lower energy consumption as RF communication systems represent ~5% - 8% of the total energy consumed globally [5]. Of the recent generations of wireless technologies, the Long Term Evolution (LTE) depends on extensive spectrum reuse and well-designed cells. The range of techniques under the LTE umbrella increase system capacity but at a cost of a complex interference management overhead [2, 6].

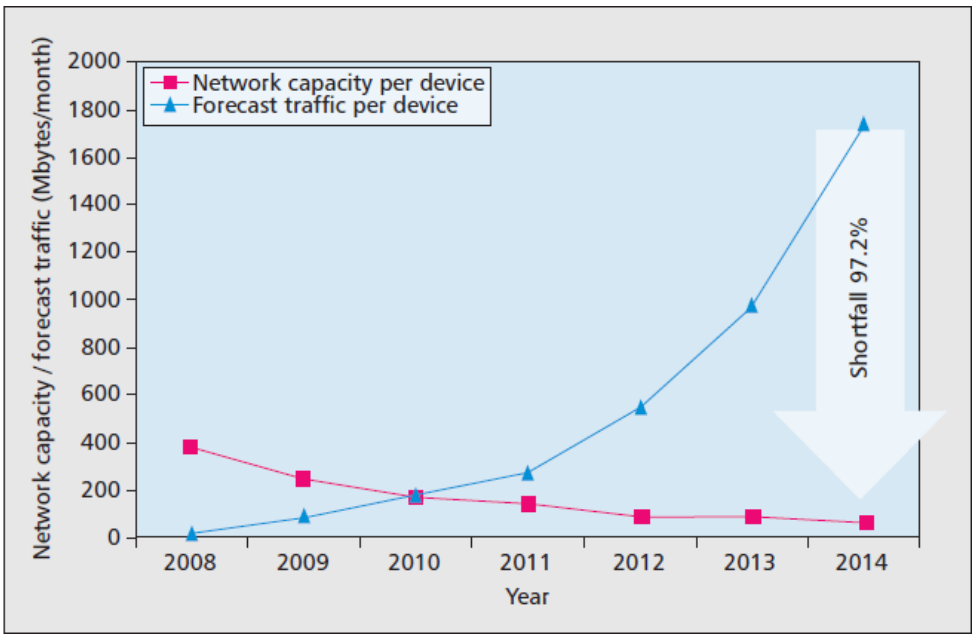


**Figure 1.1; The predicted increase in the demand for mobile communication services and the corresponding growth in network capacity [2, 7].**

The challenges of operating in the RF spectrum have stimulated research in alternative wireless network implementations such as solutions utilising the optical band of the spectrum. The market for wireless networks is extending to applications where RF interference is a fundamental barrier in the band of operation e.g. health services. Thus wireless optical communication systems are viewed as one of the options in the suite of networking schemes under the 4th Generation wireless network classification [2, 8, 9].

Visible Light Communication (VLC) is thus fats becoming a viable option in the mix of future generations of technologies with the potential to provision a rich mix of mobile services in non-conventional application sectors. VLC presents and interesting set of characteristics; low power consumption, license free and RF interference free operation and offers the option to create and isolate a wireless cell by direct control of the illumination. The implementation uses a different segment of the electromagnetic spectrum circumventing the issues of the RF "spectrum deficit". Ultimately it harnesses the unrelenting growth in the deployment of solid state lighting based on LEDs. Given that all home and office lighting will be based on

LED illumination by 2018 [10], the expansion of VLC overlays is a natural evolution that will not be hindered by the large investment required to deploy systems from scratch [11].

Although VLC systems provide many advantages, outstanding challenges remain to be mastered. A wide range of research has been undertaken to date in the design and understanding of system performance and its optimization. One issue that remains to be rigorously addressed is the impact natural light has on performance as 47% of sunlight irradiance falls within the VLC communication band of operation [12].

## 1.2 History

Light had been used as means to convey information from ancient times; humans used fire located on hilltops as signals to guide ships at sea or to alert of approaching enemies. In 1880, Bell demonstrated the" Photophone" which used light to transmit voice over distance [5] (Figure 1.2) and in 1951, Zenith invented the "Flashmatic", an early remote control unit using light to mute the sound of commercials whilst still viewing the television [13]. In the early 1970's, Nintendo introduced the light telephone transmitting sound over light [14, 15].

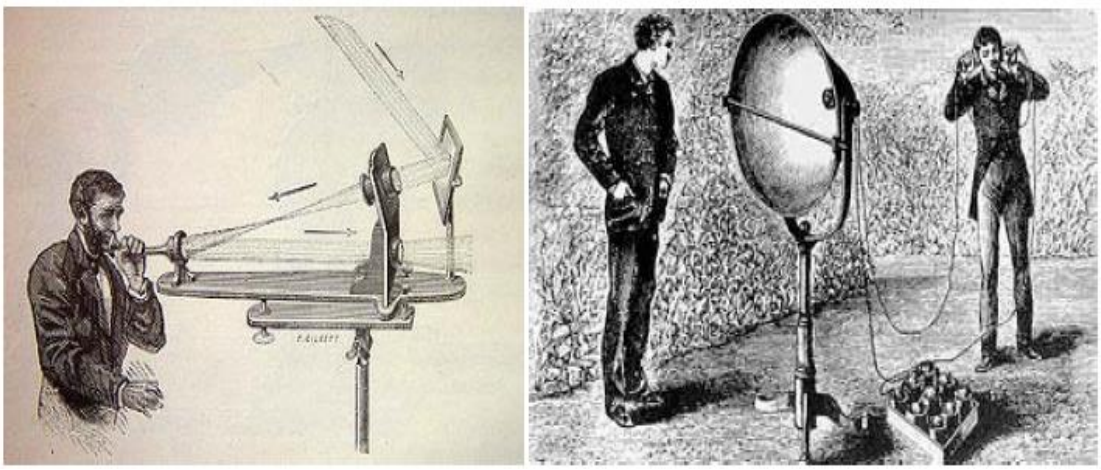

**Figure 1.2; The "Photophone" [16].**

VLC technology has its roots in the Visible Light Communication Consortium (VLCC) in Japan which triggered worldwide interest. In 2000, the VLCC, the

Infrared Data Association (IrDA) and Infrared Communication System Association (ICSA) started to co-operate in the development of VLC systems, the result being VLCC standards expanding on the original IrDA physical layer. In the same year, the ICSA issued a standard for VLC Local Area Networks (full-duplex) based on Wavelength Division Multiplexing (WDM) using both Infrared (IR) and visible light. In 2007, the Japanese Electronics and Information Technology Industries Association (JEITA) issued two Visible Light Standards - JEITA CP-1221 and JEITA CP-1221 - significant in formalising VLC system research, development and standardisation [17]. In 2010, the P802.15.7 IEEE draft standard for the physical and medium access control layers was published by the IEEE802.15.7 Working Group [1, 2].

Recent research showed that the use of Orthogonal Frequency Division Multiplexing (OFDM) can provide notable VLC system performance enhancement [3]. Thus the IEEE802.15.7 standard is being revised considering OFDM as one of main modulation techniques bringing changes to the optical frontend, lower level of the physical layer and easing integration with the LTE and IEEE 802.11 standards [18].

## 1.3 System Characteristics

VLC is considered a category of optical wireless communications (OWC) which includes Infrared, Ultra Violet and Visible Light. VLC piggybacks on visible light illumination and in essence, the input drive current applied to LED is modulated at relatively high speed with data [4, 19]. VLC is characterised by a number of features summarised in Figure 1.3.

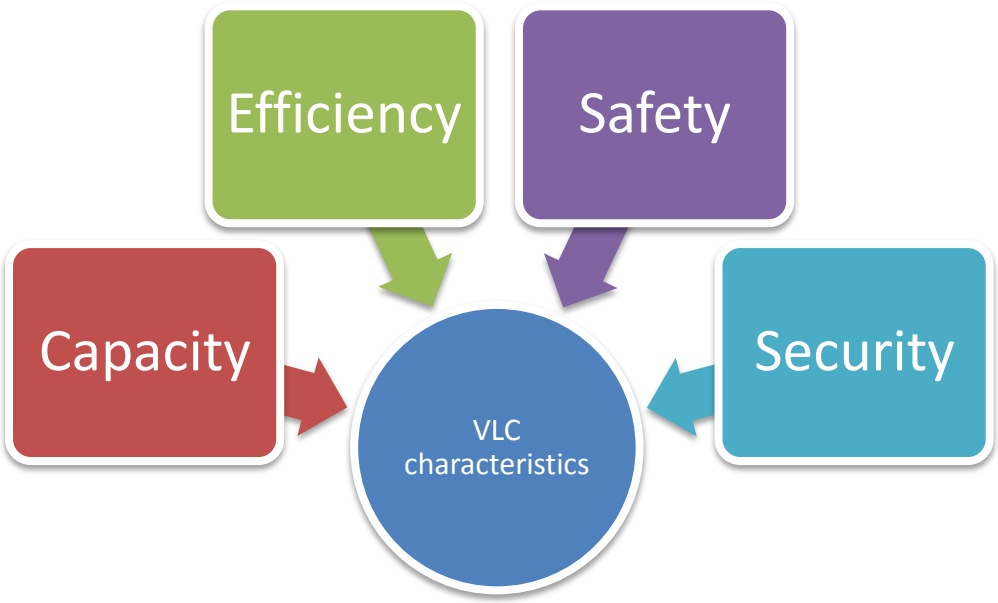


**Figure 1.3; VLC system characteristics.**

### 1.3.1 Capacity

The visible light spectrum is 1000 times wider than the RF spectrum, unlicensed and free to use, easing capacity planning [19].

### 1.3.2 Efficiency

VLC systems are lower cost than RF implementations, requiring fewer components and are significantly more energy efficient. In addition, deployment costs are minimised since an extensive lighting infrastructure already exists.

### 1.3.3 Safety

VLC systems can operate in environments where RF interference is an issue e.g. aircraft and hospitals [20, 21]. There are no health and safety concerns and an IEEE standard that governs the levels of illumination is in place [22]; RF brings a number of health and safety considerations.

### 1.3.4 Security

There are no major security concerns with VLC; signals do not penetrate through walls and the source and destination can be established physically. The signal cannot be jammed from outside the room and it is very difficult for an intruder to sample the signal [4, 19, 23].

Although the VLC feature set offers a unique set of advantages, systems are not a direct replacement for RF Wi-Fi networks. VLC system is best viewed as an enhancement to the mix of wireless network options and is a strong candidate for downlink applications like web browsing. In contrast, for uplink, VLC systems have to inter-operate with Wi-Fi or wired networks. A comparison between the Light Fidelity (LiFi) and Wireless Fidelity (Wi-Fi) is presented in Table 1.1. It must be noted that VLC systems are subject to interference from other illumination sources and natural light which impact system performance, the subject of the research reported in the dissertation [15].

## 1.4 Challenges

Although VLC offers an attractive set of features, a number of challenges remain.

### 1.4.1 Illumination On

VLC systems harness solid state illumination and consequently the LED needs to be powered to enable data transmission. In some applications subject to high levels of natural light sufficient for daily work, it is natural to switch off lighting. In these cases VLC systems are compromised; solutions such as a combination of IR sources integrated with LED lighting can increase the level of system availability.

**Table 1.1; A comparison between LiFi and Wi-Fi [2, 24-26].**

| Parameters | LiFi | Wi-Fi |
|---|---|---|
| **Data Rate** | High (> 1Gbit/s) | ~ 1.3 Gbit/s (IEEE802.11ac) |
| **Information** | Modulated over optical intensity | Modulated over electric field |
| **Device-to-Device Connectivity** | High | High |
| **Range** | Based on LED location | ~100m |
| **Data Density** | High | Low |
| **Reliability** | Medium | Medium |
| **Power Available** | High | Low |
| **Transmit/Receive Power** | High | Low |
| **Operating band** | Visible Light band | RF band |
| **Robustness** | High | Low |
| **Cost** | Low (using already installed LEDs for illumination) | High |
| **Security** | High | Medium |
| **Operation** | Can operate in any environment | Sensitive to specific environments (hospital and aviation) |
| **Congestion** | Visible Light Frequency band is 10,000 times wider than the RF band | Radio Frequency band is limited and devices compete for bandwidth |

## 1.4.2 Sunlight Interference

As 47 % of the total sunlight irradiance falls within the visible light frequency band of the spectrum, natural light incident on the receiver impacts on system

performance. Sunlight impinging on the photodiode from (say) windows within indoor and in outdoor environments generates shot noise. The prevailing meteorological conditions in network locations determine the level of sunlight. Sunlight can be categorised into two main categories; direct, not modulated by cloud coverage and indirect that has been attenuated by clouds [12, 19, 25, 27, 28].

### 1.4.3 Uplink

VLC can provision both up- and downlinks, segmented either by wavelength, time, code or optical (spatial) isolation. The use of the visible light band in the bi-directional mode may lead to interference due to crosstalk unless the path between LED and photodiode is engineered e.g. employing Time Division Duplexing (TDD) and Wavelength Division Duplexing (WDD) similar to RF systems [2]. Most often, to derive maximum benefit from the system VLC is used in the downlink and either Wi-Fi or IR provides a reliable uplink. In this context, the European Community home Optical Gigabit Access Project (OMEGA) [29] is evaluating the hybrid approach of IR in combination with VLC to provision wireless services to households. The IR path (at 850 nm) is used in the uplink in a point-to-multipoint mode as long as eye safety limits are maintained. Power Line Communication (PLC) is also a strong option for the communications backbone within the home [30]. Nevertheless, bi-directional operation is one of the main challenges to be solved before LiFi is established as a natural choice in future network deployments [2].

### 1.4.4 Line-of-Sight (LOS)

Line-of-sight paths provide the strongest received signals and in turn the best system performance. However within indoor environments, surface reflectivity is a critical factor with LOS and Non-Line-Of-Sight (NLOS) indirect paths impacting on performance. A selection of representative surfaces is considered in the evaluation of the system.

## 1.5 Motivation

To date, a large volume of research has been reported on the performance of VLC systems but all lack a rigorous analysis of the impact of sunlight irradiance. Sunlight irradiance has been considered as Gaussian noise which lacks accuracy as natural light varies according to many parameters such as metrological conditions and location. Hence an evaluation of VLC system performance in the presence of the sunlight irradiance is the major challenge under investigation. Quantification of the impact of sunlight provides a map to the range of potential services that can be offered in any location throughout the world.

LED layout is one of the main factors that influence system performance. To date, limited analyses have been reported on characterising the impact of this factor and hence design guidelines are developed to optimise the system performance and maintain the luminance at the level dictated by standards. The goal is to map performance limits as a function of room size and surfaces under different metrological conditions. Furthermore, in locations where natural light is often used as the main source of lighting during the morning hours of the day especially, the analysis considers the role of the VLC system in these scenarios.

## 1.6 Objectives

The research aims to evaluate the SNR/BER/data rate performance over a wide range of VLC system conditions to better inform on the viability of potential applications/services; LED layout, incident angle, distance between transmitter/receiver, surface reflectivity, room shape and size, receiver FOV as a function of sunlight irradiance under clear and cloudy sky conditions over the year is evaluated.

In summary, the objectives are summarised as follows;

- determine the impact of sunlight irradiance on system performance over the year
- analyse the impact of cloud coverage on performance over the year

- determine the impact of LED layout on performance in presence of the sunlight
- investigate the trade-off between energy consumption and acceptable performance of the communication link for the “lights on” scenario

## 1.7 Structure of Dissertation

The dissertation is organised into six Chapters. Chapter 1 provides an introduction to the research, the motivation, defines the overall structure, introduces the core concept underpinning visible light communication systems, the challenges and lists the original contributions arising out of the research.

Chapter 2 adds the detail on visible light communication concepts, modulation and equalisation techniques, coding schemes, LED layout design and applications. In addition, an introduction to the impact of sunlight irradiance is presented.

Chapter 3 develops the VLC system mathematical analysis framework including an extended ray tracing model that considers the Non-Line-of-Sight components for both model validation and system evaluation. Furthermore, a review of the range of sunlight irradiance models is carried out and the case is made for the selected approach to describing natural light under both clear and cloudy sky conditions.

Chapter 4 presents the results of the performance analysis of VLC systems in the presence of natural light in representative environments over the year. The impact of the cloud coverage is considered.

Chapter 5 provides an analysis of the impact of LED layout on performance in order to optimise the system in the presence of sunlight. Additionally an investigation of the “illumination on” scenario and the corresponding operating modes are discussed.

Chapter 6 provides a summary of important results relating them to the range of contributions followed by suggestions for future work.

## 1.8 Summary of Contributions

The following contributions can be identified as arising from the research;

- extension of a Ray tracing model considering Non-Line-of-Sight components up to the fifth reflection
- evaluation of the impact of natural light on the VLC system performance
- evaluation of the impact of clear sky sunlight irradiance on the VLC system over the year
- comparative analysis of VLC performance in the presence of cloud cover over the year for two representative locations.
- a comparison of the system performance is executed with a system assuming that natural light followed AWGN statistics
- analysis of the impact of LED layout on system performance. Results are compared with other research and the attainable performance enhancement is quantified
- development of a trade-off relationship between energy consumption and acceptable system performance under the "illumination on" scenario

## 1.9 Publications

**1.** Mahmoud Beshr, Ivan Andonovic, Moustafa H. Aly, "Visible Light Communications for Healthcare Applications", Proceedings of the EPSRC Network in Communications and Networking Workshop on "Photonic Communications", 28th September 2011, Oxford, United Kingdom

2. Mahmoud Beshr, Ivan Andonovic, Moustafa H. Aly, "The Impact of Sunlight on the Performance of Visible Light Communication Systems over the Year", Proceeding of the Conference on Unmanned/Unattended Sensors and Sensor Networks IX, 85400F, 19th October 2012, Edinburgh, United Kingdom
3. Mahmoud Beshr, Ivan Andonovic, Moustafa H. Aly, "The Effect of Natural Light on the Performance of Visible Light Communication Systems," Proceeding of the International Conference on Computer, Communication, Information

Sciences and Engineering, pp1327-1331, 28th-29th November 2012, Paris, France.

4. Mahmoud Beshr, Craig Michie, Ivan Andonovic, Moustafa H. Aly, "Visible Light Communication;Performance Analysis over Different Meteorological Conditions", IET Optoelectronics Journal, Special Issue of “Optical Wireless Communications”, October 2104 (submitted)
5. Mahmoud Beshr, Craig Michie, Ivan Andonovic, Moustafa H. Aly, "A LED Arrangement Methdology for Visible Light Communication Systems", submitted to IEEE Journal on Selected Areas in Communications.
6. Mahmoud Beshr, Craig Michie, Ivan Andonovic, Moustafa H. Aly, " Visible Light Communication Systems; An Energy Perspective", submitted to IEEE Photonics Technology Letters.
7. Mahmoud Beshr, Craig Michie, Ivan Andonovic, Moustafa H. Aly, " Evaluation of Visible Light Communication System Performance in the Presence of Sunlight Irradiance” , 17th International Conference on Transparent Optical Networks ICTON 2015, July 5-9, 2015, Budapest, Hungary (Invited)

# Chapter 2

# Visible Light Communication Systems;

# Designs, Performance and Applications

## 2.0. Introduction

Currently there is rapid development in the field of lighting and illumination [31]. Concerns about energy consumption are leading to the phasing out of incandescent sources and there is exponential growth in the use and development of solid-state sources. Light Emitting Diodes (LEDs) present a set of advantages compared to existing incandescent lighting in terms of low power consumption, long life expectancy, high tolerance to humidity, and minimal heat generation [25, 31]. The efficiency of solid state sources is continually increasing and their cost decreasing; consequently they are fast becoming the dominant source for general illumination.

At present solid-state sources are widely used in automotive applications for indicator and taillights and the first LED based headlights are now available [32]. They are also commonly used in feature and architectural lighting where the ability to change colour or incorporate lights into the building structure without reliability concerns, makes them preferable to alternatives. The use of solid-state sources also offers the possibility of overlaying a high data-rate communication capability, in addition to the core provision of illumination; sources can be modulated at meaningful rates providing a data channel overlay to the illumination [31].

An extensive national program in Japan promotes white LEDs as the general lighting technology of the future and many groups are developing a wireless optical communication system overlay for indoor and outdoor networking [25]. In the latter dimension, the LED is not only used as a lighting device but also as a communication transmitter device underpinning the implementation of an optical

wireless network using visible light for data transfer; this dual function enables many new and interesting applications.

## 2.1 VLC System Designs

Visible Light Communications (VLC) is now the subject of extensive development worldwide, including within bodies such as the Visible Light Communications Consortium (VLCC) [33] and the Wireless World Research Forum (WWRF) [34]. O'Brien *et al* [31, 35] outline the basic components comprising these systems, reviews the state of the art, some of the challenges and maps the potential for this new optical wireless transmission technology.

VLC offers a communications channel in an unregulated, unlicensed part of the electromagnetic spectrum [4] and in applications where a visible beam is desirable for security and safety. There are a number of technical and regulatory challenges to overcome but rapid technical progress is being made; standardisation will require cooperation and agreement from a number of different bodies [31].

Yang *et al* [36] report on a design of an indoor wireless communication system using commercial white LEDs. On-Off Keying (OOK) modulation was adopted with DC balanced coding, error check and correction. The implementation provides data links of distances up to 2.5 m at ~115 kbit/s, achieved and $10^{-7}$ Bit Error Rate (BER). The transmission data rate can be increased but most LEDs for illumination emit blue visible light and fluorescence is needed in order to emit yellow or white light [Yang, 2009 #84].

Vucic´ *et al* [37] demonstrate a VLC link at 200 Mbit/s at a $10^{-3}$ BER using thin film high power phosphorescent white LEDs modulated by Discrete Multi-Tone Modulation (DMT) with blue filtering at the receiver [37, 38]. The performance is obtained with no coding scheme and at a distance to maintain the required level of luminance for office use only, governed by the 1100 Lux (lx) standard [39]. Moreover the work demonstrated 180 Mbit/s at 550 lx (suitable for read and write) and 100 Mbit/s at 180 lx, sufficient for Internet data rates, representing improved system performance compared with Yang [36] and furthermore the BER can be improved through coding [37].

## 2.2 VLC System Equalisation

The performance of VLC systems is limited inherently by the relatively low modulation bandwidth of LEDs [40]. Equalisation techniques enhance the effective bandwidth in doing so provisioning improved data rates. Lubanzeng *et al* [40] employed first order equalisation in both the transmitter and receiver, and through both experiment and simulation show an increase in the bandwidth from 15 Mbit/s to 75 M/bits with OOK Non-Return-to-Zero (NRZ) data at a $10^{-6}$ BER.

The modulation bandwidth can also be enhanced by the multiple-resonant-drive equalisation technique. O'Brien and *et al* [31]. have demonstrated a link that uses 16 LEDs at 40 Mbit/s using NRZ OOK over a link distance of 2 m covering a radius 0.5m, sufficient to illuminate the room at the level stipulated by standards [31]. Lee and *et al* [39] also employed an equalisation technique to enhance VLC link performance. Simulations show a doubling of the bandwidth (from 16 Mbit/s to 32 Mbit/s) at a relatively low BER of $10^{-6}$ and high SNR of 81 dB with NRZ OOK modulation.

When many LEDs are distributed across a room, the optical path difference between sources triggers Inter-Symbol Interference (ISI), which significantly degrades system performance [41, 42]. Komine and *et al* [41] on installation of many high power LEDs on a ceiling to provide line of sight links, identified two problems viz. shadowing and inter symbol interference. It was shown that adaptive equalisation alleviates the impact of shadowing. The usage of the Least Mean Square (LMS) algorithm with Decision Feedback (DFE) and Finite Impulse Response (FIR) Equalisers mitigates the effects of ISI and yield data rates up to 700 Mbit/s [43], a landmark achievement in terms of the highest data rate reported to date; [42] also reports a 500 Mbit/s data rate at an acceptable level of ISI using similar approaches. Additionally, the optimum number of sources for an acceptable data rate for moderate office size applications was determined. Thus adaptive equalisation is an effective mitigation strategy; however eye and safety consideration were not discussed [43].

Nakagawa's *et al* [42] system using white LEDs which normally function as a lighting devices, is characterised by a relatively high BER, degraded significantly due to ISI. The performance of adaptive equalisation with LMS was investigated; when the data rate exceeded 400 Mbit/s, FIR equalisation and DFE were effective; when the data rate exceeded 500 Mbit/s, DFE effectively mitigates the impact of ISI [41, 42].

Other methods to enhance the limited modulation bandwidth of LED emitters have been reported. Minh *et al* [25] show that a 50 MHz bandwidth can be achieved (25 times wider than the unequalised bandwidth) when a filter is employed at the detector to pass the blue component of the signal only. By using first order analogue equalisation and NRZ OOK, a 100 Mbit/s data rate with low BER was achieved [44].

## 2.3 VLC System Analysis

In order to enhance the performance of VLC systems, the influence of interference and reflections was analysed by Komine [25]. Results corroborate the detrimental impact on performance owing to ISI and that ISI was a function of both data rate and Field Of View (FOV) of the receiver. Moreover the relationship between the data rate and FOV was defined and alternatives to LEDs as sources that enable high-speed wireless communications were suggested [25]. System performance is ultimately dependent on the environment; interference from fluorescent lighting systems can be mitigated effectively by shifting the system operational bandwidth to a higher frequency [45].

A VLC system using white LEDs was analysed (W-LED) by Hernandez *et al* [46], suggesting that VLC system could be embedded in devices like the MP3 player, PDA or virtual reality goggles provisioning data rates up to 500 kbit/s based on Pulse Width Modulation (PWM) [47]. This bandwidth is sufficient to support messaging or several audio channels. A commercial W-LED was used and the system establishes an unidirectional communication channel covering the illuminated area of the source [46].

Optical multi-paths have a significant impact on VLC system performance. Two approaches were proposed by Tanakat *et al* [48] to counter the effects of multi-paths,

using NRZ OOK and Orthogonal Frequency Division Multiplexing (OFDM) [49]. Although both approaches are proven feasible, the former was more effective at low data rates (100 Mbit/s). Conversely OFDM was much more effective at higher data rates (400 Mbit/s); guard intervals improved performance [48].

Moreover, Komine and Nakagawa [50] detail the influence of ISI and the difference between visible-light wireless and other optical wireless communications systems. The evaluation was based on numerical analyses in contrast with the work reported in [48] which was based on Monte Carlo simulations. The influence of reflections on ISI was determined and again the main conclusion drawn is that system performance degrades severely owing to ISI. The relation between the data rate and the FOV was explained and designs to implement high-speed data transmission approaching 1 Gbit/s are suggested [50].

## 2.3 Modulation Techniques

The attainable transmission data rate for use in moderate size office applications has been investigated analytically and using Monte Carlo simulations by Grubor *et al* [51]. Two transmission techniques were considered; Pulse Amplitude Modulation (PAM) and Discrete Multi-Tone Modulation (DMT) [38] using commercial white LEDs and suppressing the phosphorescent portion on detection. It was found that the channel was flat over the bandwidth of interest due to the high optical power distribution created through many LOS paths. The bandwidth available was comparable for both modulation techniques; however DMT was superior at mitigating ISI [51].

Grubor *et al* [52] also investigated the feasible data rates within a moderate-size office room illuminated with commercially available phosphor-based LEDs. It was found theoretically, that a 300 Mbit/s data rate could be achieved by using modulation schemes such as DMT and M-PAM, a substantial improvement when compared to previous work [51, 52]. The system was based on LOS yielding a good SNR and ISI was neglected owing to the nature of DMT modulation. The feasibility of the relatively complex DMT implementation is proven using FPGA and DSP [52].

An experiment to investigate the performance of the VLC system was executed using OFDM over a 1 m range using 9 commercial white LEDs and a single receiver. The SNR is enhanced by using several sources to simultaneously transmit the same data. Preliminary measurement for a 9 LED luminance - less than the required luminance by 5 times - provided a bandwidth of 20 MHz and SNR of 20 dB with no coding. On implementing 2/3 coded Quadrature Amplitude Modulation (64-QAM) [53], a 80 Mbit/s data rate was achieved, acceptable for audio and video broadcasting [54].

OOK has been the modulation scheme used most often for LED based VLC, in turn placing limitations on achievable data rates. Elgala *et al* [55] have demonstrated a VLC link based on coded OFDM with Quadrate Phase Shift Keying (QPSK) [56] with a single LED. A pilot subcarrier to correct for frequency synchronisation errors, training sequences for channel estimation and time synchronisation routines were used in addition to Forward Error Correction (FEC) [57]. A BER of $2 \times 10^{-5}$ is achieved over a distance of 90 cm between transmitter and receiver; an improved BER is achievable with LED arrays [56].

Modulating the intensity of light-emitting diodes (LEDs) with analogue signals, such as bipolar Optical Orthogonal Frequency Division Multiplexing (O-OFDM) [56], leads to significant signal degradation due to the non-linearity of the LED output characteristic. The LED transfer function distorts the signal amplitude and clips the lower peaks at the turn-on voltage. Additionally, the upper peaks are purposely clipped before modulating the LED to avoid chip overheating. Optimisation of the bias point or backing-off the average O-OFDM signal power allows the control of distortion [55, 56].

Elgala *et al* [58] determined the optimum O-OFDM signal power through Monte Carlo simulations taking into consideration amplitude distortion and upper clipping. It was shown that soft clipping was an effective approach to reducing distortion and enhancing symbol error performance [58].

The challenge of high Peak-to-Average Power Ratio (PAPR) OFDM signals was investigated by Elgala *et al* considering the LED non-linearity [55, 59]. The practical implementation of OFDM in VLC system was analysed, indicating the Cyclic Prefix (CP) length which was found to have an insignificant impact on power and bandwidth efficiencies due to the relatively low channel delay spread encountered within indoor wireless optical applications. Also shown is that the Doppler frequency shift results in a very small shift relative to the actual peak wavelength, creating insignificant variations in the SNR. The main time and frequency distortions in optical wireless communication are mainly due to sampling offsets. The optical receiver front-end is identified as the dominant source of noise, determining overall system performance through the SNR.

The Home Gigabit Access (OMEGA) programme aims to bridge the gap between mobile broadband and the wired backbone network in homes. In order to provide Gbit/s connectivity, a combination of various technologies was considered [60]: IR and visible light from illumination based on white LEDs. The IR system aims at provisioning Gbit/s hot spots at a large FOV, and although a demanding goal, the use of diffused sources and typical receivers potentially allows Gbit/s operation. The main challenge was the modulation bandwidth; however the use of PAM and DMT modulation can provide the required data rate [60].

Langer *et al* [26] present experimental results on optical wireless transmission using commercially available phosphorescent white-light LEDs. Using DMT, 125 Mbit/s is achieved over a distance of 5 m at a low BER. The level of luminance is maintained at 800 lx at the receiver. The experiment is one of the earliest that enhanced the data rate managing the limits imposed by the modulation bandwidth of phosphorescent white LEDs [61].

## 2.5 Multiple Beam Systems

One of the main challenges facing VLC system implementations in the goal to provision high data rates is the modulation bandwidth. However, a room or coverage space could typically be illuminated by an array of LEDs releasing the potential for

parallel data transmission paths, following optical Multi-Input Multi-Output (MIMO) principles [62], to achieve higher data rates. Zeng *et al* [63] investigated imaging and non-imaging optical MIMO approaches, the former approach performing well at all receiver positions whereas the non-imaging alternative fails to meet specification due to symmetry.

An imaging diversity receiver, combined with MIMO processing techniques allowed 'alignment free' high data rate communications [26, 63]. The most power efficient scheme uses a white LED channel, as the power penalties on equalised and blue filtered channels at higher bandwidths are greater than owing to simple power splitting inherent in using multiple channels. However the complexity of deploying a large number of channels makes the approach less attractive [63].

## 2.6 Effect of Multi-Paths on System Performance

Two kinds of paths predominate in VLC systems; LOS and diffused NLOS links. The performance characteristics of a VLC system with multipaths due to reflections are analysed by Fan *et al* [64]; the analysis was executed for a moderate size office room. The performance close to the wall deteriorates because of interference from reflected light is substantially larger. Nevertheless, a bit rate of ~60 Mbit/s was achieved with Pulse Position Modulation **(**8-PPM) at points near the wall and at a semi-angle of receiver FOV of 50 deg; a bit rate of ~90 Mbit/s was achieved at a point a significant distance from the wall. Thus since multipaths impact performance, mitigating its effect is core to providing high bit rates.

## 2.7 Shadowing and Blockage

Another factor that impacts Quality-of-Service (QoS) in indoor optical wireless systems is shadowing and blockage [65]. Objects create shadowing, partly or completely, in an optical path because infrared light does not penetrate opaque objects. Both cellular and Multi-Spot Diffusion (MSD )[65, 66], MIMO, MSD-MIMO configurations provide potential solutions. Jivkova and Kavehrad [67] have investigated the robustness of LOS links in cellular architectures and non-LOS links

within a MDS architecture subject to obstructions of the signal path. Further, shadowing and blockage caused by people is also considered. The maximum radiation angle at the transmitter, in both configurations, should not exceed $45^{o}$, which in turn restricts the communication cell size. The probability of blockage of a cellular link depends almost linearly on the distance of the mobile object from the centre of the communication cell.

MSD-MIMO links have been proven to be robust against blockage, though still vulnerable to shadowing. In a typical office of roof height 3 m, the probability of shadowing is less than 2 % and in the majority of cases, the shadowing causes a <50 % reduction in the received signal power. The Power Penalty (PP) due to shadowing is insignificant (< 0.1dB) in 99% of cases [67].

## 2.8 Outdoor VLC Systems

The critical parameter which governs the feasibility of outdoor VLC systems is the significant ambient-light induced noise during daylight. Existing studies related to system performance have hitherto not taken into account the effect of ambient-light noise, which varies significantly from day to night. Lee *et al* [68] propose an analytical daylight noise model based on a modified Blackbody radiation [69, 70] to treat its impact on the system, showing a peak difference of 20 dB between the level of noise in early morning compared to noon. New receiver designs were proposed based on filtering to mitigate the effect of the background noise; an enhancement of up to ~5 dB in the SNR results.

In addition an analytical daylight noise model was proposed allowing a performance evaluation with less complexity to be carried out using measured global irradiance values [70, 71] as the input parameters. Results show that the BER with the new design structure of receiver yields a better BER than the conventional receiver design by 0.6 dB, albeit at the expense of a slight increase in the cost and complexity [68].

## 2.9 LED Brightness Control

Sugiyama *et al* [72] propose two methods for controlling the LED as an illumination whilst providing wireless networking. Using Pulse Width Modulation (PWM) [73] and with control of the modulations depth, the specified data transmission rate could be met whilst at the same time LEDs brightness can be controlled from 0% to 87.5% set by the PWM duty cycle. LED brightness could be controlled from 0% to 100% to yield a better data rate, but at the expense of more complicated drive circuitry.

## 2.10 LED Layout Optimisation

The received power is the key factor in the attainable performance of VLC systems; a LED layout that provides the optimum power distribution within rooms is vital in this respect. LED layout has been analysed by Deqiang *et al* [74] from the received power viewpoint. From simulation, the received power and BER were measured for a number of LED layouts and compared. Although the investigation was executed with respect to the received power, an evaluation of the effect of illumination layout on BER was not. The investigation was also conducted without consideration of sunlight irradiance [74].

In [75], a comparison of the performance of the system with the LED source at the corner and centre of an office room was carried out through an analytical approach. A SNR in the range of 56 dB to 61 dB was calculated, although the LED layout over all possible locations across the entire room was not considered. Moreover, the NLOS components of multipaths were neglected to ease the complexity of the calculation; however it is known that the NLOS components have a significant impact on the data rate and Root Mean Square RMS delay of the system (∼10% - ∼15%) [76, 77].

The optimisation of received power is considered in [78] using the Pareto-optimal technique [79] and Strength Pareto Evolutionary Algorithm (SPEA) multi-objective optimisation [80] for LOS components only without considering reflections. The methodology to optimise the received power focuses on consideration within a

standard room of LED placement with different numbers of LEDs at different distances from the walls of the room and spacing between LEDs. The minimum level of illumination was considered as a measure. The impacts of noise owing to neither sunlight nor reflections (NLOS components) were considered. The optimisation process is confined to standard office room size and shape only.

[81] reports on an extension of the above analysis considering the impact of LED lighting profile on the VLC channel. Two LED profiles are considered including obstacles in the room for LOS components only. Reflections originating from wall surfaces and obstacles nor the impact of sunlight [82] were considered. Moreover, the effect of LED placement over different room locations was not carried out.

[83] detail an evaluation of the data rate for a point-to-point VLC system for only one ceiling mounted LED layout within a standard office room. The analysis had not considered NLOS components, room size or shape, LED layout and the impact of sunlight. A $10^{-9}$ BER was calculated at a 500 Mbit/s data rate for four LED panels.

The impact on system performance of the LED viewing angle was considered in [84]. The viewing angle was varied form 50 degrees to 90 degrees, the results highlighting the significant impact on system SNR (20 dB at 50 degrees and 18 dB at 90 degrees). The analysis only considered LOS components, neglecting the impact of NLOS components (surface reflectivity) and for one LED layout location only with four LED panels on the ceiling. Again the noise owing to sunlight was omitted.

## 2.11 Coding Schemes

Choi *et al* [85] proposes Half Bit Transmission (V5-HBT) [86] line coding for VLC applications. Half-a-bit transition to the ‘one’ bit and decoding the encoded bits was executed through measurement of the difference of the bit transition level during the ‘one’ bit duration. The coding scheme provides a 2 dB – 3 dB gain in the SNR when compared with convention line coding at the same BER ($10^{-4}$). Additional synchronisation and error correction were required in outdoor environments [85].

Spread spectrum coding has been deployed in indoor VLC systems by Ying Yi *et al.* [87]. Four spreading codes were investigated; Pseudo-Noise (PN) binary-valued codes [86], Walsh codes [86, 88], m-sequence [86] and Gold codes [86] and their BER performance on LOS and diffuse channels were compared. It was shown by experiment that spread codes militate against both multipath ISI and signal distortion due to dispersion. In conventional systems, a RMS delay spread of 0.1 over the symbol duration degrades performance significantly, exacerbated with increasing multipath dispersion; spread codes assure a high data rate even if the RMS delay is greater than 0.1 over the symbol duration and are a viable option to mitigate against multipath dispersion [87].

The use of OFDM in intensity modulation was investigated by Afgani *et al* [45]. The non-linearity of the power amplifier provides a high Peak-to-Average Ratio (PAR) in OFDM, normally considered a disadvantage in radio frequency transmission systems. However [45] have succeeded in demonstrating theoretically and through experiment, that the high PAR in OFDM can be exploited constructively in intensity modulated LED VLC systems by biasing the signal variations around an operating point determined to fall within the linear region of the LED output characteristic. Good agreement was achieved between theoretical and experimental results; the latter executed using a single LED with no channel or source coding at a 1 m distance between transmitter and receiver. LED arrays with FEC provided a higher SNR which then translated into lower BERs at much greater distances. [45].

Mase *et al* [89] proposed an improved coding scheme for VLC systems using a LED array transmitter and a high-speed camera as the receiver on a vehicle. A hierarchical coding scheme [90], which allocated data to spatial frequency components depending on priority, was proposed and the highest-priority data was received even if the receiver was at a significant distance (40 m - 60 m) from the transmitter albeit with a poor BER of $10^{-1}$. Dividing data with FEC for each spatial frequency resulted in an improvement in attainable BER [89].

## 2.12 VLC System Applications

A rich mix of VLC system applications have been reported, ranging from indoor environments such as wireless networking in offices and rooms as well as an indoor GPS-like navigation [17] through to transport systems [32] and in areas subject to high levels of electromagnetic interference such as hospitals and aircraft [91, 92].

### 2.12.1 Transport Systems

A Vehicle Information and Communication System (VICS) Intelligent Transport System (ITS) was developed for the purpose of combatting traffic accidents in Japan [93]. Kitano *et al* [32] proposed a VLC system harnessing existing deployments of LEDs for road illumination. The deployed LEDs fulfilled the standard specification for road illumination and formed the foundation for a vehicular communications solution; the viability for overlaying a vehicular communication platform was proven through numerical analysis [32].

A VLC based audio information system implemented through high brightness LEDs modulated and encoded with audio messages was reported in [94]. The system comprised a receiver combined with a speaker, located at a distance from LED traffic lights. The receiver demodulated the optically transmitted audio information and broadcasted messages. Intensity modulated direct detection was used to provision an open space, audio broadcasting information beacon for short distance communications.

A parallel MIMO-like wireless optical communication system using LED traffic lights and high-speed cameras for road-to-vehicle communication was proposed by Wada *et al* [95]. LEDs integrated into the traffic light were modulated individually, transmitting data in parallel and a camera demodulated the received data using image-processing techniques. Using this system, location and safe driving support information was disseminated locally. Due to the highly directional outputs from individual LEDs, transmitting different information for every lane of a road was possible. Transmitted information was decoded from an image; each character of the

data was matched by the camera/lens combination. Attenuation, a reduction in the number of pixels and LEDs overlap resulting in a defocused image are all degradation factors that compromised transmission channel quality. The data rate was a function of the amplitude of the signals and the number of signal frequency partitions [95].

The above system was extended to support an intelligent transport application; traffic signal LEDs acted as sources transmitting information to vehicles. However the system faced many problems; transmission distances were more challenging; the transmitter and receiver relationships changed with time; and thirdly, the communication was affected by a significant level of optical noise. Consequently, Hara *et al* [96] proposed a new receiver design comprising a photodiode, imaging optics and a tracking mechanism; the old design [32] was based solely on optical filtering. The new receiver system enabled longer distance communications (~100 m) at higher data rates (few Mbit/s). The system prototype was been validated [96].

Kumar *et al* [97] discuss system design issues relating to the use VLC concepts in road traffic control system applications. A simple model of the traffic configuration was analysed with a view to optimising VLC design parameters. The optimisation was based on the gain variation over a 100 m transmission distance, determining the gain needed at the receiver to further increase the coverage area, in turn relaxing the demands on receiver front-end design. Data transmission performance was also optimised by the judicious placement of traffic lights along both sides of the road under common control [97].

Bouchet *et al* [98] present the key goals of the OMEGA project [29] with emphasis on the hybrid optical wireless (HWO) development. The project addressed a number of significant challenges in the field of hybrid home area networks and aimed to be a catalyst to fuel a substantial consumer pull for next-generation broadband by enabling the sharing of large data user-generated content, which, in turn, stimulates the thirst for even higher data rates. The HWO work combined optical wireless communications techniques to provide robust connections by either IR for Gbit/s

LOS connections or VLC for broadcast coverage at lower data rates. In addition, an HWO 'inter-MAC' layer has been developed to control available channels. A complete HWO prototype was integral to the overall OMEGA platform [98].

Kotake *et al* [99] propose a free-space optics system implementation between a train and the ground. A BER ($10^{-3}$ ) in outdoor experiments using a test train was obtained at 100 Mbit/s data rate, the results showing that the optimal value of vertical beam angle was 0.3 degrees with optical filtering before the APD. Weather conditions were not considered but nevertheless preliminary results indicated that the solution was a promising candidate for train-to-ground communication [99].

### 2.12.2 Aerospace

Providing wireless networks on aerospace platforms using VLC brings a number of advantages primarily in terms of weight and freedom from electromagnetic interference.

Wong *et al* modelled a Boeing 777 airplane by CAD program to analyse VLC system performance [91]. Using ray-tracing, the design of the optical sources to achieve uniformity of signal distribution within the cabin was developed. The peak-to-peak variation in signal intensity for the targeted aisle positions was evaluated to be less than 5%. Ray-tracing was also used to characterise multi-paths which in turn facilitated the development of a communications model to determine the performance of the optical wireless system under ambient noise and multipath interference. For a BER of $10^{-9}$ with equalisation, a data rate of >170 Mbit/s is achieved; a transmission bit rate of >400 Mbit/s was achievable if the acceptable BER is lowered to $10^{-3}$. A 1550 nm LED source was chosen as within that segment of the spectrum, the ambient spectral noise levels are reduced compared with a 850 nm source as well as complying with the eye safety standard, the International Electro-technical Commission IEC 60825-1 [100]. The system was characterised through the BER performance, showing that multipath has a greater effect on performance than ambient noise. Additionally under fluorescent lighting, the maximum transmission data rate reduces from 440 Mbit/s to 233 Mbit/s at a BER of

$10^{-3}$ without consideration of the effect of multipath dispersion. However, the transmission capacity attained indicates that the use of broadband optical wireless within commercial aircraft cabin environments is a feasible option [91].

The path loss model for optical transmission inside the aircraft has been developed and evaluated [101]. LOS and NLOS components were considered in the evaluation of cellular network scenarios. Monte Carlo ray tracing simulations and mathematical models were utilised to evaluate system performance inside the aircraft including the impact of the shadowing components. The shadowing was modelled using a log normal distribution with zero mean and standard deviation. Signal-to-Interference Ratio (SIR) maps were developed for a number of deployment scenarios supported by a geometric Computer-Aided Design (CAD) cabin model. It was found that the LOS path loss is dominated by the direct component with consideration of multi-paths and varies between 27 dB and 69 dB with a path loss exponent of 1.92 at distances from 0.04 m to 5.6 m.

Furthermore, results show that the performance degrades by 10 dB when NLOS transmission is compared to the LOS case. The impact of shadowing is not as significant and a robust communication link can be provisioned in the aircraft cabin. SIR maps for a number of deployment scenarios showed that frequency reuse can be applied throughout the aircraft cabin; a SIR of 3 dB was achieved at the edge of the cell at a frequency reuse of 3. Full frequency reuse can be achieved through interference avoidance or mitigation techniques such as interference aware resource allocation and scheduling [102, 103]

### 2.12.3 Healthcare

Increasing the quality of any wireless communication system is core to contemporary health management strategies. Underpinning the provision of this range of services is a communications platform, the operation of which must not introduce any level of electromagnetic interference (EMI) in order to limit the impact on the operational performance of other key equipment [50, 92]. The system has to provide a flexible and reliable service for real time access to patient's information and enable more

extensive, real time monitoring of individual patient conditions. The use of LED based VLC systems potentially circumvents the problems introduced by electromagnetic interference on biomedical instrumentation whilst provisioning acceptable date rates.

A healthcare application of VLC has been reported by Hong *et al* [92]. Information was modulated onto a high brightness LED (HB-LED) for both lighting and communications, received through a portable unit. Binary Frequency Shift Keying (BFSK) [86] was used with Cyclic Redundancy Check (CRC) [86]. The overall system comprised three main elements: the Information Exchange Centre (IEC), Information Illuminating Node (IIN) and Mobile Terminal (MT) for X; here X can represent patients, doctors or nursing staff (Figure 2.1). The IEC, a PC or a workstation with direct access both to the Internet and hospital databases, collates patient information to be retrieved when needed. The connection between the IEC and Internet could be through a Digital Subscriber Loop (DSL) [92, 104] or Fibre-to-the-Premises (FTTP) [92], both of which provision an acceptable backhaul bandwidth. The hospital database was accessed through a Local Area Network (LAN) and Power-Line-Carrier (PLC), establishing a bi-direction connection between the IEC and the IIN.

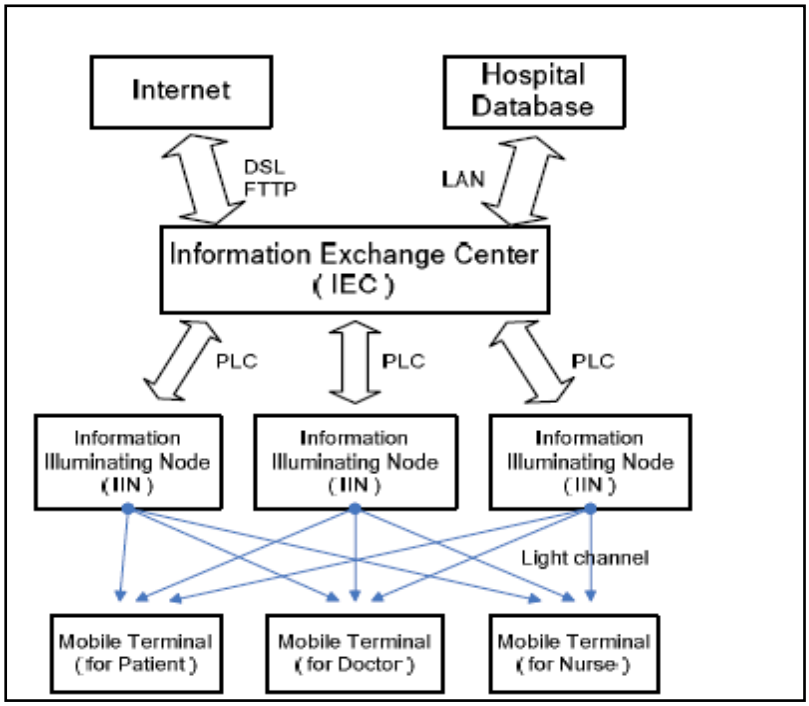


**Figure 2.1: Hospital Information VLC system (HIIS) architecture [92].**

The mobile terminal, implemented through FPGAs, was designed for use by patients, doctors and nursing staff. The information was stored and displayed and the simplified graphical user interface eases the interaction. The IIN consisted of FPGA and analogue modules, the latter implemented through MOSFET, chosen for its high switching speed so as not to comprise the driver and HB-LED illumination array response (Figure 2.2).

Environmental sensors were also installed in each IIN viz. temperature and moisture sensors; the IEC updated parameters collected by these sensors periodically. The IIN was responsible for encoding/modulating signals received from the IEC. In this work only BFSK modulation was evaluated provisioning 5.8 kbit/s; however Multi-Tone Modulation (DMT) was evaluated in [60] showing an increase in data rate to more than 200 Mbit/s at a lower BER ($10^{-3}$). The transmission frequencies were 200 kHz and 240 kHz respectively so that users were not subjected to flicker. Both uplink and downlink were implemented in the visible light range.

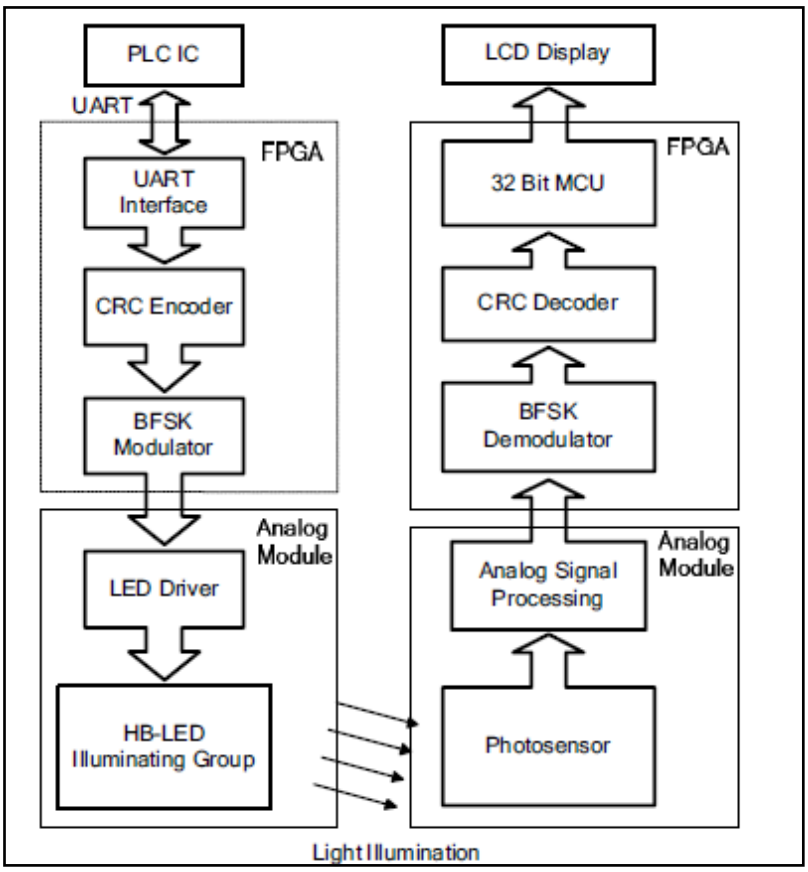


**Figure 2.2: The physical link layer between the IIN and MT [92].**

The BER performance of the system as expected indicated that as the transmission power increased, the BER decreased and as the distance between transmitter and receiver increased. Although an acceptable level of BER ($10^{-7}$) was achieved at a distance of 2 m, the BER dropped to $10^{-3}$ when the distance increased to 8 m. At a distance of 5 m between transmitter and receiver, a data rate of 125 Mbit/s was achieved [61]. The BER will be enhanced if diversity and equalisation techniques were applied [42, 105]. All system evaluation was executed at 90-degree incidence and the effect of the irradiance angle in the evaluation was not considered.

## 2.13. VLC System Integrated with Power Line Communications (PLC)

White-LEDs are primarily distributed for illumination within buildings and consequently it is possible to use power line cables as a communication medium to

connect other in-building fixed networks with the LED arrays. Power Line Communications (PLC) is becoming an accepted solution for indoor connections and that infrastructure can also be harnessed to inter-link arrays of LEDs [30]. Multipaths and noise caused by mismatches throughout the power-line network degrade system performance; thus, to attain higher data rates, impedance matching is applied. A channel model for the proposed integrated system has been developed based on modelling the Power-Line and visible Free Space Optical (FSO) channels. Signal distortions in the PLC can be minimised and the integrated system provides improved BER at high data rates [30].

The use of the current installed power line infrastructure to power LEDs and also to carry communication signals was investigated by Nakagawa *et al* [50]. The system uses visible LEDs without demodulating the signal from the power-line. The system was analysed and its feasibility shown by experiment.

## 2.14 System Receivers

VLC receivers normally comprise a receiving element, concentrator, photodiode, optical filter, amplifier and recovery circuit (Figure 2.3). The light signal is collected by a lens or/and an imaging system; the collection of light can be enhanced by the use of concentrators to mitigate the attenuation owing to beam divergence [106]. Light collection can be enhanced by increasing the Field-of-View (FOV) of the receiver; however the wider FOV impinges on the size (and hence capacitance) of the proto-sensitive area which in turn compromises the bandwidth of reception.

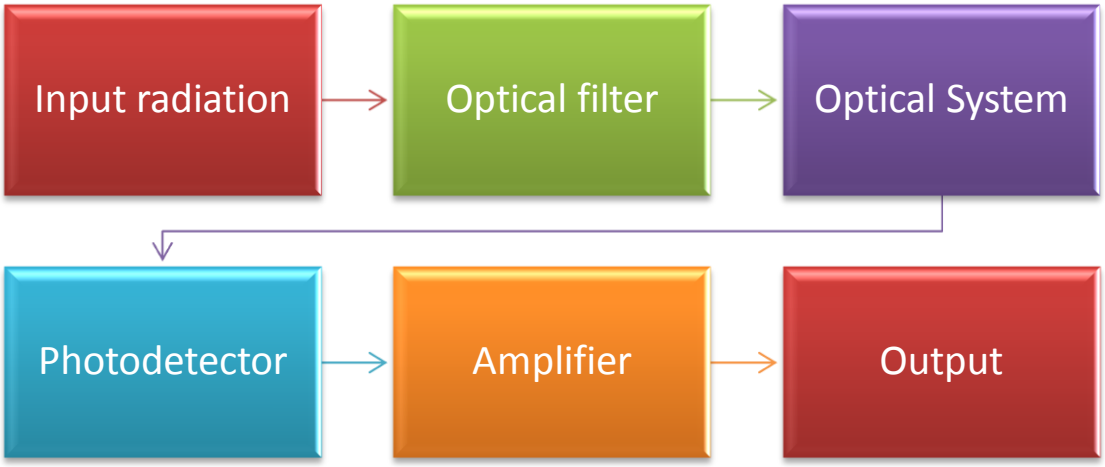


**Figure 2.3: VLC receiver components [106].**

VLC system performance is impacted by sunlight and other ambient sources of background light within the reception field of the receiver. Thus an appropriate filter is employed to mitigate the impact of the resultant noise. Silicon photodiodes operate from 400 nm to 1200 nm, the operation band of VLC systems. The signal is thus detected by utilising either a silicon p-type-insulator-n-type photodiode (Si PIN-PD) or silicon Avalanche Photodiode (Si APD).

The signal can be amplified by different types of electronic circuits but the most common are the high impedance and trans-impedance amplifier. The former senses the voltage through a series connected resistor and is simple to implement whilst the latter uses a shunt resistance around inverting amplifier converting the current input to a voltage output.

Photodiode performance is governed by the material system, usually doped to create diffusion of carriers across the interface of the p and n regions. The PIN determines the performance of the photodiode as it converts photons impinging to electron-hole

pairs. The photocurrent is generated as a function of the energy of the photon and the energy of band-gap of the semiconductor material. Silicon is the most common semiconductor material for receiver implementations in VLC systems with band-gap energy of 1.12 eV yielding a 500 nm - 900 nm operating wavelength band.

The main characteristics of photodetector important to system performance are;

- High sensitivity at the band of operating wavelengths
- Linearity: the response of the detector shall be linear to limit distortion
- Large detection area: to offer large collection of incident light and increase detection efficiency
- Short response time: for high speed system operation up to several GHz
- Minimum noise: low levels of dark current, leakage current and shunt conductance

Two main types of receivers based on the PIN photodiode and Avalanche Photodetector (APD) have been utilised in VLC implementations.

### 2.14.1 PIN photodiode

PINs offer low-cost reliable detection with a 90% quantum efficiency achievable utilising InGaAs [107]. As the gain bandwidth is relatively low for such a detector, a number approaches have been developed to provide higher bandwidth operation and 40 GHz has been demonstrated at responsivity 0.55 A/W [108]. Several approaches have succeeded in providing near to 100% quantum efficiency such as utilising AlGaAs/AlAs layers [109]. A bandwidth of 120 GHz using an air-bridged metal waveguide together with an undercut mesa structure has been demonstrated [107, 110]. However, the bandwidth of current commercially available detectors is usually up to 20 GHz due to limitations of the packaging.

### 2.14.2 Avalanche Photodiodes (APDs)

APDs provide internal gain through a more sophisticated structure than in PINs aimed at creating high electric field in the region of electron-hole pair generation. It is distinguished by a constant gain bandwidth; at low gain, the transit carrier time and RC effects dominate providing an enhanced response time. At high gain, the device bandwidth decrease proportionally with an increase of the gain. The APD is

characterised by fast rise time of between 150 psec and 200 psec and fall time of ~1 nsec. A number of approaches have been utilised to enhance operation e.g. a symmetric waveguide APD [107, 111] provides a high quantum efficiency and robustness to high input power operation. Table 2.1 summarises the characteristics of the most commonly used photodetectors in VLC systems.

**Table 2.1: A comparison of photodetector characteristics [107].**

| Characteristics | PIN | | | APD | | |
|---|---|---|---|---|---|---|
| | Si | Ge | InGaAs | Si | Ge | InGaAs |
| Operating Wavelength (μm) | 0.4-1.2 | 0.8-1.9 | 1.0-1.7 | 0.4-1.2 | 0.8-1.9 | 1.0-1.7 |
| Gain | 1 | 1 | 1 | 50-500 | 50-200 | 10-40 |
| Dark Current (nAmp) | 1-10 | 50-500 | 1-20 | 0.1-1 | 50-500 | 1-5 |
| Responsivity (A/W) | 0.4-0.7 | 0.5-0.7 | 0.6-0.9 | 80-130 | 3-30 | 5-20 |
| Response Time (ns) | 0.3-1 | 0.1-1 | 0.05-0.5 | 0.1-2 | 0.5-1 | 0.1-5 |

PIN photodetectors are most commonly used due to low cost, high reliability, tolerance to wide temperature fluctuation and operation at low bias voltages compared to APD [1].

## 2.15 Conclusions

A large body of research has been reported in the design and performance evaluation of VLC systems. Greater than 200 Mbit/sec data rates have been demonstrated within office environments. A range of other experiments conducted in both office and laboratory scenarios have highlighted similarities in system architecture which will inform the development of a more robust, flexible platform able to support a range of applications [39, 50, 64, 105].

Two main types of white LEDs have been utilised in system implementations; a blue LED coated with a phosphour or a mix of three Red-Green-Blue (RGB) chips, their combination generating white light. The first type has the advantage of low cost however the modulation bandwidth is limited due to the inherently slow response time of the phosphour.

The application of a blue filter at the receiver to restrict the amount of yellow light (inducing slower response times) impinging on the detector has been proposed to enhance the data rate; however, it leads to a power penalty at the receiver owing to a reduction in the total signal power recovered.

Two main methods are used to generate white light viz. from RGB LEDs and blue LEDs with coated phosphour, the latter being preferable due to simplicity in implementation. Several techniques have been employed to enhance modulation bandwidth such as a blue filter at the receiver to remove the slow response of the yellow component, employing multiple resonant and post equalization and advanced modulation techniques such as Discrete Multi-Tone Modulation (DMT). Employing electrical equalisation can also enhance the effective transmission rate by 2 to 10 times. A 20-fold enhancement of the direct modulation speed has been recorded utilizing Quaternary-Amplitude-Shift-Keying (4-ASK) modulation and digital filtering [106]. Multi-level modulation techniques where multiple bits can be carried through each transmitted symbols have also been used to enhance data rate e.g. Optical Orthogonal Frequency Division Multiplexing (O-OFDM) with Quadrature Amplitude Modulation (QAM) or with DMT modulation. However complex signal processing at the receiver is required at the case of multilevel modulation [24, 112].

Different approaches have been developed to enhance the data rate. Pre- and Post-equalisation has produced up to a four times enhancement (from 10 Mbit/s to 40 Mbit/s) in the data rate limit imposed by the source modulation bandwidth. A summary of equalisation techniques are provided in Table 2.2.Another approach to enhance data rate is that to employ advanced modulation formats and a number of metrics have been used to evaluate the efficacy of the modulation on system

performance i.e. spectral efficiency, sensitivity to the LED nonlinearity, sensitivity to shadowing and implementation complexity. Table 2.2 summarises the range of modulation techniques used in VLC system implementations with associated impact on performance. It is worth noting that all approaches are affected by the physical behaviour of the VLC path.

**Table 2.2: A Comparison of equalisation techniques used in VLC system implementations.**

| Equalisation Technique | Results | System Performance/ Characteristics |
|---|---|---|
| **Decision Feedback Equalization (DFE) – Adaptive Equalisation** | Data rate improvement up to 600Mb/s | NRZ-OOK, at BER of $10^{-6}$ |
| **Least Mean Square (LMS)** | Data rate improvement up to 400Mb/s | NRZ-OOK, at BER of $10^{-6}$ |
| **Pre-Equalisation using Resonant Driving** | System data rate enhanced from 10 Mbit/s to 40 Mbit/s | NRZ-OOK, 25 Mbit/s data rate at BER of $10^{-6}$ |
| **Pre-Equalisation using Resonant Driving and First Order Post-Equalisation** | System data rate enhanced from 40 Mbit/s to 120 Mbit/s | NRZ-OOK, 75MB /S data rate at BER of $10^{-6}$ |
| **Resonantly Modulated LED** | 25 Mbit/s data rate | OOK, 40 Mbit/s at a BER of $10^{-6}$ |
| **First Order Post-Equalisation** | Data rate improved from 16Mbit/s to 32 Mbit/s | NRZ-OOK, at a BER of $10^{-6}$ |
| **First order Equalisation and Filtering (Blue Light only)** | Data rate improved from 2Mbit/s to 50 Mbit/s | LXHM-LM1B LED, data rate 100 Mb/s and BER of $10^{-9}$ |

**Table 2.3: A Comparison of modulation techniques used in VLC system implementations.**

| Modulation Technique | Sensitivity to Shadowing | Spectral efficiency | Sensitivity to LED Nonlinearity |
|---|---|---|---|
| **On Off Keying (OOK )** | Medium | <1 | Low |
| **Variable Pulse Position Modulation (VPPM)** | Low | <1 | Low |
| **Colour Shift Keying (CSK)** | Medium | 2 | Medium |
| **Orthogonal Frequency Division Multiplexing (OFDM)** | High | 3-4 | High |
| **Multi-Tone Modulation (DMT)** | Medium | 2-3 | Low |
| **Multi-level Expurgated Pulse Position Modulation (MEPPM)** | Medium | 2-3 | Low |

Two principal modulation classes have been implemented in VLC systems viz. single carrier and multiple sub-carrier modulation. Single carrier pulsed modulation techniques where the time dependent characteristics of the optical pulse is used to carry the information provide high average power efficiency. Two schemes are widely used, On-Off Keying (OOK) and Pulse Position Modulation (PPM). In OOK,

LEDs are turned ON or OFF according to the data bits 1 or 0; light does not necessary to be off at bit zero but the intensity is reduced to a relatively low level. In PPM, the optical pulse is transmitted over one of *S* slots per symbol where the position of the pulse in the slot represents the bit combination in the symbol. Although the PPM spectrum is wider compared to OOK, it provides higher power efficiency at the expense of added complexity at the receiver predominately due to synchronization at both slot and symbol levels. Additionally, in order to achieve higher throughput, a multi-level scheme such as Unipolar Pulse Amplitude Modulation is utilised to overcome the impact of the limited bandwidth [2, 113].

OFDM is a practical embodiment of a multiple sub-carrier modulation technique. Although OFDM relies on transmitting orthogonal sub-carriers, it does not require complex channel equalisation as it is time variant channel; a frequency domain channel estimation can be employed with adaptive modulation according to the quality of service and the required data rate.

As OFDM outputs are complex, and it is not possible to use Quadrature Modulation with intensity modulation direct detection. Two schemes have thus been developed to adapt OFDM as used in the RF communication for use in VLC; DC-biased Optical OFDM (DCO-OFDM) and asymmetrically clipped optical OFDM (ACO-OFDM).

In the DCO-OFDM, the DC operating point is set and then the bipolar signal is utilised to module the optical carrier [1]. However DC biasing increases the power requirement in the time domain signal compared to the bipolar case. In ACO-OFDM, a clipping process is applied to convert the signal from bipolar to unipolar and only odd sub-carriers are modulated with the even sub-carriers set to zero. The approach can be applied without distortion of the encoded information owing to the symmetry of the OFDM signal.

According to the IEEE 802.15.7 standard, three physical (PHY) types for VLC systems are defined. PHY I and PHY II are defined for a single light sources and support OOK and Variable PPM modulation techniques where PHYIII concerns

multiple light sources and supports Carrier Shift Keying (CSK) modulation technique.

OOK is widely used due to hardware simplicity in implementation, providing a good balance between complexity and performance. PPM uses the position of the pulse, providing higher power efficiency compared to OOK but however is sensitive to ISI. Ultimately the absence of the need for threshold detection makes the technique preferable. OFDM is multicarrier modulation technique developed to increase the data rate for RF systems. DC-biased Optical OFDM (DCO-OFDM) and Asymmetrically Clipped Optical OFDM (ACO-OFDM) have been proposed for indoor environments with MIMO providing up to Gbit/s data rates. However the relatively long tail of the impulse response requires a long cycle prefix for OFDM to operate in addition it is not easy to control its high peak to average power ration (PAPR).

MEPPM is constructed by *N* EPPM symbols and has a spectral efficiency of between 2 and 3. It has the flexibility to provide a wide range of PAPRs and can transmit high speed data even under highly dimmed scenarios. It is an improvement on EPPM in mitigating the flicker effect as the presence of multi-light levels per symbol make light intensity changes difficult to follow with the human eye, especially if the number of levels is increased and the duration of time slots decreased. However, it is sensitive to shadowing and very sensitive to the threshold level.

Many application scenarios have been proposed for the VLC system deployment and a range of experimental demonstrations have proved that it provides acceptable performance, especially in applications subject to EMI with other wireless systems/equipment within the area of operation. Operation in healthcare, aerospace has been trialled, providing a reasonable solution for these environments. In addition deployments in conference halls, smart homes, and transport systems have demonstrated its flexibility in applications. Table 2.4 summarises the range of applications with associated performance.

**Table 2.4: A Comparison of the VLC system applications.**

| Sector | Application | System characteristics/ Performance |
|---|---|---|
| **Intelligent transport Systems (ITS)** | Vehicle Information and Communication System (VICS) for reducing traffic accidents. | 1Mbit/s for OOK modulation at level of BER= $10^{-6}$ |
| | Audio broadcasting information beacon for short distance communications. | Distance 0.4 meter, OOK modulation ant SNR level of 35 dB |
| | Wireless optical communication system using LED traffic lights and high-speed cameras for road-to-vehicle communication. | Distance communications (~100 m) at higher data rates (few Mbit/s). |
| | Road traffic control systems application | A 100 m transmission distance, the optimum Horizontal inclination of transmitter and irradiance angle as 81.4º and of 8.6º |
| | A communication link between a train and stations. | Distance 19.6 m, data rate 120 Mbit/s and BER $10^{-3}$ |
| **Aerospace** | Wireless networks on airplanes | BER of $10^{-9}$ at data rate of >170 Mbit/s; a transmission bit rate of >400 Mbit/s is achievable if acceptable BER lowered to $10^{-3}$ |
| **Indoor and Infrastructure** | Indoor GPS, Classrooms, Hotels and Conferences | 0-0.15 m accuracy with imaging sensor |
| | Integrated with PLC | Data rate 1Mbit/s, SC-PBSK modulation, BER level $10^{-6}$ |
| **Healthcare** | Real time monitoring of individual patient conditions | 0.5 m distance between transmitter and receiver, 5.8 kbit/s data rate, $10^{-5}$ BER; BER falls to $10^{-3}$ at a distance of 2 m; BER falls to $10^{-3}$ at a distance of 8 m |

The foundation research reported to date is a catalyst which stimulates a great number of other challenges. For example, the impact of room size and reflections on system data rate, SNR, BER, system availability and reliability has to date not been rigorously analysed. Although room size has been considered in [74, 75, 78, 81, 114], the evaluation is confined to a 5m×5m×3m, (a moderate size room), other potential applications require a characterisation of rooms and halls that are much larger. Signal reflections effect SNR and BER, heavily impinging on system performance [64].

Another area that has not been the subject of rigorous evaluation is the impact of sunlight irradiance on VLC system performance. Sunlight irradiance introduces noise which has an effect on BER performance, especially if the incident natural light falls directly onto the receiver. Since sunlight irradiance is at a maximum within the visible spectrum band, the probability of system unavailability increases.

[74, 75, 77-80] have considered the effect of LED layout in moderate size room environments. However, results are based on one or two LED layouts without consideration of the impact of neither sunlight irradiance nor cloud cover. LED layout optimisation minimises the power required for (number of LEDs) acceptable performance. A methodology for the optimisation of the LED layout is much sought after.

VLC system operation requires the illumination to be switched on at all times, a significant challenge for implementations in different environment especially in locations that operate with limited energy resources. Hybrid systems that co-operate with infrared IR networks when the illumination is ‘off’ have been proposed [115, 116] but at the expense of the interference with other systems within the coverage area and power consumption. A deep investigation of system performance in different environments in order to minimise the consumed power has not been carried out to date [117].

Given the state-of-the-art, the research focuses on the evaluation of the impact of sunlight on VLC system performance with the aim of creating system design guidelines. The aim is to emulate large rooms with different shapes, and to determine the optimum deployment in the presence of sunlight that maximises system data rate. Through the use of simulation, different scenarios and conditions will be estimated, in so doing informing future system design and defining the mix of potential applications.

LED layout optimisation for large rooms so as to reduce the impact of shadowing and provide the trade-off between room size and system performance as a function of LED layout and number of LEDs is a major element of work. Thus the research develops an optimisation methodology by considering the BER, SNR, illumination level required for a room (according to standards) and reflections (multipaths) from walls and surfaces in the room that may affect the performance of the system. Surface reflectivity plays an important role in system design for different environments [118].

# Chapter 3

# Modelling of Visible Light Communication (VLC) Systems and Sunlight Irradiance

## 3.1 Introduction

A review of the mathematical models describing visible light communication (VLC) system evaluation is presented. Based on the analysis of the state-of-the-art, a mathematical model of a VLC system with consideration of Non-Line-of-Sight (NLOS) components is developed; most relevant models reported to date consider only Line-of-Sight (LOS) components in the evaluation [25]. Furthermore, thus far, the impact of sunlight on VLC system availability due to direct and indirect incident irradiance has not been subject to a rigorous evaluation. In this respect, sunlight irradiance in clear and overcast sky conditions is modelled as the foundation for determining its impact on system performance.

## 3.2 Visible Light Communication Systems

The spine of a VLC system consists of a number of elements (Figure 3.1). Data originates from a Network Interface and is inputted - overlaid with brightness control to implement the dimming methodology discussed in Section 3.2.3 - to a driving circuit that modulates the LEDs through its current (Section 3.2.4). The modulation is carried either by Red (R), Green (G), Blue (B) or by Yellow-Phosphour/Blue (YB) LEDs (Section 3.2.1). During transmission, the light is subject to reflections in the path from transmitter to receiver where the optical concentrator captures rays that fall within its collection angle. An optical filter rejects (ambient) light falling outwith the spectrum of interest. The signal is transduced through a photo-detector, amplified and the data recovered. The following Sections provide more detailed descriptions of the core system blocks.

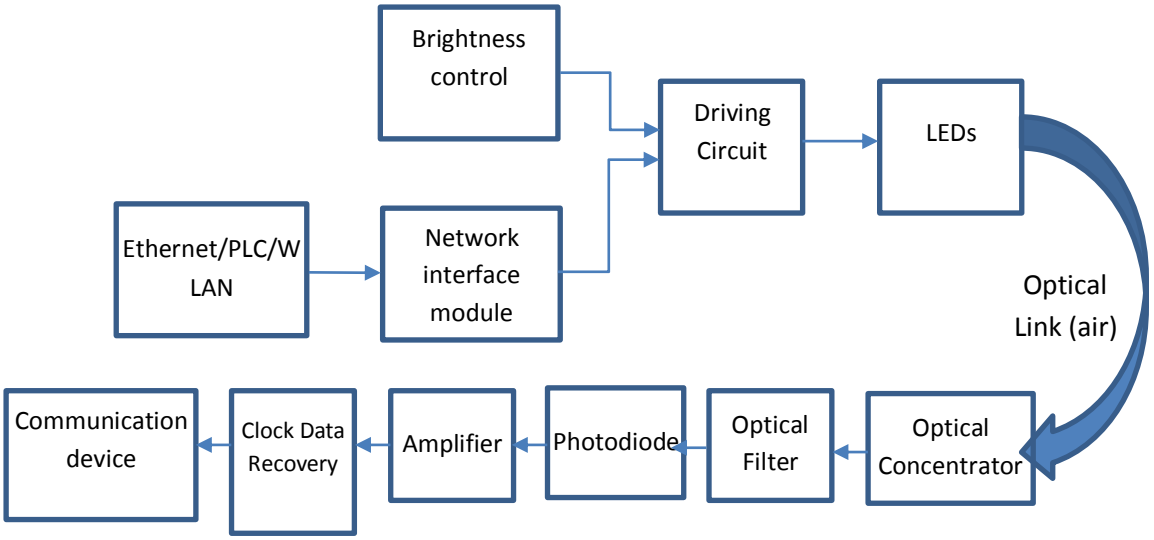


**Figure 3.1 VLC communication system block diagram.**

### 3.2.1 VLC Transmitters

VLC transmitters use LEDs (high brightness) as sources of a visible light optical carrier. Since these LEDs are used primarily for illumination, the transmitter must comply with existing lighting standards for indoor environments, which are between 200 lx –1000 lx following the International Standards Organisation (ISO) recommendations [118].

### 3.2.2 Light Emitting Diodes (LEDs)

There are two types of visible wavelength (white) LEDs; the first category is single colour - Red (R), Green (G) or Blue (B) - the other White (W-LED), normally comprising a chip emitting a short wavelength and wavelength conversion layer e.g. phosphour for converting the emission wavelength from an active area [25]. The phosphour absorbs short wavelength radiation from and the re-radiated light from the phosphour is subject to shifts to longer wavelengths; many wavelength components are generated. Red, Green, and Blue LEDs emit a spectrum around a central

wavelength governed by the material characteristics; R-LEDs emit a wavelength of ~625 nm, G-LEDs ~525 nm, and B-LEDs ~470 nm.

From the communication viewpoint, the response time of each LED is core, since the maximum data rate to be transmitted is related to its response time. In this respect, the phosphour based W-LEDs have longer rise/fall times due to a combination of absorption/re-emission times [38, 119]. It must however be noted that both LED types have found appropriate VLC system applications [27, 120, 121].

### 3.2.3 LED Brightness Control

For illumination, LED brightness control is a prerequisite feature and consequently a number of dimming methods have been implemented [27, 122]. Amplitude modulation (AM) dimming [123] controls the DC forward injection current into the LED (Figure 3.1); changing the DC forward current controls the luminous flux but the method also produces colour shifts of the emitted light as the LED spectral power distribution (SPD) is a function of drive current [123, 124].

Pulse Width Modulation (PWM) based methods [27, 125] can control the average current into the LED through the width of the injection pulses. PWM pulses are of constant amplitude and thus the spectrum of the emitted light remains constant with the pulse width varying according to the dimming level (duty ratio) within the PWM period. Moreover the PWM method is preferred due to superior linearity compared to AM [123, 124]. Similarly, Pulse Frequency Modulation (PFM) can be used to [27, 126] control the average current into the LED through the frequency variation of constant width and amplitude pulses [27].

### 3.2.4 LED Drive Circuits

The drive current is injected with an appropriate DC bias to impart LED modulation, comprising a DC level for illumination (the dimming current) and a to mix the digital data input signals for modulation applied through a bias Tee.

The drive circuit normally comprises a transistor or a FET to feed the current [53]; latterly integrated circuit based driver chips have been developed [127]. Input voltage (~700 Vpp/mV), output voltage and maximum LED drive current (~600 mA) are the main specifications in the design of the drive circuit [53, 127]. However there are other parameters that determine the selection of the drive circuit such as the current requirement to control modulation depth and bias current, the rise and fall times of LEDs which impact on the maximum data rate; LEDs rise and fall times vary from a few nanoseconds to a few hundreds of nanoseconds [27, 40]. Additionally the switching speed of the drive circuit must not compromise data rate in order to minimise the impact of inter-symbol interference on system performance [27, 127]. Power dissipation and thermal performance are also factors that govern the design.

### 3.2.5 VLC Receivers

The VLC receiver is a critical element of the overall implementation, defining the noise level of the overall system. A typical receiver comprises an optical concentrator, optical filter, photodiode, amplifier and a signal recovery circuit. The optical concentrator compensates for the high (spatial) attenuation owing to beam divergence from LEDs, usually designed to illuminate as extensive an area as possible. The use of an appropriate concentrator increases the effective capture area (Field-of-View (FOV)) and hence recovered signal levels; examples are the Compound Parabolic Concentrator (CPC) and imaging lens specifically designed for infrared communications [53, 121].

Photodiodes with good Responsivity (R) [128] to visible light are normally silicon p-type-insulator-n-type (Si pin-PD [129]) and Avalanche Photodiode (Si APD [53, 130]). The silicon material system responds efficiently to light from 400 nm to 1200 nm, which includes the visible wavelength range. There are many photodiodes whose bandwidths exceed 200 MHz [27], significantly wider than the modulation bandwidth of typical VLC LED transmitters.

Post detector pre-amplification is also an important stage of the receiver. High impedance and trans-impedance amplifiers are used typically, the former being simplest to implement. A series resistor is connected to the anode of the photodiode and the high input-impedance amplifier senses the voltage across that resistor, thereby amplifying the low level input current from the photodiode. The trans-impedance amplifier provides current-to-voltage conversion by using a shunt feedback resistor around an inverting amplifier [53, 121].

### 3.2.6 Ambient Light Noise

Generally, the noise components at the VLC receiver are similar to those encountered in most optical communication receivers viz. thermal noise from the load resistor, shot noise from the photodiode and the excess noise from the amplifier [4, 25, 27, 53].

Background radiation impinging on the receiver varies widely depending on factors such as time of day, meteorological conditions, the communication path relative to the sun, receiver FOV and receiver optical parameters e.g. photodiode sensitivity to the wavelengths of sunlight. Direct sunlight may impact system performance to affecting availability and reliability.

Two classes of sunlight impact receiver performance;

- Direct
- Indirect (diffuse)

The level of Shot Noise is highly dependent on the amount of ambient light falling within the receiver FOV and its intensity depends on the class viz. direct or indirect. It is important to characterize the likelihood and the frequency of direct and indirect sunlight to fully determine system performance across many environments [4, 27, 118]. The calculation and modelling of sunlight irradiance is discussed in detail in Section 3.6.

## 3.3 Models

The section presents the relevant models that form the basis of the evaluation of the impact of sunlight on VLC system performance. Models for the physical channel transmission properties in the visible light band, the distribution of the diffuse optical radiation field and the bandwidth limitations imposed by multipath signal dispersion on system SNR/BER are presented.

The key features of a diffuse optical channel are derived from the idealised model [131]. An optical source is assumed to be incident on an arbitrarily shaped surface (Figure 3.2) with radiant emmitance $W$ and the surface is assumed to be an ideal Lambertian reflector. A photodiode with photosensitive area $A_R$ and FOV is then subject to diffusely scattered radiation from surface $A$.

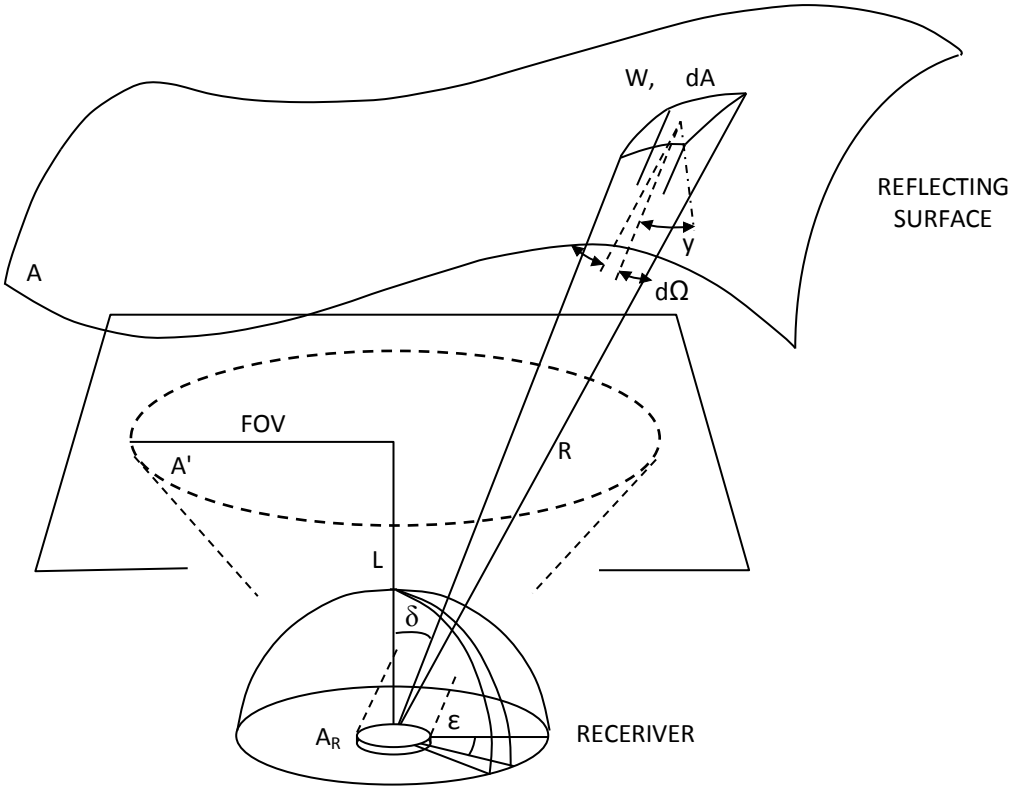


**Figure 3.2: Optical power received from a diffusely reflecting surface [121, 131].**

The optical power incident on the photosensitive area $A_R$ from the surface element $d_A$ is given by [121];

$$dP_R = \frac{1}{\Pi} W \cos\gamma dA d\Omega \tag{3.1}$$

where

$$d\Omega = \frac{1}{R^2} A_R \cos\delta \quad if\ A_R \ll R^2 \tag{3.2}$$

$$dA = \frac{1}{\cos\gamma} R^2 \sin\delta\, d\delta\, \mathrm{d}\epsilon \tag{3.3}$$

where all variables are functions of coordinates δ and $\epsilon$; $R$ is the distance between the receiver and reflectance surface; $d\Omega$ is the spectral angle element and δ is the angle between the incident ray from surface $A$ and the perpendicular on the receiver surface. $A_R$ is the photosensitive area and Assuming a homogeneously illuminated surface $A$ with $W$ a constant, then the total power incident on $A_R$ is obtained by integrating over the entire FOV;

$$P_R = \frac{W}{\Pi} A_R \int_0^{FOV} \int_0^{2\Pi} \sin\delta \cos\delta d\delta d\epsilon \tag{3.4}$$

and

$$P_R = wA_R \sin(FOV)\ 0 < FOV < 90 \tag{3.5}$$

Thus the received optical power $P_R$ is independent of the position of the photo-detector with respect to surface $A$. In the case of an isotropic source located in the centre of the room with a wall $A$, an estimate of the optical power $P_S$ for the source illuminating the room is given by:

$$P_S \cong \frac{AP_{min}}{A_R \rho \sin(FOV)} \tag{3.6}$$

where $P_{min}$is the minimum power required by the receiver and ρ is the reflection coefficient indicating the proportion of diffusively reflected incident radiation [131].

### 3.3.1 Multipath Dispersion

In order to gain an accurate model for multipath dispersion, a plane reflecting surface $\grave{A}$ at distance L from the photodiode (Figure 3.2) at time $t = 0$ is assumed. A Dirac pulse from the source is reflected by surface $\grave{A}$, producing an impulsive with uniform radiant emmitance $W$ over the entire surface. The optical power incident on the photodiode with propagation delay $\tau$ given by Equation (3.1) and expressing $R$ in terms of $\tau$ is;

$$dp_R(\tau) = 2wA_R\tau_o^{\,2}\frac{1}{\tau^3}d\tau, \qquad \tau_o \le \tau \le \frac{\tau_o}{\cos(FOV)} \tag{3.7}$$

where

$$\tau = \frac{L}{c\cos\delta}$$

and

$$\tau_o = \frac{L}{c}$$

$\boldsymbol{c}$ is the speed of light, $\tau_o$ the minimum delay and $dp_R(\tau)$**)** the contribution within the time element $d\tau$ originated from an annular surface element $d\grave{A}$**.** The normalised impulse response $F(\tau)$ is calculated using Equation (3.3) and Equation (3.7);

$$F(\tau) = \frac{dP_R}{P_R d\tau} = \begin{cases} \frac{2\tau_o}{\tau^3 \sin(FOV)}, & \tau_o \le \tau \le \frac{\tau_o}{\cos(FOV)} \\ 0 & elsewhere \end{cases} \quad (3.8)$$

$$F(\tau) = \frac{dP_R}{P_R d\tau} = \begin{cases} \frac{2\tau_o}{\tau^3 \sin(FOV)}, & \tau_o \le \tau \le \frac{\tau_o}{\cos(FOV)} \\ 0, & elsewhere \end{cases}$$

In a diffuse optical channel, the photodiode is exposed to ambient light, introducing additional noise at the receiver [27]. The most commonly encountered ambient light sources are sunlight, tungsten and fluorescent lamps. In general, although a number of significant sources of stationary or slowly fluctuating ambient light generating shot noise can be identified, sunlight represents the major source [1, 4, 27, 132]. Sunlight modelling will be addressed in Section 3.6.

### 3.3.2 Channel DC Gain

The frequency response of VLC transmission channels is relatively flat near DC. For most purposes, the most important quantity characterising a channel is the DC gain, related to the transmitted and received average powers through $P_R = H(0)P_s$, where $P_R$ is the received power, H(0) is the channel DC gain, $P_S$ is the transmitted power and $R_O$ is the transmitter radiant intensity. The DC gain estimate is developed for a common VLC link configuration [133] only considering LOS propagation paths.

For the link geometry considered, assume the transmitter emits an axially symmetric radiation pattern described by the radiant intensity (W/sr). Assuming the signal at the receiver is $P_S R_O(\emptyset)$, located at distance $d$ and angle $\emptyset$ with respect to the transmitter, then the irradiance is given by [131];

$$I_s = (d, \varnothing) = P_s R_o / d^2 \quad (3.8)$$

The received power is given by;

$$P_R = I_S(d,\varnothing)\,A_{eff}(\Psi)$$

and

$$A_{eff}(\Psi) = \begin{cases} AT_S(\Psi)\,g(\Psi)\cos\Psi, & 0 \le \Psi \le \Psi_c \\ 0, & \theta > \Psi_c \end{cases} \qquad (3.9)$$

The channel DC gain is then obtained by:

$$H(0)_{LOS} = \begin{cases} \frac{A}{d^2} R_0(\varnothing) T_s(\Psi)\, g(\Psi), & 0 \le \Psi \le \Psi_c \\ 0, & \theta > \Psi_c \end{cases} \qquad (3.10)$$

where $A_{eff}$ is the effective signal detection area of the detector, $\Psi$ is the angle of incidence with respect to receiver axis, $T_s(\Psi)$ is the signal transmission of the filter, $g(\Psi)$ is the concentrator gain and $\Psi_c$ is the concentrator FOV (semi angle) (n.b. the DC gain is proportional to $d^{-2}$). Since d and $R_O(\emptyset)$ are normally fixed, the most effective means of increasing H(0) are to increase the detector area A, increase the concentrator gain $g(\Psi)$, increase the refractive index n or decrease the FOV ($\Psi_c$).

The emission from a variety of practical LOS transmitters can be modelled reasonably using the generalised Lambertian radiation pattern given by [118, 121];

$$R_0(\varnothing) = \left[(m+1)/2\pi\right] cos^m\varnothing \qquad (3.11)$$

The order m is related to the transmitter semi angle at half power $\emptyset_{1/2}$ by;

$$m = -\ln 2 \,/\, \ln(\cos\varnothing_{1/2}) \qquad (3.12)$$

Thus the channel DC gain is given by:

$$h(0)_{LOS,Gen,Lamb} = \begin{cases} \dfrac{(m+1)A}{2\pi d^2} cos^m \varnothing T_S(\Psi) g(\Psi) \cos\Psi, 0 \le \Psi \le \Psi_c \\ 0, \qquad\qquad \theta > \Psi_c \end{cases} \quad (3.13)$$

The development of an estimate of the DC gain for directed non-LOS propagation paths is carried out with reference to the link geometry in

Figure 3.3. The assumptions are that the transmitter illuminates a small region of the reflector, the channel DC gain depends only on the distance $d_{sr}$, the horizontal distance between the illumination LED and the photodiode and not on the distance between the transmitter and receiver, However, the latter assumption does not affect the accuracy of the model [118, 121].

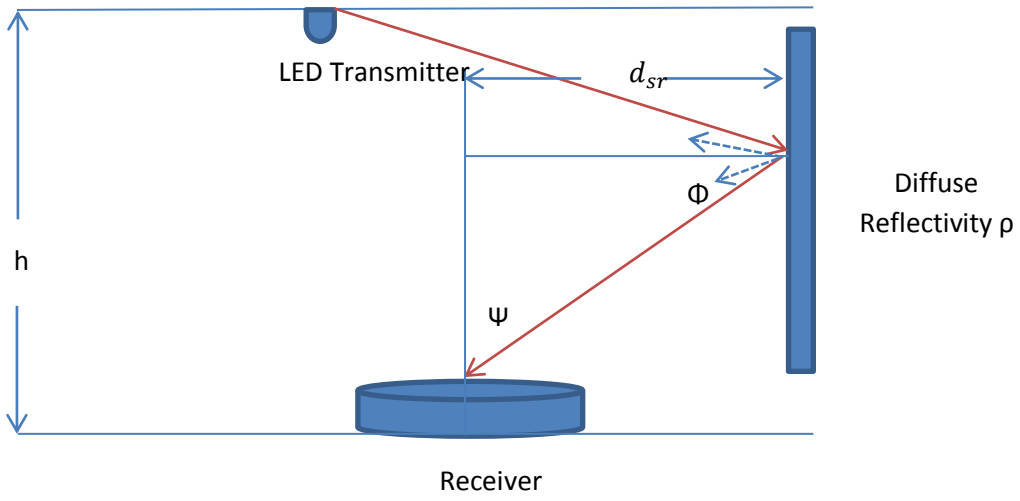


**Figure 3.3: Direct and Non-Line-of-Sight (NLOS) links.**

If the ceiling diffusion reflectivity ρ is located a distance h above the receiver, then the received signal irradiance is given by [134];

$$I_S(d_{sr},h) = \rho h p_s / \pi (h^2 + {d_{sr}}^2)^{3/2} \quad (3.14)$$

the received power is;

$$P = I_S(d_{sr}, h)A_{eff}(\Psi) \tag{3.15}$$

and the channel DC gain is;

$$H(0)_{directed\ non-LOS} = \begin{cases} \dfrac{\rho A h}{\pi\left(h^2 + d^2{}_{sr}\right)^{3/2}} T_S\left(\Psi\right) g\left(\Psi\right)\cos\left(\Psi\right), 0 \le \Psi \le \Psi_c \\ 0, \qquad\qquad \theta > \Psi_c \end{cases} \tag{3.16}$$

where A is the receiver area, $T_S$ is the filter transmission, $\Psi$ is the angle from which rays are received, $g\left(\Psi\right)$ is the concentrator gain and $\Psi_c$ is the concentrator FOV.

### 3.3.3 Signal to Noise Ratio (SNR)

In order to evaluate the system SNR and BER, it is assumed that data using ON-OFF keying (OOK) with NRZ pulses is transmitted at a bit rate $R_b$. The transmitted average power is $P_s$, the received average power is $p_R = H(0)P_S$, where the channel DC gain is as defined in Section 3.3.3. The channel is assumed to be distortion less, has gain H(f) = H(0) for all frequencies, and that the receiver pre-amplifier is followed by an equaliser. Each sample of equaliser output contains Gaussian noise with total variance as [53, 121, 131];

$$\sigma_{total}{}^2 = \sigma_{shot}{}^2 + \sigma_{thermal}{}^2 \tag{3.17}$$

The shot noise is given by;

$$\sigma_{shot}{}^2 = 2qRp_nI_2R_b \tag{3.18}$$

The shot noise owing to sunlight irradiance impinging at the photodetector ($P_n$) is defined in the sunlight irradiance model presented in Section 3.6

The thermal noise variance is given by:

$$\sigma_{thermal}^{\ 2} = \frac{4KT}{R_F} I_2 R_b + \frac{16\pi^2 KT}{g_m}\left(\Gamma + \frac{1}{g_m R_D}\right) C_T^{\ 2} I_3 R_B^{\ 3} + \frac{4\pi^2 K I_D^{\ a} C_T^{\ 2}}{g_m^{\ 2}} I_f R_b^{\ 2} \tag{3.19}$$

In a FET-based trans-impedance pre-amplifier, the total receiver input capacitance is dominated by the detector capacitance (Cd) because of the large detector area required to achieve a high SNR. K is Boltzmann's constant, $C_T$ is the input capacitance, T is absolute temperature (in Kelvin), $R_b$ is the data rate, $R_F$ is feedback resistor, Γ is the FET channel noise factor, $g_m$ is a FET trans-conductance, k and a are the FET $1/f$ noise coefficients, q is the electron charge, R detector responsivity, $I_2$ is the FET parameter, $P_n$ is the sunlight noise power, $I_D$ is the FET drain current and gm is a FET parameter.

Using the calculated received power $P_R$ (Equation (3.10), Equation (3.11), Equation (3.12), Equation (3.13), Equation (3.14) and Equation (3.15)), the SNR is expressed using Equation (3.22), Equation (3.23) and Equation (3.24) as;

$$SNR = \frac{(RP_R)^2}{\sigma_{total}^{\ 2}} \tag{3.20}$$

and the BER by;

$$BER = Q(\sqrt{SNR}) \tag{3.21}$$

where

$$Q(x) = \frac{1}{\sqrt{2\pi}} \int_x^{\infty} e^{-y^2/2} dy \tag{3.22}$$

Equation (3.22) supported by Equation (3.19), Equation (3.20) and Equation (3.21) are integral to the Monte Carlo simulation, the results of the analysis discussed in detail in Chapter 4.

## 3.4 Multiple Reflections and Multipath Dispersion

The optical signal suffers many reflections on the path between transmitter and receiver; thus modelling multi-paths is invaluable in order to better define VLC system performance. Reflections may induce severe attenuation of the received signal and hence degrade the BER below that acceptable to users. The following model therefore estimates multiple reflections up to and including the fifth reflection. Prior studies have shown the accuracy of models considering beyond the fifth reflection have little impact on the accuracy of the analysis [121].

A model based on optical ray tracing for indoor environments is developed to calculate the response after *k*-reflections from the *n*th LED source assuming the path geometry shown in Figure 3.4. The aim is to calculate the impulse response in the case of multiple reflections of optical paths from multiple optical sources.

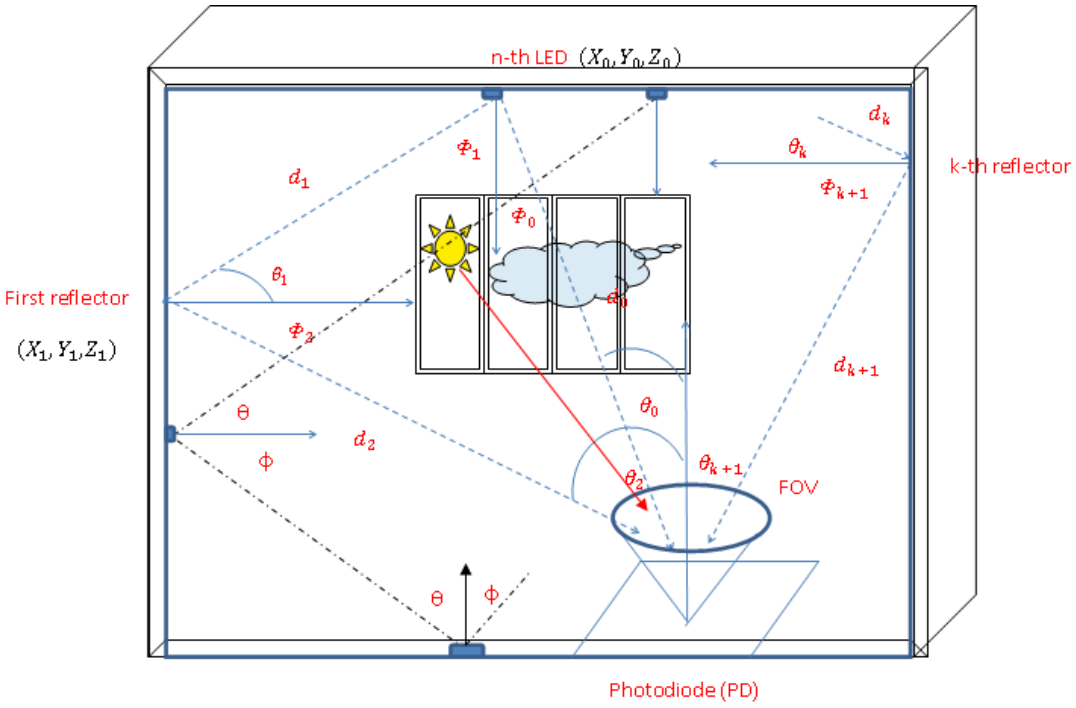


**Figure 3.4: Geometry of the n*th* LED and PD location for multiple reflections.**

The scenario is confined to an empty room; the transmitter is placed on the ceiling whilst the receiver is located on the floor of the room. The transmitter is assumed to emit an axially symmetric radiation pattern described by radiant intensity (W/sr). $P_s R_O(\emptyset)$ is the signal at the receiver, located at distance *d* and angle $\emptyset$ with respect to the transmitter.

To obtain the channel response, the area of reflection of the incident optical ray on a surface is calculated to yield the magnitude of the reflection and the change in direction. The area of the reflection, the incident angle, the reflection angle, the reflection point index, the distance between reflections and the distance between the last reflection and receiver is calculated for each reflection.

The impulse response is thus given by [118];

$$h(t) = \sum_{n=1}^{N_{LED}} \sum_{k=0}^{\infty} h^{(k)}(t; \Phi_n) \tag{3.23}$$

where $N_{LED}$ is the total number of LEDs. The assumption is that each LED transmits an equal power output. The response after *k*-reflections of the *n*-th LED source is then;

$$h^{(k)}(t; \Phi_n) = \int_s \left[ L_1 L_2 \ldots\ldots L_{K+1} \Gamma_n{}^{(k)} rect(\frac{\theta_{k+1}}{FOV}) \times \delta(t - \frac{d_1 + d_2 + \ldots d_{k+1}}{c} \right] dA_{ref}, \; k \geq 1 \tag{3.24}$$

where

$$L_1 = \frac{A_{ref}(m+1)cos^m \Phi_1 cos\theta_1}{2\pi d_1{}^2} \tag{3.25}$$

$$L_2 = \frac{A_{ref} \cos\Phi_2 cos\theta_2}{\pi d_2{}^2} \tag{3.26}$$

$$L_{k+1} = \frac{A_{PD} \cos\Phi_{k+1} \cos\theta_{k+1}}{\pi d_{k+1}{}^2} \tag{3.27}$$

$L_{k+1}$ represents the path-loss terms for each path. The integration in Equation (3.30) is performed with respect to the surface $\mathcal{S}$ of all reflectors, and $\mathcal{A}$ref is the area of the reflecting element. The mode number of a radiation lobe, $m = -1/\log 2\,(\mathrm{Cos}\phi 1/2)$, is a measure of the directivity of the light beam and is related to the viewing angle of an LED as ($2\phi 1/2$).

In order to calculate the reflecting elements and the area of the reflectors, the following ray tracing algorithm is applied up to the fifth reflection.

**In the first reflection;**

$$\theta_1 = 90 - \varphi_1 \tag{3.28}$$

the distance between reflection being;

$$d_1 = {x_1}\Big/{\cos\left(90 - \varphi_1\right)} \tag{3.29}$$

$$y_1 = y_{room} - \left(d_1 \times \sin\left(90 - \varphi_1\right)\right) \tag{3.30}$$

and reflection area radius;

$$R_1 = d_1 \times \tan\left(f\right) \tag{3.31}$$

Thus the reflection area is:

$$A_{ref1} = \pi \times R_1^{\,2} \tag{3.32}$$

where

$\mathrm{y_{room}} = \mathrm{y} - \mathrm{axis\ of\ the\ room}$

$\mathrm{X_{room}} = \mathrm{x} - \mathrm{xis\ of\ the\ room}$

f is the Full Width Half Maximum (FWHM) angle of the light beam, $R_i$ is the radius of the reflecting area, $\mathcal{A}_{refi}$ is the reflecting area and $x_i$ = x-axis of the transmitter.

**Second reflection;**

$$\theta_2 = 90 - \varphi_2 \tag{3.33}$$

$$y_2 = y_{room} - y_1 \tag{3.34}$$

$$d_2 = {y_2}/{\cos(90 - \varphi_2)} \tag{3.35}$$

$$x_2 = d_2 \times \sin(90 - \varphi_2) \tag{3.36}$$

$$\varphi_3 = \theta_2 \tag{3.37}$$

$$R_2 = (d_1 + d_2) \times \tan(f) \tag{3.38}$$

$$A_{ref\,2} = \pi \times R_2^{\,2} \tag{3.39}$$

**Third reflection;**

$$x_3 = x_{room} - x_2 \tag{3.40}$$

$$\theta_3 = 90 - \varphi_2 \tag{3.41}$$

$$d_3 = {x_3}/{\cos(90 - \varphi_3)} \tag{3.42}$$

$$y_3 = d_3 \times \sin(90 - \varphi_3) \tag{3.43}$$

$$\varphi_4 = \theta_3 \tag{3.44}$$

$$R_3 = (d_3 + d_1 + d_2) \times \tan(f) \tag{3.45}$$

$$A_{ref\,3} = \pi \times R_3^{\,2} \tag{3.46}$$

**Fourth reflection;**

$$\theta_4 = 90 - \varphi_4 \tag{3.47}$$

$$y_4 = y_{room} - y_3 \tag{3.48}$$

$$d_4 = {y_4}\Big/{\cos(90 - \varphi_4)} \tag{3.49}$$

$$x_4 = d_4 \sin(90 - \varphi_4) \tag{3.50}$$

$$R_4 = (d_4 + d_3 + d_1 + d_2) \times \tan(f) \tag{3.51}$$

$$A_{ref\,4} = \pi \times R_3^{\,2} \tag{3.52}$$

**Fifth reflection;**

$$x_5 = x_{room} - x_4 \tag{3.53}$$

$$\theta_5 = 90 - \varphi_5 \tag{3.54}$$

$$d_5 = {x_5}\Big/{\cos(90 - \varphi_5)} \tag{3.55}$$

$$y_5 = d_5 \times \sin(90 - \varphi_5) \tag{3.56}$$

$$R_5 = (d_5 + d_4 + d_3 + d_1 + d_2) \times \tan(f) \tag{3.57}$$

$$A_{ref\,5} = \pi \times R_3^{\,2} \tag{3.58}$$

All reflections are obtained by the substitution of Equation (3.34) into Equation (3.64) in Equation (3.30) giving the response after $k$-reflections of the $n$th LED.

The angles of irradiance and incidence are governed by $\phi k$ and $\theta k$ respectively. The received power is inversely proportional to the square of the distance $dk$, the distance

between source and receiver. The photodiode detects light whose angle of incidence is less than field of view (FOV*)* viz. the acceptance angle of the detector. The rectangular function rect(*x*) is given by [118, 121];

$$rect(x) = \begin{cases} 1 & for|x| \le 1 \\ 0 & for|x| > 1 \end{cases} \tag{3.59}$$

*c* is the speed of light. Letting $\Gamma_n^{(k)}$in Equation (3.30) denote the power of the reflected ray after *k*- reflections from the *n*th LED given by;

$$\Gamma_n^{(k)} = \int_{\lambda} \Phi_n(\lambda)\rho_1(\lambda)\rho_2(\lambda)\ldots\ldots\rho_k(\lambda)d\lambda \tag{3.60}$$

The simplified form (lower accuracy) of Equation (3.66) is described by;

$$\overline{\Gamma_n}^{(k)} = P_n\bar{\rho}_{n,1}\bar{\rho}_{n,2}\ldots\ldots\ldots\ldots\bar{\rho}_{n,k} \tag{3.61}$$

where $\bar{\rho}_{n,k} = \frac{1}{P_n}\int_{\lambda}^{??} \Phi_n(\lambda)\rho_k(\lambda)d\lambda$ is the average reflectance and $P_s = \int_{\lambda} \Phi_n(\lambda)d\lambda$ is the radiant power from the *n*th LED source. For k=1, Equation (3.66) and Equation (3.67) have the same value as;

$$\Gamma_n^{(1)} = \bar{\Gamma}_n^{(1)} = \int_{\lambda}^{??} \Phi_n(\lambda)\rho_1(\lambda)d\lambda \tag{3.62}$$

However, the differences become significant as the order of the reflection increases. The channel DC gain for LOS is given as;

$$h^{(0)}(t;\Phi_n) = L_O P_n rect(\frac{\theta_o}{FOV})\delta(t - \frac{d_o}{c}) \tag{3.63}$$

where

$$L_O = \frac{A_R(m+1)cos^m\Phi_o cos\theta_o}{2\pi d_0^{\,2}} \tag{3.64}$$

$A_R$ is the area of the photodiode, m is the mode number of a radiation lobe, $\Phi_o$ is the irradiance angle, $d_0$ is the distance between transmitter and receiver and $\theta_o$ is the incidence angle.

Thus the power level up to and including the fifth reflection of the optical signal is estimated and considered in the system evaluation. To date the impact of multiple reflections up to the fifth reflection on VLC system performance has not been evaluated; most analysis has been restricted to LOS paths only.

## 3.5 System Model Validation

The VLC system was modelled and simulated using a Matlab software package [135]. The validation process was executed by simulating the performance of the system configuration as detailed in [118].

A 5m×5m×3m room with plaster walls and plastic walls was modelled. The otherwise room was equipped with a single transmitter, emitting a 1W power output, located on the ceiling (2.5 m, 2.5 m, 3 m) and directed towards the receiver on floor of the room (0.5 m, 1.0 m, 0 m). The simulation parameters are summarised in Table 3.1.

**Table 3.1 System simulation parameters.**

| System parameter | Value |
|---|---|
| **Photodiode Responsivity** | $0.54\ {}^{A}/_{W}$ |
| **Data rate ($R_b$)** | 100 Kbit/s |
| **photosensitive area( $A_R$)** | 0.5×10-4 |
| **electron charge( q)** | 1.6×10.^-19 |
| **The viewing angle of the LED $\Phi_1$** | 60 degrees |
| **Modulation Type** | ON-OFF keying (OOK) with NRZ pulses |
| **Surface Reflectivity** | ≅ 0.82 |
| **Power Transmitted** | 1W |
| **Photodiode Area** | $1cm^2$ |
| **Filter Transmission** | 0.6 |
| **N filter reflective index** | 1.3 |
| **Receiver Field Of View (FOV)** | 85degrees |
| **Transmitter FWHM Angle** | 9 degrees |

Simulation parameters are selected based on commercially available off-the-shelf components and are the same simulation parameters used in [118] for comparison purposes. Table 3.2 is a summary of a results comparison between the simulation and the reported performance in [118]. The results at the first three reflections agreed well - ∼94- ∼97 % and ∼95%-∼97% - with the results reported in [118] for plastic and plaster walls respectively.

**Table 3.2: A comparison of results; simulation and the results reported in [118].**

| Reflection Number | Received power (Model under test) (μw) | | Received power (Reference model [118]) (μw) | |
|---|---|---|---|---|
| | **Plaster wall** | **Plastic wall** | **Plaster wall** | **Plastic wall** |
| k=1 | 0.43 | 0.059 | 0.467 | 0.063 |
| k=2 | 0.201 | 0.0135 | 0.221 | 0.015 |
| k=3 | 0.098 | 0.00287 | 0.107 | 0.003 |
| Line-of -Sight (LOS) component | 1.29 | | 1.232 | |

Furthermore the system model was tested within large room sizes and different configurations to provide further validation. The performance of the system was evaluated for a (15 m × 15 m × 3 m) room with the 1W transmitter positioned on the ceiling and the receiver on the floor and a range of surfaces reflectivities were considered.

The room is assumed to be empty and unfurnished and diffusely reflected light form plastic walls, plaster walls, floors and ceiling are considered. The room is equipped with five identical transmitters at different locations and the assumption is that all transmit at the same data rate in phase. Performance up to the fifth reflection was evaluated and the results are summarized in Table 3.3.

**Table 3.3: Reflections for a single source in a 15m×15m×3m room.**

| Surface / Reflection | Plaster Wall (W) | Floor (W) | Ceiling (W) | Plastic Wall (W) | Time Delay (S) |
|---|---|---|---|---|---|
| **First Reflection** | 0.0014 | 0.0011 | 7.5239 e-004 | 1.7914e-004 | 3.000e-008 |
| **Second Reflection** | 3.6878 e-006 | 2.8581e-006 | 1.9361 e-006 | 4.6098e-007 | 6.000e-008 |
| **Third Reflection** | 9.8873 e-010 | 7.6626e-010 | 5.1908 e-010 | 1.2359e-010 | 1.300e-007 |
| **Fourth Reflection** | 4.7477 e-012 | 3.6795e-012 | 2.4925 e-012 | 5.9346e-013 | 1.500e-007 |
| **Fifth Reflection** | 1.4578 e-015 | 1.1298e-015 | 7.6537 e-016 | 1.8223e-016 | 2.300e-007 |
| Transmitter location (10,15,3) | | | | | |
| Receiver location (8,8,0) | | | | | |
| Line of sight component = 0.0022 W | | | | | |

The results of the system model for this room size are in good agreement with those reported in [118] for the same simulation parameters. The results validate that the model can be applied to various scenarios and system configurations.

Four LED panels are installed in 5m×5m×3m room, each panel containing100 LED chips and each LED emitting an optical power of 0.45 W. The photodiode receiver was placed at the horizontal surface at height 0.85 m. LED panels were placed on the ceiling and the photodiode has 0.54 A/W Responsivity and 500 kbit/s data rate. The analysis estimated the average system SNR for a winter day, overcast sky when the sunlight irradiance varies between 900-2000 Lx in a room with consideration of the LOS and Non-LOS components up to the fifth reflection.

An empty 5m×5m×3m room is assumed with all room surfaces being plaster (0.82 reflectivity) and plastic walls (0.2 reflectivity). The SNR evaluation was conducted for NLOS components up to the fifth reflection. It was found that the fifth reflection only become significant when the room wall is made of high reflectivity surfaces such as plaster; the SNR was 89 dB, 18.4 dB, 12.7 dB at the first, fourth, and the fifth reflections respectively (Figure 3.5).

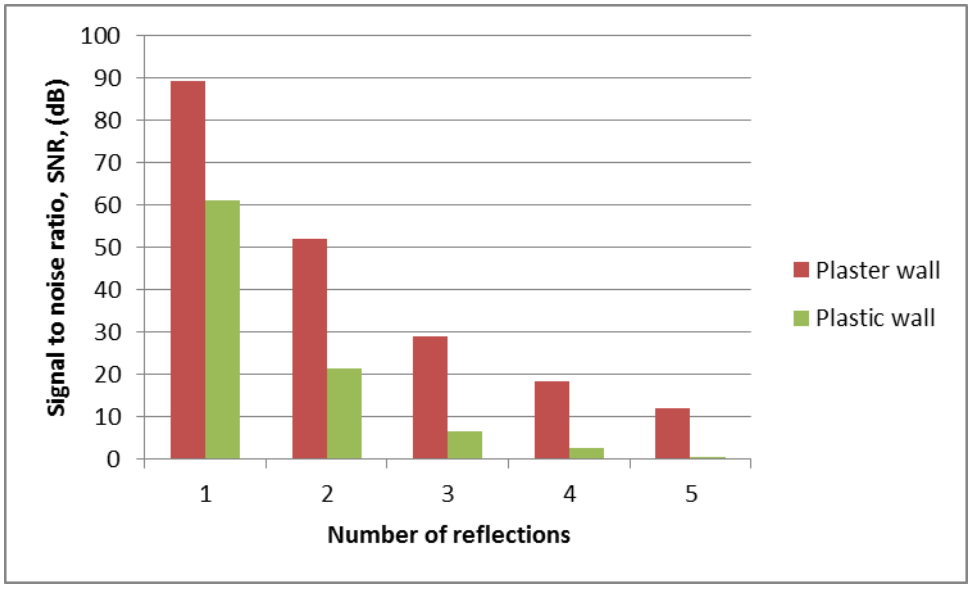


**Figure 3.5: SNR at different reflections.**

However the SNR degraded greatly for plastic walls due to low surface reflectivity; the SNR was 61 dB, 21.3 dB, 2.65 dB, 0.52 dB at the first, second, fourth and fifth reflection respectively. NLOS components can provide an enhancement in system performance especially in the mitigation of the impact of shadowing [67] and the fifth reflection components have significance in environments with high surface

reflectivity. Consideration up to the second reflection is adequate in environments with poor surface reflectivity.

In order to provide further validation of the model under evaluation, different deployment scenarios were considered. The simulation parameters and criteria of [136] are input to the model under evaluation for comparison purposes. Three empty rooms of different shapes and sizes were considered. Transmitters were placed on the ceiling at different positions and receivers were placed at the floor at different locations (Table 3.4). All walls were assumed to have the same surface reflectivity of 0.8. The Cree Xlamp® MC-E Color (RGBW) LED [137] with Lambertian distribution and a viewing angle of 110° is assumed.

**Table 3.4: Simulation parameters - time delay**

| Configuration | Room size ($m^3$) | Position of transmitter (m) | Position of receiver (m) | Surface reflectivity |
|---|---|---|---|---|
| A | 5×5×3 | (0,0,3) | (2.3,2.3,0) | 0.8 |
| B | 9×9×3 | (0,0,3) | (2.3,2.3,0) | 0.8 |
| C | 13×13×5 | (0,0,5) | (2.3,2.3,0) | 0.8 |

Time dispersion parameters for the power delay profile of the VLC channel have been evaluated through simulation for three system configurations (Table 3.5). A comparison of the mean excess delay ($T_o$) and RMS delay spread ($T_{rms}$) for the different configurations was conducted. A comparison of results arising from the model under evaluation and results of [136] is summarised in Table 3.5.

**Table 3.5: A comparison of time dispersion results.**

| Configuration | Reference Model[136] | | Model under Evaluation | |
|---|---|---|---|---|
| | Mean excess delay (ns) | RMS delay spread (ns) | Mean excess delay (ns) | RMS delay spread (ns) |
| A | 36.6 | 15.98 | 37.42 | 16.347 |
| B | 57.06 | 19.028 | 58.4413 | 19.469 |
| C | 95.57 | 28.598 | 98.526 | 29.09 |

Results of the model under evaluation show good agreement with the reference research results of [136] viz. ~94 % to~ 96%. As the room dimension increases, the mean excess delay and RMS delay spread values increase as the light ray traverses longer distances and the power at the receiver decreases due to higher path losses.

## 3.6. Sunlight Irradiance

The location of the VLC deployment is a key factor in the performance of the system. Sunlight irradiance varies throughout the regions of the world and may compromise system SNR which in turn sets limits to the range of viable applications (Figure 3.6).

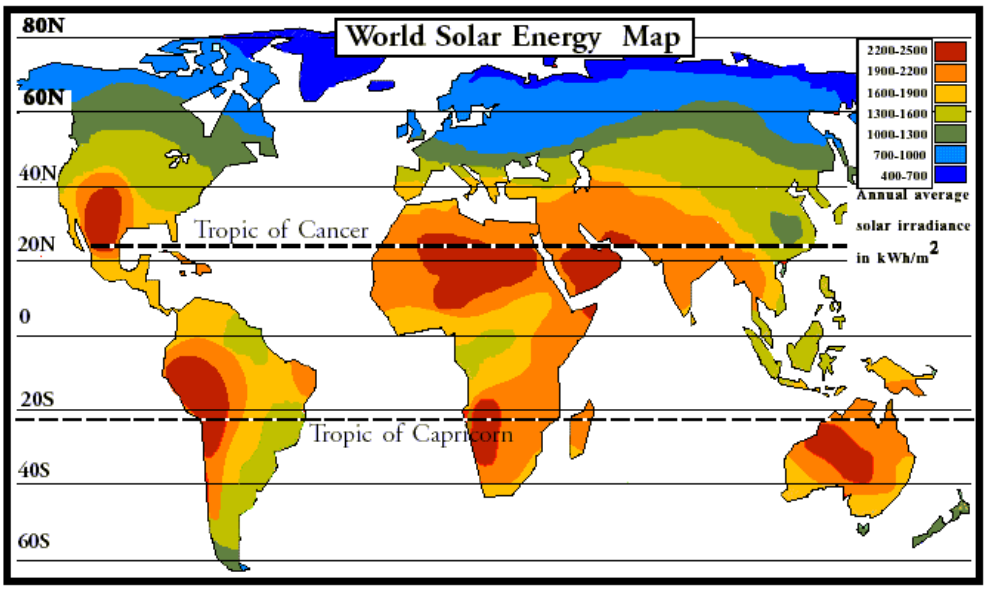


**Figure 3.6: Solar radiation levels by regions of the world [138].**

The empirical approach to determining sunlight irradiance is to install measurement devices such as the pyrometer [139] at particular locations to monitor and record levels on an hourly basis. However the cost of this approach is prohibitive in terms of resources and the captured data is relevant only to specific locations. Although sunlight irradiance is an important economic and social factor for many developing and developed countries, nevertheless the cost of implementing this approach remains a major barrier. Hence, a number of models have been developed to

accurately estimate sunlight irradiance over the world based on the available metrological data generated at already deployed stations.

### 3.6.1. Sunlight Irradiance; Empirical Model Factors

There are therefore a number of models available to estimate the sunlight irradiance and a number of correlations exist between them which make the selection difficult.

Many correlations have been developed to determine the relationship between sunlight irradiance and metrological parameters [140, 141]. Empirical models are selected for implementation according to the availability of input metrological parameters; empirical models can be classified into four categories based on metrological parameters as shown in Figure 3.7.

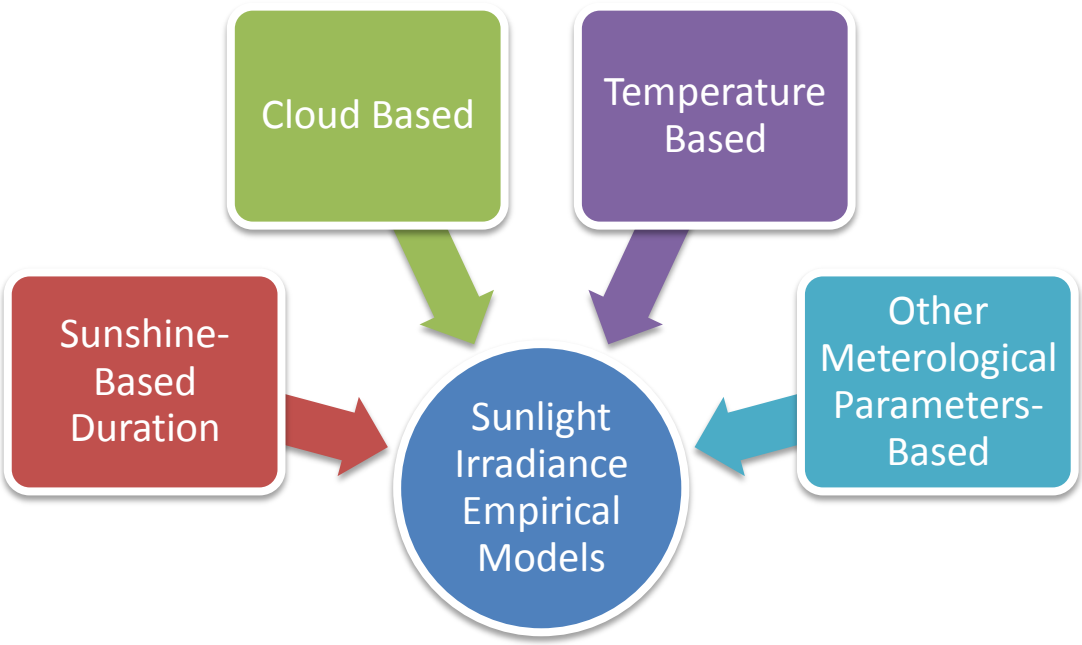


**Figure 3.7: Classification of sunlight irradiance models.**

The range of models that have been developed are thus most readily classified by factors applied to estimate sunlight irradiance [28, 139, 142];

- **Astronomical**; use the solar constant, earth-sun distance, solar declination and hour angle to estimate sunlight irradiance on a horizontal surface

- **Geometrical**; use the azimuth angle of the surface, tilt angle of the surface, sun elevation angle and sun azimuth angle to estimate sunlight irradiance on a horizontal surface on an average daily basis

- **Geographical;** use the latitude, longitude and elevation of the location to estimate sunlight irradiance on a horizontal surface

- **Physical;** the scattering of air molecules, water vapour content, scattering of duct and other atmospheric constituents such as $O_2$, $N_2$ and $CO_2$

- **Meteorological**; extra-terrestrial solar radiation, sunshine duration, temperature, precipitation, relative humidity, effect of cloudiness, soil temperature and evaporation are used for the sunlight irradiance model.

### 3.6.1.1 Sunshine Based Model

The sunshine model is used widely as it is based on sunshine duration which is easily measureable in a reliable way [139].

#### 3.6.1.1.1 Angstrom-Prescott Model

The Angstrom model is most widely used in determining sunlight estimation [143]. Angstrom derived the linear relationship between the ratio of the average daily global radiation to a corresponding value for a completely clear sky. Prescott modified Angstrom's method by basing it on the level of extraterrestrial radiation on a horizontal surface rather than clear sky radiation [144];

$$\frac{H}{H_0} = a + b\left(\frac{s}{s_0}\right) \tag{3.65}$$

H is the monthly average global radiation on a horizontal surface, Ho is the monthly average daily radiation, S is the daily sunshine hours, $S_0$ is the maximum possible monthly average daily sunshine hours and a and b are constants.

The value of the monthly average daily extra-terrestrial radiation can be calculated by;

$$H_O\left(\frac{Wh}{m^2 day}\right) = \frac{24}{\pi} I_{SC}\left[1 + 0.033\cos\left(\frac{360 n_{day}}{365}\right)\right]\left[\cos\varphi\cos\delta\sin\omega_s + \frac{\pi}{180}\omega_s\sin\varphi\sin\delta\right] \tag{3.66}$$

where $I_{SC}$ is the solar constant, $\varphi$ is the latitude of the location under consideration, $\omega_s$ is the sunset hour angle in degrees, $n_{day}$ is the day of the year and $\delta$ is the declination angle.

Glower and McCulloch [142, 145] developed the Angstrom-Prescott model further to consider the effect of latitude of the location as an additional input;

$$\frac{H}{H_o} = a\cos\varphi + b\left(\frac{s}{S_o}\right) \tag{3.67}$$

$$\frac{H}{H_0} = 0.29\cos\varphi + 0.52\left(\frac{S}{S_0}\right) \tag{3.68}$$

provided the coefficients derived from the Angstrom Prescott model can be applied at any location in the world to yield the sunlight irradiance for that location;

$$\frac{H}{H_O} = 0.23 + 0.48\left(\frac{S}{S_0}\right) \tag{3.69}$$

A number of models have been proposed which are correlations of the regression coefficients of the Angstrom-Prescott model based on the specific location and climate zone [145-151].

### 3.6.1.2. Cloud-Based Model

Any model that estimates the level of sunlight irradiance must take into account clouds as a factor. A number of models have been reported that estimate sunlight irradiance considering the prevailing cloud conditions [142]. The model developed by Paltridge *et al* [152] is particularly relevant defining the sunlight irradiance at any location based on the solar zenith angle ($\theta$), length of day ($S_0$) and Cloud Factor (CF) [153]. The model assumes that the regional albedo, atmospheric water vapour and aerosol optical air mass are negligible values and are thus neglected.

The hourly beam radiation ($I_b$) and diffuse radiation($I_d$) in ($MJ/m^2h$) are determined by;

$$I_b = 3.42286\left(1 - e^{0.075(90-\theta)}\right) \tag{3.70}$$

$$I_d = 0.00913 + 0.0125(90 - \theta) + 0.723CF \tag{3.71}$$

and

$$H = (1 - CF)\int_{sunrise}^{sunset} I_b(\theta)\cos\theta dt + \int_{sunrise}^{sunset} I_d(\theta)dt \tag{3.72}$$

where $I_b$ is the hourly beam radiation, $I_d$ is the diffuse radiation, CF is the Cloud Factor and $\theta$ the solar zenith angle.

The Cloud Factor (CF) [142] varies from zero (clear sky) to one (overcast sky). Cloud cover is observed every three hours in ranges from (0-2) octas, (3-6) octas and (7-8) octas where octas is a unit used in meteorology to measure cloud cover, equivalent to a *cloud* cover of one eighth of the sky [154]. The *CF* is obtained from the cloud cover by;

$$CF = \frac{n_1 + 4.5 \times n_2 + 7.5 n_3}{8 \times (n_1 + n_2 + n_3)} \tag{3.73}$$

where $n_1$, $n_2$ and $n_3$ are the total number of days in each month from zero to 2/8, 3/8, 6/8 and 7/8 to 8/8 octas respectively [152, 155-157].

### 3.6.1.3. Temperature Based Models

Data on cloud coverage are not available in all locations. Thus a number of solar radiation models based on the maximum and minimum air temperature have been developed; however there are other factors that affect air temperature such as humidity, latitude, elevation and topography e.g. large area of water. These factors influence model estimates especially from the photovoltaic aspects [142, 158, 159].

However, some of those factors are not available for developing countries, making the selection of this type of model for VLC system evaluation restrictive. The sunshine based models (Angstrom-Prescott) are preferred where input data do not exist or are difficult to obtain.

### 3.6.1.4 Other Meteorological Parameters Based Models

An accurate representation of the value of solar radiation for a given location requires consistent metrological data not readily available in all geographies. Nevertheless, many researchers have attempted to harness a range of available metrological data such as relative humidity, soil temperature and evaporation. These models were developed using multiple regression methods which consume significant computational resources and their estimates are only valid for specific locations [142, 160].

### 3.6.2. Sunlight Irradiance Model

Based on the review of the sunlight irradiance models, the Angstrom-Prescott formulation is deemed the most appropriate in the goal of evaluating the impact of noise owing to sunlight on the performance of VLC systems. Model extensions [142, 160] enhance the granularity of the evaluation through estimating the hourly sunlight irradiance for any location as a function of longitude, latitude, day and time of the year. The model is proven to provide more accurate data for any location worldwide compared to other reported models. Furthermore, the model is based on existing data for many locations especially in the developing world; most of these countries enjoy clear skies with high levels of sunlight irradiance throughout the year. The model requires less computational resources for processing in contrast to many other models which require long term data analysis and significant resources for the continual acquisition and processing of data whilst ultimately yielding less accurate estimations.

VLC systems are impacted by irradiance over the day, varying from sunrise to sunset. Incident solar radiation is a function of several variables including the time of day, the day of the year, geographic location and atmospheric conditions. Direct solar radiation, $q_{sun}$ could be measured at the proposed locations. However in the absence of accurate measurements, the sunlight irradiance can be calculated from the approximation of clear sky solar radiation on a horizontal surface (in W/m$^2$) as [28, 139];

$$q_{sun}^{\backslash} = 1350.3\left[1+0.033\cos\left(\frac{360n_{day}}{365}\right)\right]\left[\sin\phi\sin\delta+\cos\phi\cos\delta\cos\omega\right] \qquad (3.74)$$

where Φ is the latitude of the location in degrees, defined as the angular location north or south of the equator (-90 °≤ $\Phi$≤ 90°, $\Phi$ > 0 for north), $n_{day}$ is the number of the day of the year, δ is the declination of the sun in degrees, defined as the angular position of the sun at solar noon with respect to the plane of the equator (-

$23.45° \leq \delta \leq 23.45°$, $\delta>0$ for north) and $\omega$ is the solar hour angle in degrees, defined as the angular displacement of the sun east or west of the local meridian due to the rotation of the earth on its axis at 15°/hour, negative before and positive after the solar noon. The direct solar radiation falling within the receiver FOV and contributing shot noise that impacts the SNR is calculated using Equation (3.20), Equation (3.21) and Equation (3.22). The main source of Pn in Equation (3.20) is the direct solar radiation (Equation (3.76)) which varies resulting in a variation of the level of shot noise and hence the SNR.

Two corrections in time are used to convert from a local clock time into the Apparent Solar Time (AST) [139]. The first takes into consideration the variation in the earth's rate of rotation; the second is an adjustment for the difference in local longitude and the standard meridian for the local time zone [28, 139].

The declination, in degrees, is;

$$\delta = 23.45 \sin\left[360\left(\frac{284+n_{day}}{365}\right)\right] \tag{3.81}$$

where $n_{day}$ is the day of the year.

The angular displacement of the sun, east or west of the local meridian due to the earth's rotation (afternoon positive) is the Angle Hour (AH). The AH, in degrees, is;

$$\omega = 15(12 - AST) \tag{3.82}$$

The AST, related to the Local Standard Time (LST), is given in minutes from midnight by;

$$AST = LST + E \pm 4(\eta - \psi) \tag{3.83}$$

where, $\eta$ is the Standard Meridian for the local time zone in degrees west of the Greenwich meridian, $\psi$ is the local longitude in degrees east or west of the Greenwich meridian, E is the equation of time, which can be calculated for the day of the year ($n_{day}$) and divided into four main periods. The positive sign signifies west and the negative sign east of the Greenwich meridian (zero longitude) [28, 139];

Between 1st January and 15th April, (1<= $n_{day}$ <=105);

$$E = -14.2\sin\left[0.028303\left(n_{day}+7\right)\right] \tag{3.84}$$

Between 16th April and 15th June, (106<= $n_{day}$ <=165);

$$E = 4\sin\left[0.053247\left(n_{day}-106\right)\right] \tag{3.85}$$

Between 16th June and 31st August, (166 <= $n_{day}$ <= 245);

$$E = -6.5\sin\left[0.03927\left(n_{day}-166\right)\right] \tag{3.86}$$

Between 1st September and 31st December, (246 <= $n_{day}$ <= 365);

$$E = 16.4\sin\left[0.027802\left(n_{day}-246\right)\right] \tag{3.87}$$

The above formulation is used to calculate the hourly solar radiation for two locations viz. Egypt and Scotland; the cities of Cairo and Glasgow are selected to represent two contrasting meteorological environments. Cairo enjoys clear skies for most of the year and the sunlight irradiance is high whilst Glasgow suffers from cloudy conditions for most of the year and thus is characterised by a low level of sunlight irradiance. Comparison of the impact of sunlight irradiance over the year is estimated using a Matlab software package for these two widely different weather conditions.

## 3.7. Conclusions

A review of potential mathematical models for VLC system design and evaluation comprising multiple sources and multiple reflections has been presented. Table 3.6 provides a high level comparison of VLC models.

**Table 3.6: A comparison of VLC mathematical models.**

| Model / Criteria | Selected | Kwon Hyung ([118]) | Kaiyum [132] |
|---|---|---|---|
| **Model Outputs** | LOS and diffuse components | LOS and a few diffuse components | LOS only |
| **Number of Reflections** | Up to the fifth reflection | Few Reflections | None |
| **Noise Sources** | Accurate modelling of sunlight irradiance over the year | Additive White Gaussian noise | Additive White Gaussian noise |
| **Application** | Applied in any location in the world | Applied in any location in the world | Applied in any location in the world |

The selected model treats both LOS and NLOS components in the evaluation of VLC system performance while most others are confined to only LOS components, thus reducing the accuracy of the estimation. The model also takes into account up to fifth reflection, not been considered before in other models (Table 3.4) and has been validated through a comparison with an established set of results reported in the literature.

In addition, the model provides an evaluation of the impact of sunlight irradiance. While others treat this source of noise as Additive White Gaussian (AWG), the model utilised here provides results under different meteorological environments and geographies. Sunlight irradiance has been modelled by a number of researchers; a comparison of the sunlight irradiance models is summarised in Table 3.7.

**Table 3.7: A comparison of sunlight irradiance models.**

| Model / Criteria | Sunshine | Cloud-Based | Temperature | Other Meteorological Parameters |
|---|---|---|---|---|
| **Input data** | Sunshine duration, latitude and longitude of the location | Solar zenith angle ($\theta$) , length of day ($S_0$) and Cloud Factor (CF) | The maximum and minimum air temperature, cloudiness, humidity, latitude, elevation and topography | Relative humidity, soil temperature and evaporation |
| **Accuracy** | High | Medium | Low | High |
| **Computational Resources** | Medium | High | High | High |
| **Availability of Input Data** | Easily available at any location | Available | Not for developing world | Not for developing world |
| **Application** | Any location | Specific locations | Specific locations | Specific locations |

The sunshine duration model developed by Angstrom-Prescott has been chosen for modeling the impact of sunlight irradiance in system evaluation. The Angstrom-Prescott Model uses data which can be easily obtained in any location throughout the world to provide an accurate estimation for the local hourly sunlight irradiance. Moreover, the Angstrom-Prescott Model can be applied in the developing world and consumes less computational resources. The model includes the effect of the cloud coverage on the level of sunlight irradiance.

# Chapter 4

# VLC System Performance in the Presence of Sunlight Irradiance

## 4.1 Introduction

Major global concerns on continually escalating energy consumption and the level of greenhouse gas emissions are driving the phasing out of incandescent sources thereby stimulating the rapid growth in the deployment of solid-state sources [25, 40]. In parallel, Visible Light Communication (VLC) overlays are being developed to harness these widespread LEDs deployments for data communication purposes. VLC has the potential to provide license free high data rates at relatively low power consumption, especially in environments where issues with RF interference are a fundamental barrier.

The performance of VLC systems has been evaluated extensively but without rigorous consideration of the impairments owing to natural light [40, 118, 161, 162]. In reported research, natural light has been treated as Additive Gaussian White noise; this research takes into consideration the variation of natural light intensity over the year under different metrological conditions.

The performance of VLC in the presence of sunlight is presented. A brief introduction on the treatment of sunlight irradiance is given along with the sunlight spectrum and the manner it impacts on VLC system performance, complementary to the background detailed in Chapter 2. Clear sky sunlight irradiance is estimated on an hourly basis in order to fully characterise system behaviour under different environmental conditions. The understanding of the impact of sunlight irradiance is further enhanced through consideration of cloud coverage throughout the year. The Chapter ends with conclusions on the evaluation of system performance from the perspective of future system design and implementation.

## 4.2 System Evaluation Framework

Inspection of the sunlight spectrum (Figure 4.1) clearly shows that the visible light frequency band - the VLC system band of operation - occupies ~47% of the overall spectrum. This segment of the sunlight irradiance spectrum is a source of shot noise at the receiver, further impairing system performance. Research [1, 25, 50, 56, 118] to date has treated this noise as Gaussian with no accurate estimate of the level of irradiance at the receiver as a function of a number of factors such as location and hour of the day.

The sunlight irradiance originating from windows and doors impinging on the receiver located in the room is a function of the size of the window. The window size is one of the main factors in its architecture design with regulations stipulating that the total area of window space shall be not less than 10% of the total room area [163]. The sunlight irradiance is a function of the location, day of the year, time of the day and metrological conditions; so changes in any of the parameters will affect the sunlight irradiance impinging the receiver and hence the SNR performance.

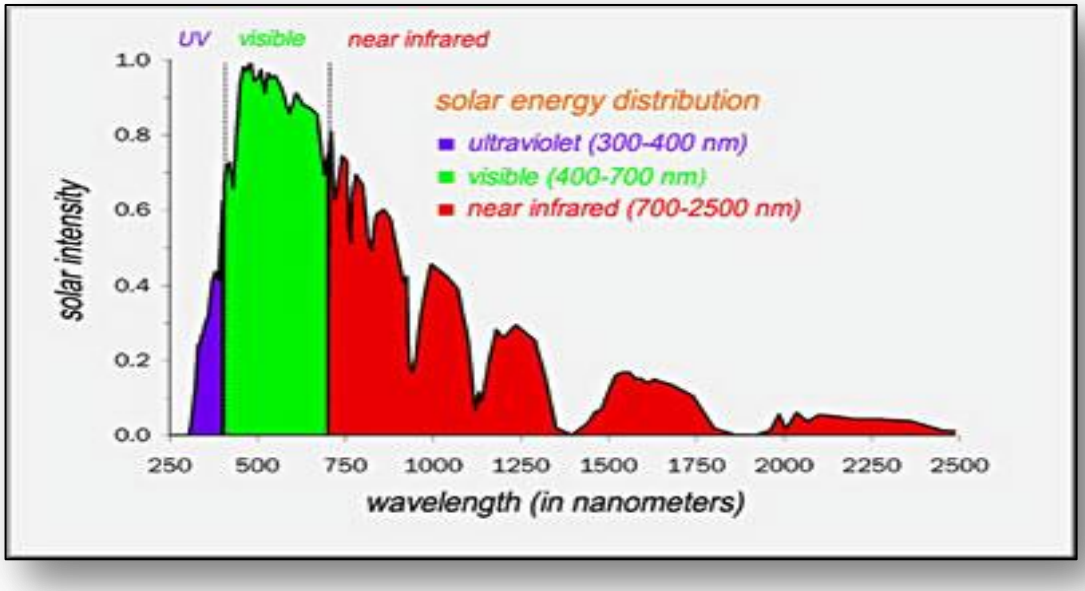


**Figure 4.2: The sunlight spectrum [28].**

The characterization of VLC system performance is executed by segmenting natural light into five main categories and the concomitant system performance is evaluated

for each category as a function of metrological conditions. The categories are mapped based on empirical measurements [161]; clear night with full moon, summer day with clear sky, summer day with overcast sky, winter day with clear sky and winter day with overcast sky. Two representative locations characteristic of different meteorological conditions are selected for the evaluation under the clear sky environment, segmented into hourly levels of sunlight irradiance. The evaluation finishes with a determination of the impact of cloud coverage on the sunlight irradiance over the year for extreme cloud cover conditions.

### 4.2.1 Research Methodology

The goal of the research is to provide a deeper understanding on the performance of VLC systems in order to inform the design and planning of deployments. The output is system design guidelines in the presence of the sunlight as a function of different environmental conditions. The evaluation is referenced through comparison with research reported in the literature. The review of the state-of-the-art serves a number of purposes, the most important being highlighting the gaps in previous research and the importance of the sunlight irradiance on system performance.

#### 4.2.1.1 Evaluation Methodology

In order to provide a meaningful evaluation of system performance, a number of representative system operational scenarios are considered. Analytical methods are a proven approach to providing valuable insights but in cases where the number of scenarios is widespread, it is prohibitively challenging to develop an analytical framework able to treat all scenarios [164, 165].

The alternative is evaluation through simulation. A number of simulation approaches are commonplace but here, Monte Carlo is adopted since it has been proven to be the most efficient and commonly used for the evaluation of communication systems [166, 167]. The methodology provides the chronological behaviour of each system component taking into account all possible operational scenarios. Monte Carlo simulations are characterised by a long simulation time to convergence compared to

analytical methods owing to the large number of operational scenarios considered in the system evaluation.

Thus a combination of Monte Carlo simulation with Matlab software is used in the performance evaluation. Other available software [168] does not offer the flexibility and scope to yield an extensive range of analysis. Since Monte Carlo simulation consumes significant computational resources, a high performance computer facility [169] has been harnessed to provide evaluation for such complex system scenarios.

A number of key assumptions are adopted in the evaluation;

- Empty, unfurnished room; system performance is evaluated for an empty, unfurnished room for different surface reflectivities, room sizes, location and room shapes. Shadowing and blockage due to (say) furniture in the room has not been considered due to time limitations. Shadowing has been investigated [67, 170] and Multi-Input Multi-Output (MIMO) techniques[62] have been proven to provide an acceptable solution to this challenge (Chapter 2)
- Receiver located on the floor of the room; the receiver is assumed to be on the floor of the room for most evaluation scenarios
- Lambertian reflectors; all surface reflections are treated as purely Lambertian. The radiation intensity pattern emitted by a Lambertian reflector is dependent on the incident angle. Many sources of reflections within the indoor environment such as plaster walls, acoustic-tiled walls, carpets and unvarnished wood are approximated well as Lambertian reflectors [42]

#### 4.2.1.4 Research Scope

In order to provide the full spectrum of the impact of natural light on system performance, the research examines its impact in different locations (meteorological environments); Glasgow (Scotland), Cairo, (Egypt) and Berlin (Germany). In summary the scope of the evaluation are as follows;

- considering the LOS and NLOS components up to the fifth reflection
- impact of the natural light on system performance in the presence of sunlight for clear and cloudy skies
- optimisation of LED layout design to mitigate the impact of sunlight
- optimisation of system performance with a minimum number of transmitter LEDs to limit power consumption whilst maintaining the luminance level dictated by standards [100]
- investigation of illumination 'off' mode to determine the trade-off between system performance and power consumption

### 4.2.2 System under Evaluation

A schematic diagram of the VLC system under evaluation is depicted in Figure 4.2. A stream of data is generated from source and is input with brightness control (discussed in Section 3.2.3) to modulate LEDs through the drive current (Chapter 3) [171]. Light rays are subject to many reflections in the path from the LED to receiver and the optical concentrator collects rays impinging from different directions. An optical filter rejects the energy from fluorescent lights around the receiver location. The received signal is amplified and data are recovered. The simulation considers the impact of the physical link. All system parameters are selected from off-the-shelf commercial components and are listed in Table 4.2.

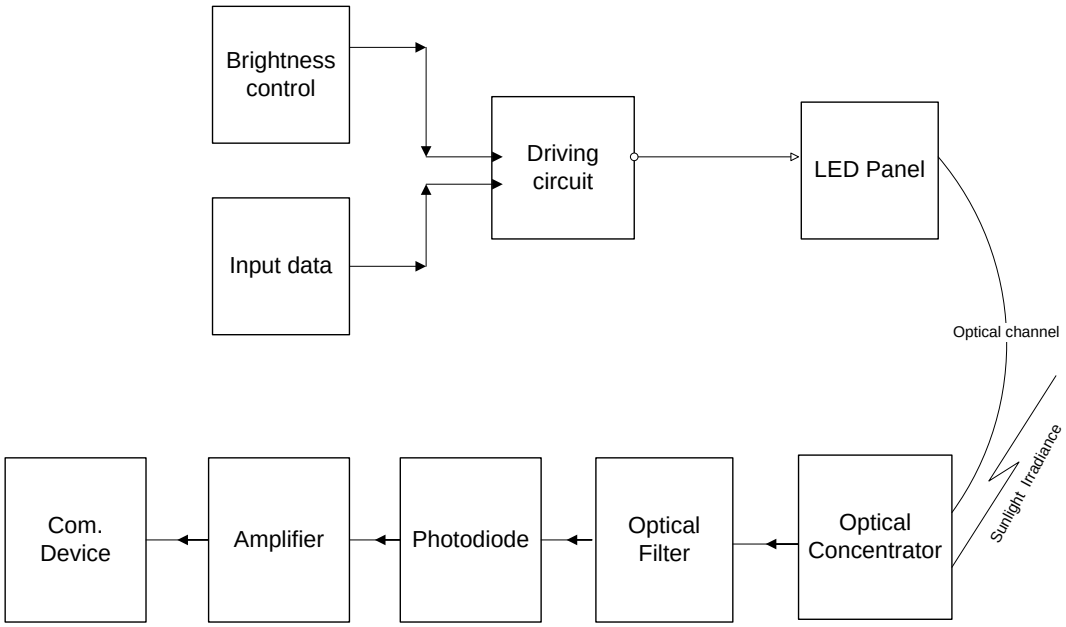


**Figure 4.2: Schematic diagram of the system under evaluation.**

## 4.3 Natural Light

Two classes of natural light impact system performance: direct and indirect and both vary as a function of cloud cover over a particular location [172]. Shot Noise is dependent on the sunlight level captured within the receiver FOV, its intensity dependent on whether it is direct, indirect or reflected. Thus core to the evaluation is the characterisation of the likelihood and the frequency of direct against indirect sunlight impinging on the receiver [120, 172].

According to [25, 161], natural light can be categorised in five main categories defined by the level of irradiance;

- clear night with full moon
- summer day with clear sky
- summer day with overcast sky
- winter day with clear sky
- winter day with overcast sky

These categories are characterised using a cosine corrected light sensor [25, 161] which captures irradiance levels through a 180 degrees hemisphere (Table 4.1).

**Table 4.1: Classes of natural light [161].**

| Natural Light Class | Intensity (lx) |
|---|---|
| **Clear night, full moon** | 0.3 |
| **Winter day, overcast sky** | 900-2000 |
| **Summer day, overcast sky** | 4000-20000 |
| **Winter day, clear sky** | up to 9000 |
| **Summer day, clear sky** | up to 100,000 |

According to [161, 172], no fixed conversion factors exist to convert light intensity from lx [161] to W/m$^2$. For the evaluation, lx is converted to watts/m$^2$ for day light by multiplying with 0.00402, only appropriate for the visible light band of interest [25].

### 4.3.1 System Performance Analysis; Natural Light

The estimation of the SNR and concomitant BER is carried out for a system where the transmitter is assumed to be mounted on the ceiling and the receiver on the floor in an empty room of 15m×15m×3m size. The transmitter sends data at a bit rate $R_b$ using ON-OFF keying (OOK) with NRZ pulses. The transmitted average power is $P_t$, the received average power is $p = H(0)P_t$, where the channel DC gain is determined as detailed in Chapter 3.

Shadowing and blocking occurs in real life scenarios within (say) the office due furniture and people. Shadowing and blocking due to a human body near the receiver (LOS paths) has been investigated [170]; network cell design [173] and MIMO

techniques [66, 67] mitigate the effect. Additionally NLOS components can also be affected by a human body (~1.8 m tall) near the receiver (50 cm) and may increase channel path loss by as much as 5dB [170]. However, a relatively wide incident angle can mitigate its impact but at the expenses of ISI which in turn can be corrected through equalisation [42] and use of Time Division Multiple Access (TDMA) [41].

The channel is assumed to be distortion free with gain H(f) = H(0) at all frequencies. The receiver pre-amplifier is followed by an equalizer. Each sample of the equaliser output contains noise with a total variance given by [2,[53, 121, 131];

$$\sigma_{total}{}^2 = \sigma_{shot}{}^2 + \sigma_{thermal}{}^2 \tag{4.1}$$

The shot noise is;

$$\sigma_{shot}{}^2 = 2qRp_nI_2R_b \tag{4.2}$$

while the thermal noise variance is given by;

$$\sigma_{thermal}{}^2 = \frac{4KT}{R_F}I_2R_b + \frac{16\pi^2KT}{g_m}\left(\Gamma + \frac{1}{g_mR_D}\right)C_T{}^2I_3R_B{}^3 + \frac{4\pi^2KI_D{}^aC_T{}^2}{g_m{}^2}I_fR_b{}^2 \tag{4.3}$$

The SNR is expressed using Equation (4.1), Equation (4.2) and Equation (4.3);

$$SNR = \frac{(RP)^2}{\sigma_{total}{}^2} \tag{4.4}$$

and the BER is;

$$BER = Q(\sqrt{SNR}) \tag{4.5}$$

where

$$Q(x) = \frac{1}{\sqrt{2\pi}}\int_x^\infty e^{-y^2/2}dy \tag{4.6}$$

All parameters in the equations are defined in Table 4.2.

**Table 4.2: Simulation parameters.**

| System Parameter | Value |
|---|---|
| **Photodiode Responsivity** | 0.54 $A/W$ |
| **Data Rate ($R_b$)** | 100 Kbit/s |
| **Photodiode area $A_{pd}$** | $0.5\times10^{-4}$ |
| **Electron charge q** | $1.6\times10.^{\wedge-19}$ |
| **FET parameters $I_2$** | 0.562 |
| **FET parameters $I_3$** | 0.0868 |
| **FET parameters $g_m$** | $40 \times 10.^{\wedge-3}$ |
| **detector capacitance $C_d$** | $10\times10.^{\wedge-9}$ |
| **FET parameter ($R_f$)** | 10.^4 |
| **FET channel noise factor($\Gamma$)** | 0.2 |
| **FET parameter ($R_D$)** | $4\times10^{\wedge3}$ |
| **Total capcitance $C_T$** | $18\times10.^{\wedge-12}$ |
| **FET drain current $I_D$** | 10×10^-3 |
| **FET parameter ($I_f$)** | 0.184 |
| **$T$ absolute temperature (in Kelvin)** | 300 |
| **$K$ Boltzmann's constant** | 1.38×10.^-23 |
| **$K_{cap}$ FET noise coefficient** | 567 |
| **A FET noise coefficient** | 1 |
| **Filter transmission** | 0.6 |
| **N receiver reflective index** | 1.3 |
| **FET parameter ($R_B$)** | 10^3 |
| **$\phi$ irradiance angle** | 60 |
| **Receiver field of view (FOV)** | 45 |
| **Transmitter full width half maximum (FWHM) angle** | 9 |
| **Floor surface reflectivity** | ~ 0.62 |
| **Plastic wall surface reflectivity** | ~ 0.2 |
| **Plaster wall surface reflectivity** | ~ 0.8 |
| **Ceiling surface reflectivity** | ~ 0.4 |

The SNR is evaluated for each natural light category (Table 4.1). The evaluation of the system is carried out at a 100 kbit/s data rate, 0.54 $A/W$ photodiode Responsivity, 5 LEDs, each emitting 1W of power. Table 4.2 summarises the simulation parameters used in the evaluation.

The total receiver input capacitance is dominated by the photodiode capacitance ($C_d$), because of the large detector area required to achieve a high SNR. K is Boltzmann's constant, $\Gamma$ is the FET channel noise factor, K and a are the FET $^1/_f$ noise coefficients, $I_D$ is the FET drain current, and gm is the FET parameter. System parameters are representative of available commercial components.

#### 4.3.1.1 Clear Night, Full Moon

Figure 4.3 shows a typical average system SNR characteristic for a clear night, full moon as a function of reflections from plaster walls, ceilings, floors and plastic surfaces. The effect of natural light is weak as the SNR remains relatively high. During the simulation, all operational conditions are evaluated to converge on an accurate value. The most relevant average SNR value is taken after the curve converges, the point that the moving average is minimised and the simulation reaches stability. Equation (3.22) supported by Equation (3.20) and Equation (3.21) is employed within the Monte Carlo simulations at varying levels of sunlight irradiance ($P_n$ in Equation (3.20)). The characteristic starts at the calculated value of 58 dB, thereafter changes in the parameters producing the behaviour captured in Figure 4.3.

Simulations are initiated with different seed numbers and the characteristic converges to stable estimates after 100 iterations. The number of iterations varies on a case by case basis e.g. the case from sunrise to sunset in different locations (8760 hours/year) is significantly more demanding scenario requiring many more iterations to converge. The average system SNR for a plastic wall (lowest surface reflectivity) is ~30 dB; ~46 dB for a plaster wall (highest surface reflectivity); ~42dB and ~45dB for a ceiling and floor respectively. The system can provide a $10^{-11}$ BER at the specified data rate.

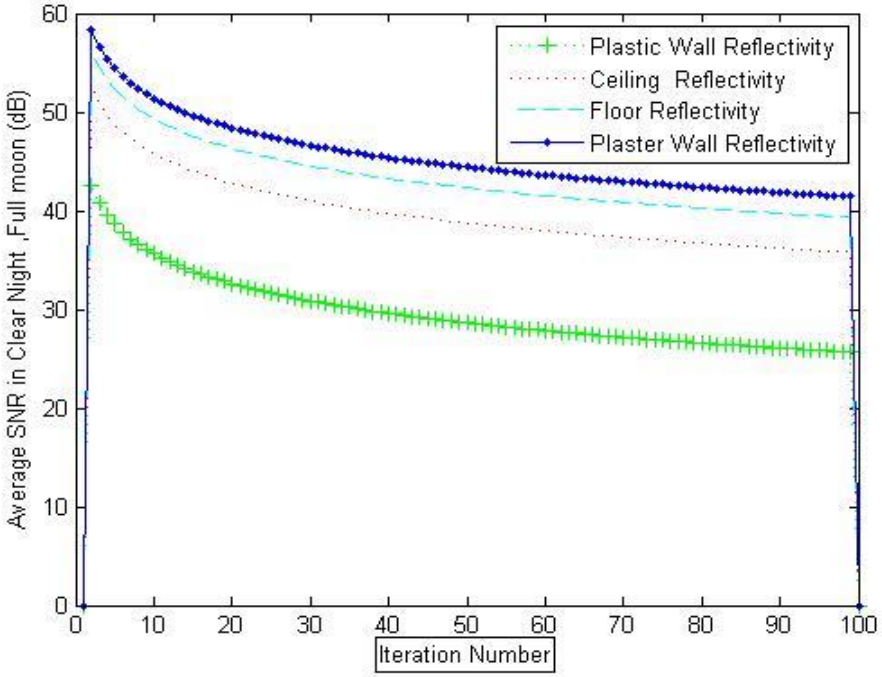


**Figure 4.3: Average system SNR; clear night, full moon.**

Similar characteristics for all of the scenarios considered are presented in Appendix I. Henceforth the results of the estimation of the system average SNR for the range of scenarios under consideration is presented in a tabular format.

### 4.3.1.2 Winter, Overcast Sky

For the case of a winter day with overcast sky, the average system SNR for a plastic wall reduces to ~28 dB (Table 4.3) compared to the clear night, full moon scenario. For a plaster wall, a slight decrease to ~44 dB is observed; for a ceiling and floor surface the SNR decreases to ~39dB and ~42dB respectively.

**Table 4.3: Average system SNR; winter, overcast sky.**

| Surface Reflectivity | Average SNR (dB) |
|---|---|
| **Plaster wall** | ~44 |
| **Ceiling** | ~39 |
| **Floor** | ~42 |
| **Plastic wall** | ~28 |

### 4.3.1.3 Winter Day, Clear Sky

A clear sky condition further degrades the SNR, reducing to ~27 dB for a plastic wall and ~43 dB for a plaster wall (Table 4.4). The SNR for a floor and ceiling surface is even lower, but the required level of BER is still attainable.

**Table 4.4: Average system SNR; winter, clear sky.**

| Surface Reflectivity | Average SNR (dB) |
|---|---|
| **Plaster wall** | ~43 |
| **Ceiling** | ~37 |
| **Floor** | ~40 |
| **Plastic wall** | ~27 |

### 4.3.1.4 Summer, Overcast Sky

In the summer months when sunlight intensity is highest - in the 4000 lx to 20000 lx range - the shot noise increases reducing the SNR from ~40 dB to ~24dB for a plastic wall (Table 4.5) compared to the clear night full moon case. The SNR for ceiling, floor and plaster wall surfaces also decreases to ~35 dB, ~39 dB and ~41 dB respectively. A slight degradation is also evident on comparison of winter to summer for the overcast sky case.

**Table 4.5: Average system SNR; summer, overcast sky.**

| Surface Reflectivity | Average SNR (dB) |
|---|---|
| **Plaster wall** | ~41 dB |
| **Ceiling** | ~35 |
| **Floor** | ~39 |
| **Plastic wall** | ~24 |

### 4.3.1.5 Summer, Clear Sky

During a clear, sunny day, sunlight intensity may reach up to 100,000 lx. As a consequence, the SNR decreases to ~20 dB for a plastic wall. In the case of a plaster wall, the SNR does not degrade by the same percentage due to the high reflectivity of the surface, being ~39dB (Table 4.6). The SNR decreases to ~34 dB and ~37 dB for a ceiling and floor surface respectively.

**Table 4.6: Average system SNR; summer, clear sky.**

| Surface Reflectivity | Average SNR (dB) |
|---|---|
| **Plaster wall** | ~39 |
| **Ceiling** | ~34 |
| **Floor** | ~37 |
| **Plastic wall** | ~20 |

Thermal noise dominates shot noise when the level of sunlight is low. The evaluation considered a comparison of system performance when there is no shot noise and at different levels of natural light. The average SNR is thus evaluated at the six metrological conditions as listed in Table 4.7, the first scenario being when there is no shot noise due to the sunlight irradiance and only the impact of the thermal noise is relevant. The remaining scenarios consider the impact of both thermal noise and varying levels of shot noise.

**Table 4.7: Metrological conditions classes.**

| Scenario | Metrological Condition | Sunlight Intensity (lx) |
|---|---|---|
| 1 | Sunlight not considered | 0 |
| 2 | Clear night, full moon | 0.3 |
| 3 | Winter day , overcast sky | 900-2000 |
| 4 | Winter day , clear sky | Up to 9000 |
| 5 | Summer day , overcast sky | 4000-20000 |
| 6 | Summer day , clear sky | Up to 100000 |

Results indicate that in the absence of sunlight irradiance, the average SNR was 58 dB and 42 dB for plaster and plastic walls respectively (Figure 4.4). In clear nights when the shot noise was small compared to thermal noise, the shot noise had little impact on the average SNR viz. ~53 dB and ~ 32 dB for plaster and plastic walls. As the level of sunlight irradiance increases, the shot noise dominates and the average SNR degrades to 38 dB and 20 dB for plaster and plastic walls respectively.

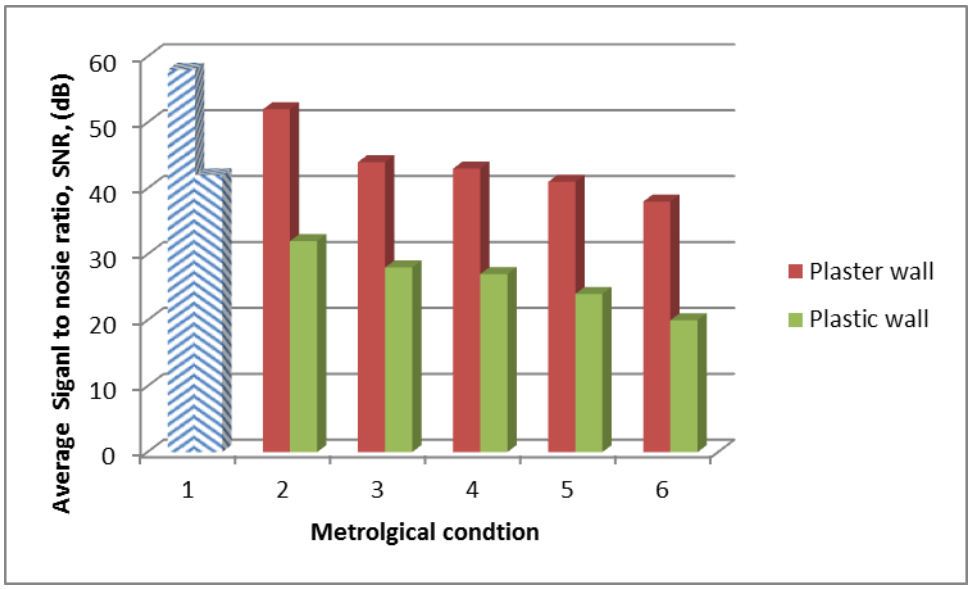


**Figure 4.4: A comparison of the system performance with thermal noise and varying levels of shot noise.**

### 4.3.1.6 Room design

The system peformance is evaluted as a function of window size; three empty rooms are simulated with the same illumination configurations and varying number of windows. According to building regulations [163], the window area should be at least 10% of total room area.

A 5m × 5m×3m room is equipped with 4 LED panels, each panel comprising 100 LED chips and each chip emittimg 0.45 W. All LED panels transmit the same data at the same viewing angle of 80 degrees. The LED panels are located on the ceiling and the 49 photodiodes with 0.54 A/W Resposivity are placed on a horizontal disk at height of 0.85 m from the floor; the room walls are made of plaster. Three window area are considered in the evaluation (Tabel 4.8).

**Tabel. 4.8: Window areas.**

| Room Number | Area |
|---|---|
| 1 | 2 windows (1.25 m× 1 m) |
| 2 | 5 windows (1.25 m× 2 m) |
| 3 | 9 windows (1.25 m× 2 m) |

The average SNR for the different window areas listed in Table 4.8 are shown in Figure 4.5. The evaluation considers a Cairo summer, clear sky scenario when the sunlight irradiance is high. It was found that when the window size was 10 % of the room area, the average SNR is ~ 43 dB, degrading to 32 dB as the window size increases to 50 % of the room area. When the room comprises a significant number of windows (90 % of the room area), the average SNR degrades further to 27 dB since the level of sunlight irradiance is highest.

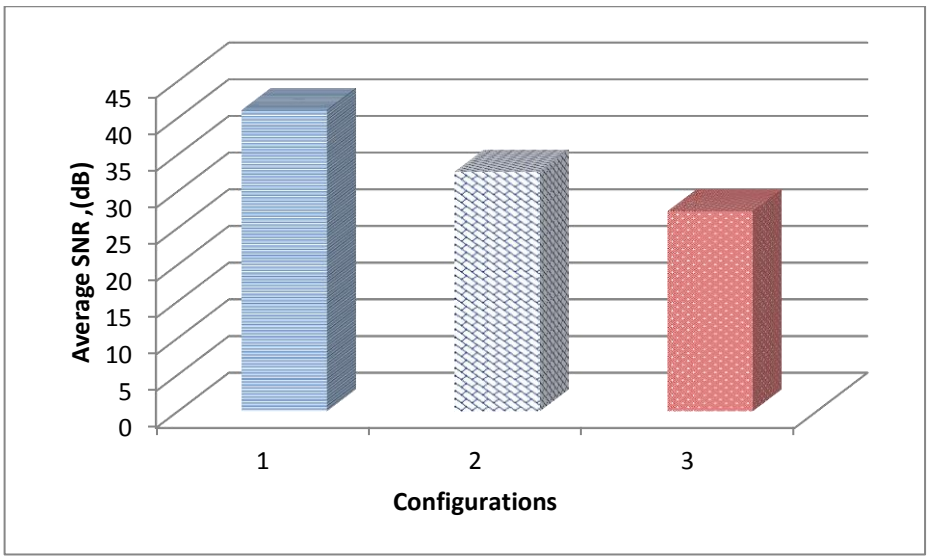


**Figure 4.5: A comparison of average SNR for different window areas (Table 4.8).**

The impact of sunlight suggests that it is advisable to locate receivers away from areas of sunlight generation such as a window. An analysis of the placement of the receiver as function of the distance to the window is given in Chapter 5. The remaining analyses are confined to rooms with window area equal to 10 % of the total room area.

### 4.3.2 System Performance; Clear Sky

VLC systems are dynamically impacted by sunlight irradiance over the day, varying from sunrise to sunset. Incident solar radiation is a function of several variables including the time of day, the day of the year, geographic location, and atmospheric conditions. Thus in order to estimate the performance of the VLC system in the presence of sunlight (clear sky) more rigorously, hourly sunlight irradiance is calculated using the model detailed in Chapter 3.

Two representative locations are selected for the estimation; Cairo and Glasgow. These locations represent characteristics of environments at the opposite ends of the spectrum since Cairo enjoys sunlight throughout the year whereas Glasgow suffers from a limited number of sunny days. Hourly sunlight irradiance values over the year of 2011 are calculated considering the longitude and latitude of the locations, the day of the year and the time of the day.

### 4.3.2.1 Clear Sky Sunlight Irradiance

Direct solar radiation, $q_{sun}$ in the absence of accurate measurements, can be estimated from the approximation of clear sky solar radiation on a horizontal surface in W/m$^2$ as [28, 139];

$$q_{sun}^{\backprime} = 1350.3\left[1 + 0.033\cos\left(\frac{360n}{365}\right)\right]\left[\sin\varphi\sin\delta + \cos\varphi\cos\delta\cos\omega\right] \tag{4.7}$$

where δ is the solar declination, $\omega$ is the angular displacement and φ is the location longitude. Two corrections in the time are used to convert from a local clock time into an apparent solar time. The first correction takes into consideration the variation in the earth's rate of rotation; the second correction is an adjustment for the difference in local longitude and the standard meridian for the local time zone [28, 139].

The sunlight irradiance is a function of the location longitude, latitude, time of the day, day of the year, the location of the sun relative to the earth and the metrological conditions. In order to provide a comparative analysis of system performance over different metrological conditions, performance is evaluated for Glasgow-Scotland, Cairo–Egypt and Berlin-Germany. Table 4.9 comprises the coordinates for the three locations.

**Table 4.9: Coordinates of the locations of the system evaluation.**

| Location | Longitude | Latitude |
|---|---|---|
| Glasgow-Scotland | 4.2590° W | 55.8580° N |
| Cairo–Egypt | 31.2333° E | 30.0500° N |
| Berlin-Germany | 52.5167° N | 13.3833° E |

### 4.3.2.2 System Performance; over the Year

The average system SNR is calculated for each season of the year.

#### 4.3.2.2.1 Winter Season

Table 4.9 and Table 4.10 show that average system SNR for a plaster wall, ceiling, floor and plastic wall surfaces during winter; the effect of sunlight is weak since its intensity is relatively low. The average system SNR for plastic walls (lowest reflectivity) is ~17 dB in Cairo and ~ 19 dB in Glasgow; ~36 dB and ~33 dB for plaster walls (highest reflectivity) respectively; for ceiling and floor surfaces the average system SNR is ~27 dB/~29 dB and ~28.5 dB/~31.5 dB for Cairo and Glasgow. The system provides a $10^{-12}$ BER for plaster walls, plastic walls and ceilings and $10^{-10}$ for floor surfaces. An average data rate of 10 Mbit/s is achievable at a $10^{-9}$ BER.

**Table 4.10: Average system SNR; winter, Cairo.**

| Surface Reflectivity | Average SNR (dB) |
|---|---|
| **0.8 (Plaster wall)** | ~36 |
| **0.4 (Ceiling surface)** | ~27 |
| **0.62 (Floor surface)** | ~28.5 |
| **0.2 (Plastic wall)** | ~17 |

**Table 4.11: Average system SNR; winter, Glasgow**

| Surface Reflectivity | Average SNR (dB) |
|---|---|
| **0.8 (Plaster wall)** | ~33 |
| **0.4 (Ceiling surface)** | ~29 |
| **0.62 (Floor surface)** | ~31.5 |
| **0.2 (Plastic wall)** | ~19 |

#### 4.3.2.2.2 Summer Season

During the summer season, sunlight intensity increases up to 1175 W/m$^2$ and the average system SNR for plastic wall surfaces degrades to ~15 dB and ~13.5 dB and 31 dB and 30 dB for plaster walls in Glasgow and Cairo (Table 4.12 and Table 4.13). A decrease in the average system SNR for floor and ceiling surfaces is evident but a $10^{-9}$ BER at is still attainable at the specified data rate.

**Table 4.12: Average system SNR summer, Cairo.**

| Surface Reflectivity | Average SNR (dB) |
|---|---|
| **0.8 (Plaster wall)** | ~30 |
| **0.4 (Ceiling surface)** | ~26.5 |
| **0.62 (Floor surface)** | ~29 |
| **0.2 (Plastic wall)** | ~13.5 |

**Table 4.13: Average system SNR; summer, Glasgow.**

| Surface Reflectivity | Average SNR (dB) |
|---|---|
| **0.8 (Plaster wall)** | ~31 |
| **0.4 (Ceiling surface)** | ~27.5 |
| **0.62 (Floor surface)** | ~30 |
| **0.2 (Plastic wall)** | ~15 |

#### 4.3.2.2.3 Autumn Season

As sunlight intensity decreases in the autumn period, as expected, the average system SNR increases for plastic and plaster walls to ~17 dB /~32 dB and ~ 18 dB/~34dB in Cairo (Table 4.14) and Glasgow (Table 4.15). Furthermore, increases in the average SNR to ~28 dB/~27 dB and ~33 dB/~30 dB for ceilings and floors are observed. A BER of $10^{-10}$ for plastic walls and ~$10^{-11}$ for other surfaces is attainable at the specified data rate.

**Table 4.14: Average system SNR; autumn, Cairo.**

| Surface Reflectivity | Average SNR (dB) |
|---|---|
| **0.8 (Plaster wall)** | ~32 |
| **0.4 (Ceiling surface)** | ~27 |
| **0.62 (Floor surface)** | ~30 |
| **0.2 (Plastic wall)** | ~17 |

**Table 4.15: Average system SNR; autumn, Glasgow.**

| Surface Reflectivity | Average SNR (dB) |
|---|---|
| **0.8 (Plaster wall)** | ~34 |
| **0.4 (Ceiling surface)** | ~28 |
| **0.62 (Floor surface)** | ~33 |
| **0.2 (Plastic wall)** | ~18 |

### 4.3.2.2.4 Spring Season

The sunlight intensity increases to 1314 $W/m^2$ compared to winter and thus the average system SNR also increases (Table 4.16, Table 4.17). The SNR is ~15 dB for plastic walls in both Glasgow and Cairo, 25 dB, 28 dB, 30 dB for ceilings, floors and plaster walls in Cairo and ~27dB, ~30dB, ~31dB in Glasgow. The BER ranges from $10^{-10}$ for plastic walls, $10^{-11}$ for ceilings and $10^{-12}$ for both floors and plaster walls at the specified data rate.

**Table 4.16: Average system SNR; spring, Glasgow.**

| Surface Reflectivity | Average SNR (dB) |
|---|---|
| **0.8 (Plaster wall)** | ~31 |
| **0.4 (Ceiling surface)** | ~27 |
| **0.62 (Floor surface)** | ~30 |
| **0.2 (Plastic wall)** | ~15 |

**Table 4.17: Average system SNR; spring, Cairo**.

| Surface Reflectivity | Average SNR (dB) |
|---|---|
| **0.8 (Plaster wall)** | ~30 |
| **0.4 (Ceiling surface)** | ~25 |
| **0.62 (Floor surface)** | ~28 |
| **0.2 (Plastic wall)** | ~15 |

### 4.3.2.3 Impact of Cloud Cover on System Performance

The impact of direct and indirect sunlight irradiance (due to cloud cover) is considered in the evaluation of average system SNR. Sunlight irradiance is moderated by cloud cover over a day; the type and thickness of clouds reduce the level of irradiance impinging on a horizontal surface. Further, clouds diffuse irradiation with, for example, days with heavy cover diffusing the total irradiance by as much as 90%. The sun's declination and height changes over the year for different locations; thus the level of sunlight irradiance depends on the longitude and latitude of locations, day of year and time of day.

Diffuse irradiance changes significantly for different locations and in the evaluation, two representative locations have been chosen – Cairo (Egypt) and Berlin (Germany) - to evaluate its impact on VLC performance. The selection of these cities is based upon the study of locations subject to the heaviest and lowest levels of cloud cover. The variation of direct irradiance (without any reflections) and diffuse irradiance for these locations over the year is presented in Table 4.18 and Table 4.19 [28, 139].

**Table 4.18: Diffuse sunlight irradiance over a year; Cairo, Egypt [139].**

| Month | Direct Irradiance (KWh/$m^2$ Day) | Diffuse Irradiance (KWh/$m^2$ Day) | Percentage of Diffuse Irradiance | Percentage of Irradiance Sunshine to 11am from clear sky | Percentage of Irradiance From 11AM to 3PM from clear sky | Percentage of Irradiance From 3PM to sunset from clear sky |
|---|---|---|---|---|---|---|
| **Jan.** | 1.74 | 1.35 | 43.6% | 56.31% | 73.83% | 65.12% |
| **Feb.** | 2.37 | 1.63 | 40.75% | 59.25% | 75.55% | 67.4% |
| **March** | 3.07 | 2.08 | 40.38% | 59.62% | 75.77% | 67.696% |
| **April** | 3.78 | 2.49 | 39.7% | 60.3% | 76.18% | 68.24% |
| **May** | 4.56 | 2.47 | 35.1% | 64.9% | 78.94% | 71.92% |
| **June** | 5.16 | 2.40 | 31.74% | 68.26% | 80.9566 % | 74.608% |
| **July** | 4.93 | 2.41 | 32.8.% | 67.2% | 80.32% | 73.76% |
| **August** | 4.57 | 2.19 | 32.39% | 67.61% | 80.566 % | 74.088% |
| **Sept.** | 3.86 | 2.01 | 34.24% | 65.76% | 79.456 % | 72.608% |
| **Oct.** | 3.07 | 1.62 | 34.54% | 65.46% | 79.276 % | 72.368% |
| **Nov.** | 1.96 | 1.49 | 43.18% | 56.82% | 74.092 % | 65.456% |
| **Dec.** | 1.58 | 1.28 | 44.75% | 55.25% | 73.15% | 64.2% |

**Table 4.19: Diffuse sunlight irradiance over a year; Berlin, Germany [139].**

| Month | Direct Irradiance (KWh/m2 Day) | Diffuse Irradiance (KWh/m 2Day) | Percentage of Diffuse Irradiance (%) | Percentage of Irradiance Sunshine to 11am from clear sky (%) | Percentage of Irradiance From 11AM to 3PM from clear sky (%) | Percentage of Irradiance From 3PM to sunset from clear sky (%) |
|---|---|---|---|---|---|---|
| **Jan.** | 0.17 | 0.44 | 72.13% | 27.86% | 56.722% | 42.296% |
| **Feb.** | 0.40 | 0.74 | 64.9% | 35.08% | 61.06% | 48.08% |
| **Mar.** | 1.03 | 1.41 | 57.78% | 42.213% | 65.332% | 53.776% |
| **Apr.** | 1.42 | 2.07 | 59.31% | 40.687% | 64.414% | 52.552% |
| **May** | 2.13 | 2.64 | 55.345% | 44.654% | 66.793% | 55.724% |
| **Jun.** | 2.58 | 2.86 | 52.573% | 47.42% | 68.456% | 57.944% |
| **Jul.** | 2.29 | 2.97 | 56.463.% | 43.536% | 66.122% | 54.82% |
| **Aug.** | 2.05 | 2.53 | 55.24% | 44.759% | 66.856% | 55.808% |
| **Sept.** | 1.38 | 1.67 | 54.75% | 45.245% | 67.15% | 56.2% |
| **Oct.** | 0.54 | 1.05 | 66.037% | 33.962% | 60.3778% | 47.1704% |
| **Nov.** | 0.22 | 0.54 | 71.05% | 28.94% | 57.37% | 43.16% |
| **Dec.** | 0.211 | 0.49 | 69.90% | 26.2% | 52.3% | 22.5% |

The percentage of diffuse irradiance is based upon a monthly average of direct irradiance [28]. Further the diffuse irradiance varies over the day; Table 4.20 summarizes its variation over a day.

**Table 4.20: Variation of diffuse irradiance over a day.**

| Time Period | Diffuse Irradiance (%) |
|---|---|
| **Sunrise to 11 AM** | 100 |
| **11AM to 3 PM** | 60 |
| **3PM to Sunset** | 80 |

The maximum and minimum sunlight irradiance in each season for both locations is summarised in Table 4.21 and Table 4.22.

**Table 4.21: Sunlight irradiance, Cairo.**

| Seasons | Max Irradiance Clear sky | Max Irradiance clouds effect | Min Irradiance Clear sky | Min Irradiance clouds effect |
|---|---|---|---|---|
| **Autumn** | 1175.087 | 890.552 | 3.280 | 1.059 |
| **Spring** | 1314.609 | 1030.823 | 1.861 | 1.388 |
| **Summer** | 1312.911 | 1036.15 | 0.48 | 0.348 |
| **Winter** | 1185.579 | 876.997 | 1.446 | 0.814 |

**Table 4.22: Sunlight irradiance, Berlin.**

| Seasons | Max Irradiance Clear sky | Max Irradiance clouds effect | Min Irradiance Clear sky | Min Irradiance clouds effect |
|---|---|---|---|---|
| **Autumn** | 822.627 | 368.981 | 0.281 | 0.0813 |
| **Spring** | 1151.26 | 586.064 | 2.668 | 1.09277 |
| **Summer** | 1150.806 | 586.9389 | 0.565 | 0.271 |
| **Winter** | 823.107 | 347.58 | 0.49 | 0.838 |

### 4.3.3 Average system SNR under Cloud Cover

Monthly average levels of sunlight irradiance are assumed as the main source of shot noise. The average system SNR for both environments in clear and cloudy skies over the year is evaluated.

#### 4.3.3.1 Winter Season

The sunlight irradiance during winter in Cairo is 1185w/$m^2$ (clear sky) and 876w/$m^2$ (cloudy sky). The average SNR (Table 4.23 and Table 4.24) is evaluated to be at a minimum of 17 dB for plastic walls with clear sky and 39 dB for plaster walls in the presence of cloud cover; for the ceiling and floor the SNRs are 27.5 dB/31 dB and 28.5 dB/37 dB respectively. The average SNR in Berlin ( Table 4.25 and Table 4.26) was in the range of 40 dB (plaster wall) to 18 dB (Plastic wall) in the cloudy and clear skies respectively.

**Table 4.23: Average system SNR; Cairo for winter, clear sky.**

| Surface Reflectivity | Average SNR (dB) |
|---|---|
| **0.8 (Plaster wall)** | ~37 |
| **0.4 (Ceiling surface)** | ~27.5 |
| **0.62 (Floor surface)** | ~31 |
| **0.2 (Plastic wall)** | ~17 |

**Table 4.24: Average system SNR; Cairo for winter, cloud cover.**

| Surface Reflectivity | Average SNR (dB) |
|---|---|
| **0.8 (Plaster wall)** | ~39 |
| **0.4 (Ceiling surface)** | ~28.5 |
| **0.62 (Floor surface)** | ~37 |
| **0.2 (Plastic wall)** | ~20 |

**Table 4.25: Average system SNR; Berlin for winter, clear skies.**

| Surface Reflectivity | Average SNR (dB) |
|---|---|
| **0.8 (Plaster wall)** | ~38 |
| **0.4 (Ceiling surface)** | ~32 |
| **0.62 (Floor surface)** | ~35 |
| **0.2 (Plastic wall)** | ~18 |

.

**Table 4.26: Average system SNR; Berlin for winter, cloud cover.**

| Surface Reflectivity | Average SNR (dB) |
|---|---|
| **0.8 (Plaster wall)** | ~40 |
| **0.4 (Ceiling surface)** | ~33 |
| **0.62 (Floor surface)** | ~38 |
| **0.2 (Plastic wall)** | ~21 |

### 4.3.3.2 Summer Season

During summer, as expected, the sunlight irradiance is at a maximum especially in Cairo, ~1313 w/$m^2$ in clear and 1036 w/$m^2$ in cloudy sky; the average system SNR is 13 dB and 17 dB respectively for plastic wall surfaces (Table 4.27and Table 4.28). The corresponding SNR for plaster wall surfaces is 35 dB and 38 dB.

In Berlin, the irradiance reaches 1150 W/$m^2$ and 586 W/$m^2$ for clear and cloudy sky; the corresponding average SNR is 16 dB/27.5 dB, 31 dB/33.5 dB, 18 dB/30 dB and 33 dB/35 dB for plastic, ceiling, floor and plaster wall surfaces (Table 4.29 and Table 4.30).

**Table 4.27: Average system SNR; Cairo for summer, clear sky.**

| Surface Reflectivity | Average SNR (dB) |
|---|---|
| **0.8 (Plaster wall)** | ~35 |
| **0.4 (Ceiling surface)** | ~27 |
| **0.62 (Floor surface)** | ~32 |
| **0.2 (Plastic wall)** | ~13 |

**Table 4.28: Average system SNR; Cairo for summer, cloudy sky.**

| Surface Reflectivity | Average SNR (dB) |
|---|---|
| **0.8 (Plaster wall)** | ~38 |
| **0.4 (Ceiling surface)** | ~29 |
| **0.62 (Floor surface)** | ~35 |
| **0.2 (Plastic wall)** | ~17 |

**Table 4.29: Average system SNR; Berlin for summer, clear sky.**

| Surface Reflectivity | Average SNR (dB) |
|---|---|
| **0.8 (Plaster wall)** | ~33.5 |
| **0.4 (Ceiling surface)** | ~27.5 |
| **0.62 (Floor surface)** | ~31 |
| **0.2 (Plastic wall)** | ~16 |

.

**Table 4.30: Average system SNR; Berlin for summer, cloudy sky.**

| Surface Reflectivity | Average SNR (dB) |
|---|---|
| **0.8 (Plaster wall)** | ~35 |
| **0.4 (Ceiling surface)** | ~30 |
| **0.62 (Floor surface)** | ~33 |
| **0.2 (Plastic wall)** | ~18 |

### 4.3.3.3 Spring Season

During spring, the average SNR is 14 dB and 17 dB for plastic wall surfaces (Table 4.31 and Table 4.32) and 30 dB and 37 dB for plaster wall surfaces for clear and cloudy sky. In the Berlin spring, the average SNR is 18.5 dB/16 dB, 37 dB/32.5 dB for plastic and plaster surfaces for clear and cloudy sky (Table 4.33 and Table 4.34).

**Table 4.31: Average system SNR; Berlin for spring, clear sky.**

| Surface Reflectivity | Average SNR (dB) |
|---|---|
| **0.8 (Plaster wall)** | ~30 |
| **0.4 (Ceiling surface)** | ~26 |
| **0.62 (Floor surface)** | ~29 |
| **0.2 (Plastic wall)** | ~14 |

**Table 4.32: Average system SNR; Cairo for spring, cloudy sky.**

| Surface Reflectivity | Average SNR (dB) |
|---|---|
| **0.8 (Plaster wall)** | ~36 |
| **0.4 (Ceiling surface)** | ~28.5 |
| **0.62 (Floor surface)** | ~31 |
| **0.2 (Plastic wall)** | ~17 |

**Table 4.33: Average system SNR; Berlin for spring, clear sky.**

| Surface Reflectivity | Average SNR (dB) |
|---|---|
| **0.8 (Plaster wall)** | ~32.5 |
| **0.4 (Ceiling surface)** | ~29 |
| **0.62 (Floor surface)** | ~31 |
| **0.2 (Plastic wall)** | ~16 |

**Table 4.34: Average system SNR; Berlin for spring, cloudy sky.**

| Surface Reflectivity | Average SNR (dB) |
|---|---|
| **0.8 (Plaster wall)** | ~37 |
| **0.4 (Ceiling surface)** | ~30 |
| **0.62 (Floor surface)** | ~33 |
| **0.2 (Plastic wall)** | ~18.5 |

### 4.3.3.4 Autumn Season

During autumn in Cairo, sunlight irradiance reaches 1175w/$m^2$ and the corresponding average system SNR (Table 4.35 and Table 4.36) for clear and cloudy sky are 16 dB/30 dB, 32.5 dB/35 dB; 18 dB/32 dB and 35 dB/37.5 dB for plastic wall, ceiling, floor and plaster wall surfaces. In Berlin, cloud cover is more pronounced and consequently sunlight irradiance reduces to 822w/$m^2$ and 368w/$m^2$ for clear and cloudy skies. The average system SNR is 14.5 dB and 18 dB (Table 4.37 and Table

4.38) for a plastic wall and 38d B and 34.5 dB for plaster wall surfaces for clear and cloudy sky.

**Table 4.35: Average system SNR; Cairo for autumn, clear sky.**

| Surface Reflectivity | Average SNR (dB) |
|---|---|
| **0.8 (Plaster wall)** | ~35 |
| **0.4 (Ceiling surface)** | ~30 |
| **0.62 (Floor surface)** | ~32.5 |
| **0.2 (Plastic wall)** | ~16 |

**Table 4.36: Average system SNR; Cairo for autumn, cloudy sky.**

| Surface Reflectivity | Average SNR (dB) |
|---|---|
| **0.8 (Plaster wall)** | ~37.5 |
| **0.4 (Ceiling surface)** | ~32 |
| **0.62 (Floor surface)** | ~35 |
| **0.2 (Plastic wall)** | ~18 |

**Table 4.37: Average system SNR; Berlin for autumn, clear sky.**

| Surface Reflectivity | Average SNR (dB) |
|---|---|
| **0.8 (Plaster wall)** | ~34 |
| **0.4 (Ceiling surface)** | ~28.5 |
| **0.62 (Floor surface)** | ~31 |
| **0.2 (Plastic wall)** | ~14.5 |

**Table 4.38: Average system SNR; Berlin for autumn, cloudy sky.**

| Surface Reflectivity | Average SNR (dB) |
|---|---|
| **0.8 (Plaster wall)** | ~38 |
| **0.4 (Ceiling surface)** | ~31 |
| **0.62 (Floor surface)** | ~36.5 |
| **0.2 (Plastic wall)** | ~19 |

### 4.3.4 Data Rate

The following assumptions are adopted in order to evaluate system performance in terms of data rate;

- four LED panels (2m×2m)
- each panel contains a 10×10 LED array (LXH LW6C LEDs [171]) at 4 cm between each chip. This source is representative of a typical commercial LED currently available on the market
- each panel is placed in four locations; A (1 m, 1 m, 3 m), B (4 m, 1 m, 3 m), C (1 m, 4 m, 3 m) and D (4 m, 4 m, 3 m)
- the irradiance angle is 80 degrees
- each LED transmits at a power of 0.452 W
- the receiver is located on a desk at a height of 0.85m

The evaluation is confined solely to the plaster wall case; the intention is to illustrate the data rate behaviour for one scenario only. All other simulation parameters remain as in Table 4.2. An evaluation of performance is carried out for Cairo at summer/clear sky (high sunlight irradiance) and Berlin at winter/cloudy sky (lowest sunlight irradiance). 50 receivers are normally distributed over the area of room and the arithmetic mean of the evaluated data rate is presented. Equation (3.19), Equation (3.20), Equation (3.21), Equation (3.22), Equation (3.23) and Equation (3.24) are employed to evaluate the BER from the SNR estimation for different data rates over different metrological conditions.

### 4.3.4.1 Summer

The BER performance as a function of data rate in Cairo is presented in Figure 4.6. The BER decreases dramatically as the data rate increases owing to the impact of sunlight irradiance induced noise and inter symbol interference. A $10^{-9}$ BER is achieved at 10 Mbit/s but as the data rate increases to 200 Mbit/s and 500 Mbit/s, the BER degrades to $10^{-4}$ and $10^{-2}$ respectively. As a comparison, a $10^{-6}$ BER at 200 Mbit/s has been reported [41] when shot noise owing to sunlight is treated as Gaussian.

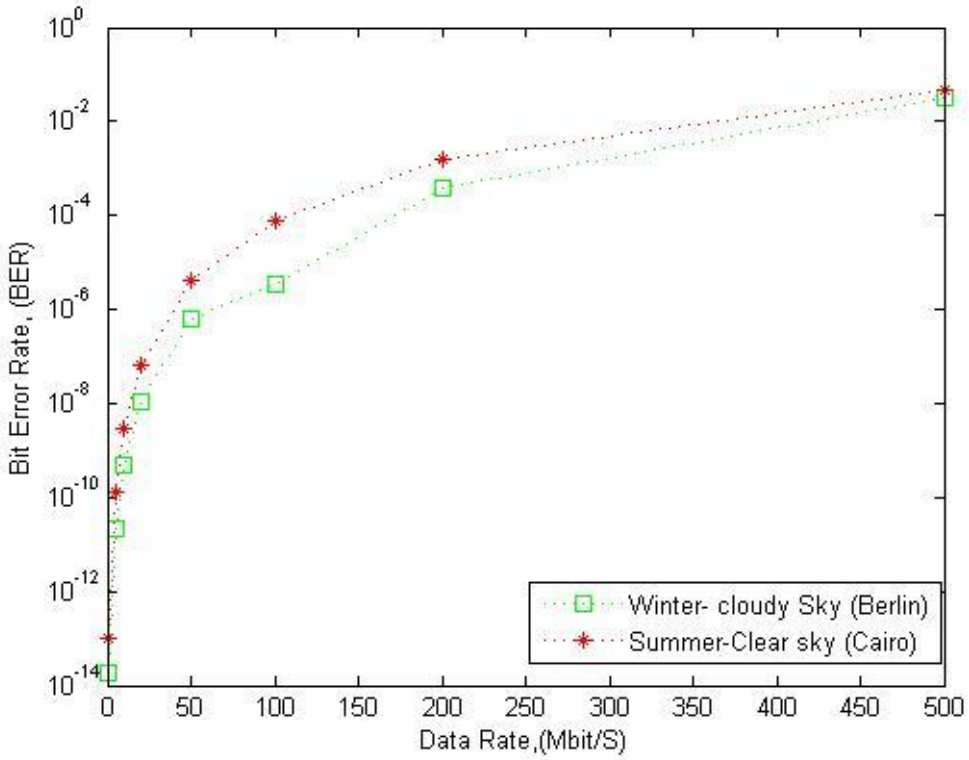


**Figure 4.6: A comparison of BER performance as a function of data rate; Cairo-summer and Berlin-winter**

### 4.3.4.2 Winter

During a Berlin winter, sunlight irradiance decreases dramatically and the BER performance as a function of data rate mirrors the change in environment (Figure 4.6). A $10^{-13}$ BER is achieved at a relatively low data rate of 1 Mbit/s. As the data rate increases to 150 Mbit/s, 200 Mbit/s and 500 Mbit/s the BER degrades to $10^{-6}$,

$10^{-5}$, and$10^{-3}$ respectively; a $10^{-9}$ BER is achieved at 50 Mbit/s, a threefold increase in data rate at the same BER compared to the Cairo summer, clear sky condition. The BER performance as a function of data rate for other scenarios lies between the two cases.

## 4.4 Conclusions

The results of an evaluation of the level of impact of sunlight irradiance on the performance of VLC systems through the average SNR and BER are presented (Figure 4.6). Sunlight irradiance is modelled for clear and cloudy skies to provide granularity on the estimation of the detrimental impact under different environmental conditions. Clear night-full moon, summer day-clear sky, winter day-clear sky, summer day-overcast sky and winter day-overcast sky conditions are considered and represented as 1, 2, 3, 4, 5. The evaluation also considers a range of surfaces; plaster walls provide the best SNR performance compared to floor, plastic wall and ceiling surfaces. The magnitude and hence impact of NLOS components decrease for every reflection considered, especially in relatively spacious environments (15m×15m×3m). As expected, the lowest average SNR (and BER) occurs for a summer day, clear sky since natural light intensity is at maximum.

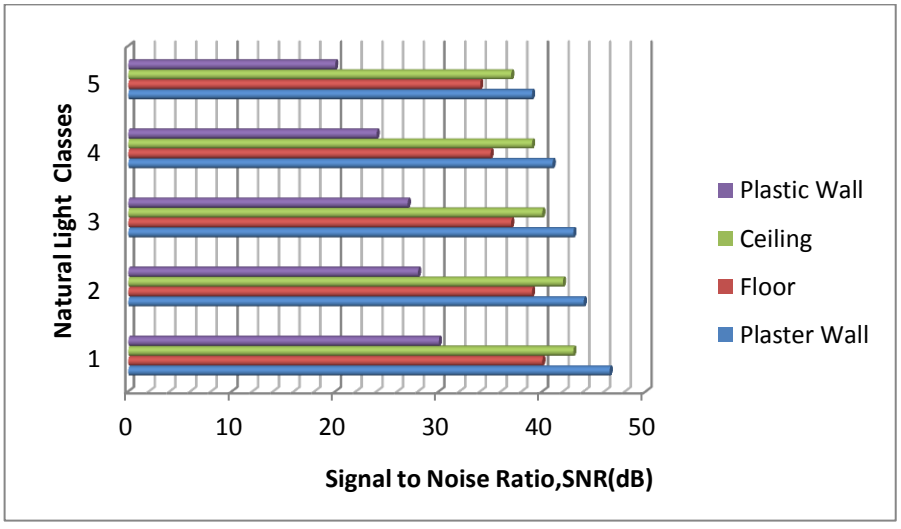


**Figure 4.7: Summary of the average system SNR over the main five environmental categories.**

Furthermore sunlight irradiance (clear sky) was modelled over the year of 2011 for two representative locations viz. Cairo and Glasgow. The impact on system performance is evaluated for summer, spring, autumn, and winter seasons (Table 4.39). The evaluation considered the BER for a range of surfaces; plaster walls, floors, plastic walls and ceilings. The attainable BER ranges from $10^{-9}$ to $10^{-12}$, evaluated using hourly estimations (8760 hours) of sunlight irradiance. The lowest SNR (and BER) occurred for summer days in Cairo where sunlight intensity is at maximum.

**Table 4.39: Average system SNR over the four seasons of the year (clear sky).**

| SNR / Season | Plaster wall (dB) | | Floor (dB) | | Ceiling(dB) | | Plastic wall (dB) | |
|---|---|---|---|---|---|---|---|---|
| | **Cairo** | **Glasgow** | **Cairo** | **Glasgow** | **Cairo** | **Glasgow** | **Cairo** | **Glasgow** |
| **Summer** | ~ 30 | ~ 31 | ~ 27.5 | ~ 29.5 | ~ 23.5 | ~ 25 | ~13.5 | ~ 15 |
| **Autumn** | ~ 32 | ~ 34 | ~ 30 | ~ 33 | ~27 | ~ 28.5 | ~ 17 | ~ 18 |
| **Winter** | ~ 33 | ~ 36 | ~ 28.5 | ~ 33 | ~ 27.5 | ~ 29 | ~ 17 | ~ 19 |
| **Spring** | ~ 30 | ~ 31 | ~ 28 | ~ 30 | ~ 25 | ~ 27 | ~ 14 | ~ 15.5 |

The evaluation moved to consider two locations representative of the sunniest and cloudiest areas of the world (Cairo and Berlin) to determine the impact of cloud coverage on system performance. A comparative performance analysis of attainable average SNR (and BER) is determined on an hourly basis over the year for both clear and cloudy sky conditions (Table 4.40 and Table 4.41). The minimum SNR is obtained in Cairo, summer-clear skies (~13.5 dB) and the maximum SNR is achieved in Berlin, winter-cloudy sky (~39.5dB). The BER lies in the range of $10^{-13}$ (plaster walls) to $10^{-10}$ (plastic walls) at the specified data rate. Moreover, the maximum data rate at $10^{-9}$ BER is 10 Mbit/s and 50 Mbit/s for summer-clear sky (Cairo) and winter-cloudy sky (Berlin) respectively (plasters). Plaster walls are recommended for locations with high sunlight irradiance due to high reflectivity but plastic walls should be avoided in such environments as they lead to a significant impact on system performance.Sunlight irradiance can impact system performance with 10%

variation of the SNR over the year for clear skies. A ~5% improvement in the system SNR occurs under cloudy scenarios compared to clear sky. A comparative analysis of the BER performance at different data rates for Berlin, winter (cloudy sky), Cairo- summer (clear sky) and when the shot noise is treated as Gaussian shows that the performance degrades by ~40% for the Berlin case compared to when Gaussian Noise is assumed.

**Table 4.40: Average system SNR; for Cairo and Berlin, clear skies.**

| SNR / Season | Plastic wall (dB) | | Ceiling surface (dB) | | Floor surface (dB) | | Plaster wall (dB) | |
|---|---|---|---|---|---|---|---|---|
| | **Cairo** | **Berlin** | **Cairo** | **Berlin** | **Cairo** | **Berlin** | **Cairo** | **Berlin** |
| **Winter** | ~ 17 | ~ 20 | ~ 29.5 | ~ 31 | ~ 34 | ~36 | ~ 36 | ~ *37.5* |
| **Autumn** | ~17.5 | ~ 19 | ~ 29 | ~*30* | ~32.5 | ~33.5 | ~33 | ~*34.5* |
| **Spring** | ~17.5 | ~ 18.5 | ~ 27.5 | ~ 29 | ~31.5 | ~33 | ~33.5 | ~ 35 |
| **Summer** | ~13.5 | ~ 17 | ~ 25.5 | ~ 27 | ~ 30 | ~32.5 | ~33 | ~35.5 |

**Table 4.41: Average system SNR; for Cairo and Berlin, cloudy skies.**

| SNR / Season | Plastic wall (dB) | | Ceiling (dB) | | Floor (dB) | | Plaster wall (dB) | |
|---|---|---|---|---|---|---|---|---|
| | **Cairo** | **Berlin** | **Cairo** | **Berlin** | **Cairo** | **Berlin** | **Cairo** | **Berlin** |
| **Winter** | ~ 19 | ~21.5 | ~ 32 | ~ 34 | ~ 35.5 | ~38 | ~38 | ~ 39.5 |
| **Autumn** | ~ 20 | ~20.5 | ~ 31.5 | ~ *32.5* | ~34 | ~ 35 | ~ 36.5 | ~38 |
| **Spring** | ~18.5 | ~ 19 | ~ 30 | ~ 31.5 | ~33.5 | ~ 34.5 | ~ 36 | ~ 37.5 |
| **Summer** | ~ 15.5 | ~18 | ~28 | ~ 29.5 | ~ 32.5 | ~ 34 | ~ 34 | ~ 37 |

The BER performance is evaluated in comparison with results obtained assuming natural light induced noise follows Gaussian statistics [41]. The data rate limits for a BER of $10^{-6}$ are 65 Mbit/s and 120 Mbit/s in Cairo and Berlin respectively compared to 200 Mbit/s reported at the same BER level for the same system configuration but when shot noise due is assumed as Gaussian.

This comparative evaluation estimates the expected system performance over the year as a function of location and metrological conditions, a basis for system reliability and availability assessment planning. Moreover, it informs the selection of applications that can be implemented in different locations over the year, anywhere in the world.

# Chapter 5

# LED Layout and System Performance

## 5.1 Introduction

The impact of LED layout on the performance of VLC systems is presented. Optimum LED layout placement is developed with consideration of sunlight irradiance and cloud cover over the year. The analysis is carried out as function of room shape, size and surface reflectivity.

LED layout is defined as the distribution of transmitters across the ceiling of a room, a key factor that modulates system performance. The location of the transmitters and in turn the relative positions of the transmitters with respect to receivers, limits network coverage across a room. In addition, just as important, is the optimisation of LED layout that mitigates the impact of sunlight on performance.

The impact owing to LED layout has been reported extensively [74-76, 78, 83, 84] but only considering a limited number of system configurations; circular or square shapes for a standard room office only without the impact of sunlight irradiance. Also, the arrangement of LEDs has also been considered [174] from a statistical perspective, specifically the SNR variance over the room. One constellation was proposed and analysed but a wider optimisation of the layout to maximise system performance has not been addressed. Although the path loss of the system has been characterised in [132], only LOS path components were considered and sunlight was treated as Additive White Gaussian noise. The level of sunlight irradiance was measured in the room under consideration, a point evaluation as sunlight irradiance varies dramatically according to the time of day, the location, day of year and metrological conditions. Furthermore, different room sizes and shapes were not considered.

In summary, the state-of-the-art in terms of layout optimisation is thus limited viz. two LED constellations, restricted to LOS components only with the impact of sunlight irradiance treated as AWG noise. LED layout design has been considered with consideration of the impact on communication system performance [74] for specific room geometries not subject to constrains imposed by illumination requirements [175]. The variation of received signal strength to minimise fluctuations over the room has also been investigated but without consideration of NLOS paths and sunlight irradiance. The goal here is to enhance the understanding of VLC system designs under an extended range of environmental conditions. System planning must draw on design guidelines that treat different room shapes and sizes which include NLOS effects and sunlight irradiance over the year to enhance the quality of service provided.

Here, two room sizes are considered; 12 m × 12 m × 3 m and 6 m × 6 m × 3 m as well as the impact of sunlight irradiance emanating from windows and doors. Moreover, as in previous analyses, the investigation considers two representative environments - Cairo and Berlin - locations characteristic of extreme metrological conditions. The analysis is driven by the lighting requirement stipulated by established standards of luminance for the two room sizes with the additional aim of conserving the energy consumed.

Monte Carlo simulation is used. LED panels with irradiance angle $\emptyset_{1/2}$ are deployed across the ceiling and directed towards receivers distributed uniformly on the floor and/or on desks (at 0.85 m height from the floor). Both LOS and NLOS components (up to fifth reflection) are considered. The room geometry and window and door placements are as shown in Figure 5.1.

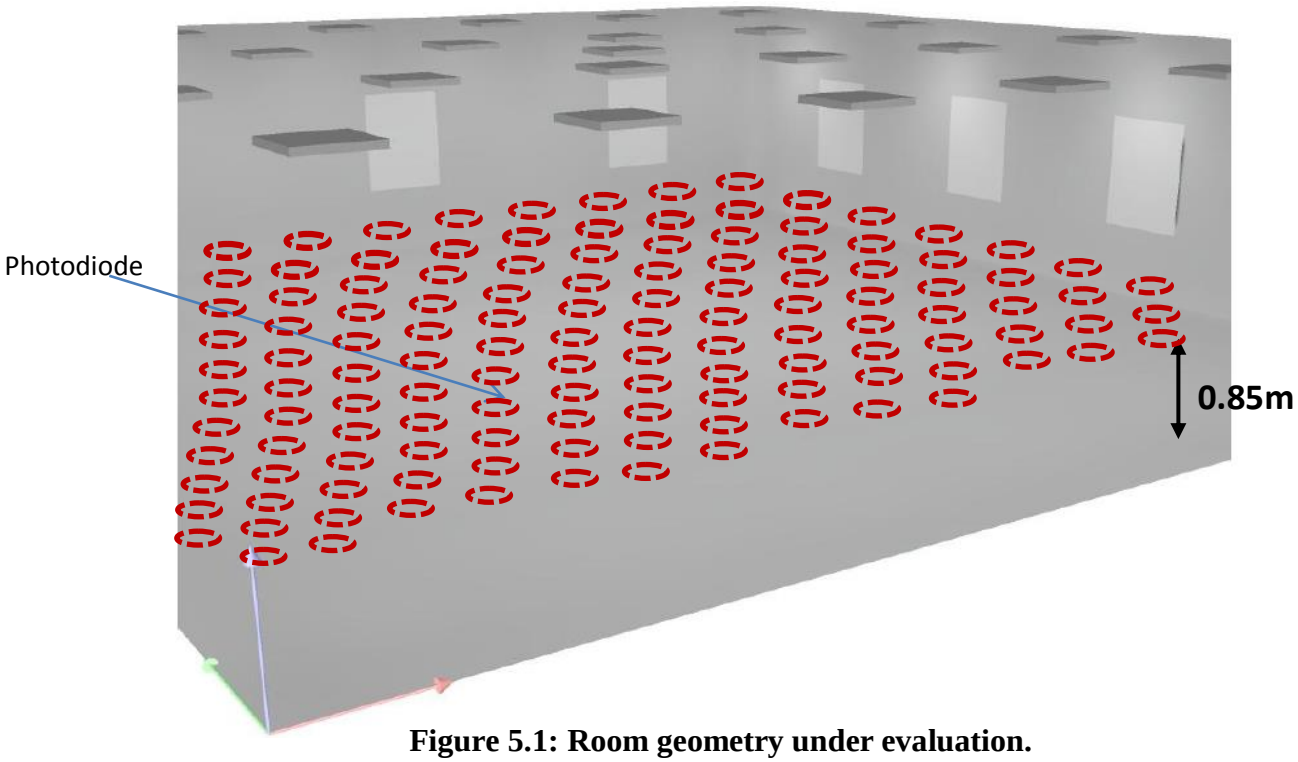


**Figure 5.1: Room geometry under evaluation.**

Sunlight irradiance emanates from windows and doors and is manifest as shot noise at the receiver. The room is assumed to be furnished with either plaster or plastic walls for the purpose of the analysis.

Equation (3.19), Equation (3.20), Equation (3.21), Equation (3.22), Equation (3.23) and Equation (3.24) are revisited to illustrate the methodology employed to find the optimum placement of LED panels that maximise the SNR in the room. The optimisation problem formulation for optimum placement of LED panels is as follow;

- **Find variables:**

  $x_1, x_2, x_3 \ldots x_n; y_1, y_2, \ldots . y_n$

  where $x_1$, $x_2$ are the coordinates of x-axis and $y_1$, $y_2$ are the coordinates of -axis of the LED panel location for *n* LED panels.
- **Criteria:**

  Max E[SNR]

- **Constrains**
  - $0 < x_1, x_2, x_3 \ldots x_n <$ Room length
  - $0 < y1, y2, \ldots . yn <$ Room width
  - $400\ Lx < E_h < 1100\ Lx$
  - $x_i \neq x_j$
  - $y_i \neq y_j$

where

$$E_h \equiv I_O \cos^n(\phi)^{\cos(\theta)/R_{distance}}$$

$$f = \max\left( E\left[ SNR = \frac{(RP_R)^2}{2qRp_n I_2 R_b + \frac{4KT}{R_F} I_2 R_b + \frac{16\pi^2 KT}{g_m}\left(\Gamma + \frac{1}{g_m R_D}\right) C_T{}^2 I_3 R_B{}^3 + \frac{4\pi^2 K I_D{}^a C_T{}^2}{g_m{}^2} I_f R_b{}^2} \right] \right)$$

$E_h$ is the horizontal illuminance at a point, $\emptyset$ is the irradiance angle, $\theta$ is the incidence angle, $R_{distance}$ is the distance to the illuminated surface and $I_o$ is the maximum luminous intensity. The remaining parameters are discussed in Chapter 3, Section 3.3.3.

## 5.2 LED layout

LED layout and placement are major parameters that impact system performance. A mapping of system performance as a function of LED layout allows the optimisation of network performance for the number of LEDs or the energy consumed on reaching an acceptable network performance at a minimum number of LEDs.

### 5.2.1 Distance to the wall

The section focuses on the characterisation of the impact on system performance of the placement of LED panels as a function of distance between the sources and the wall. A room 5 m × 5 m × 3 m is modelled with four LED panels mounted on the ceiling. Receivers are uniformly distributed at the horizontal plane at a height of 0.85

m. The simulations parameters are as stated in Chapter 4, Section 4.3.4, Table 4.3 except for the following;

- four LED panels (2 m × 2 m)
- each panel comprises of a 10×10 LED array (LXH LW6C LEDs [171]) at 4 cm between each chip, a source representative of a typical commercial LED available on the market
- each panel is placed in four locations; A (1 m, 1 m, 3 m), B (4 m, 1 m, 3 m), C (1 m, 4 m, 3 m) and D (4 m, 4 m, 3 m)
- the irradiance angle is 80 degrees
- each LED transmits at a power of 0.452 W

Initially LED panels are placed close to the wall (Figure 5.2(a)) and are then moved simultaneously (Figure 5.2(b)) away from the wall in 0.25 m steps. All LEDs transmit the same information in the same direction and it is assumed that there is no interference.

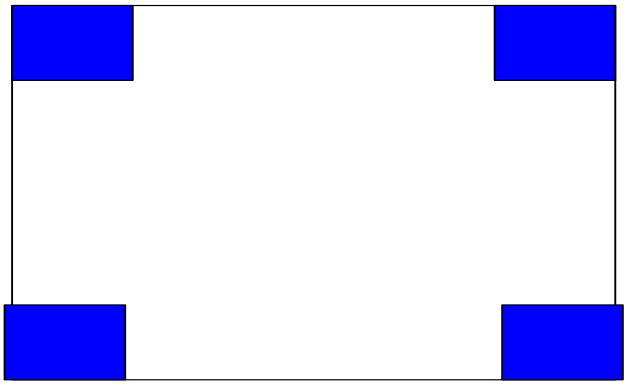

**Figure 5.2(a): Initial LED panel layout.**

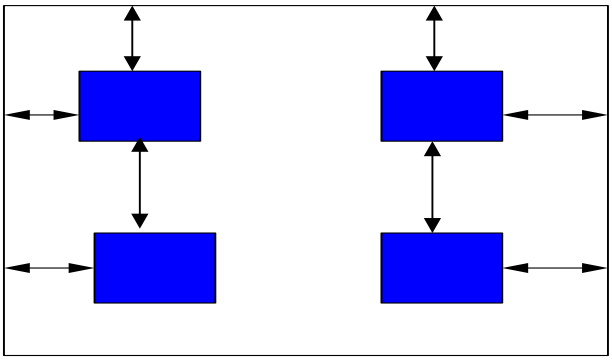

**Figure 5.2(b): LED panel movement.**

The average SNR (arithmetic mean of 49 receivers) at the horizontal plate and at height 0.85 m from the floor is generated as a function of LED panel to wall separation. The evaluation considers the performance for a Berlin winter, cloudy sky for plaster (Figure 5.3) and plastic (Figure 5.4) walls.

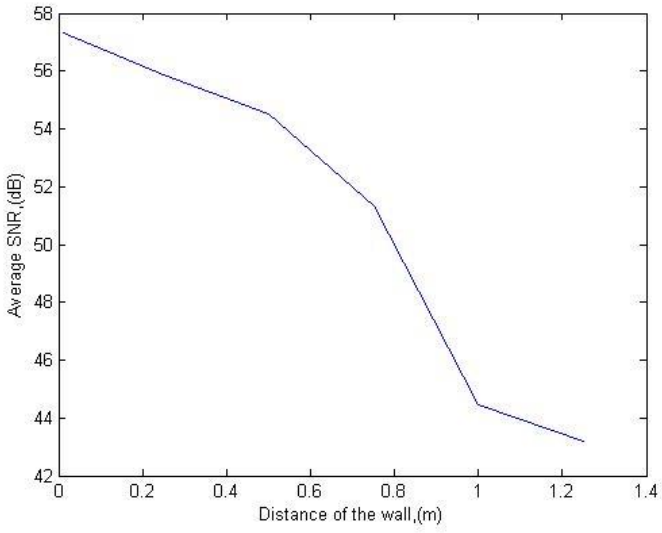


**Figure 5.3: Average SNR as a function of LED panel distance from a plaster wall (Berlin, winter, cloudy sky).**

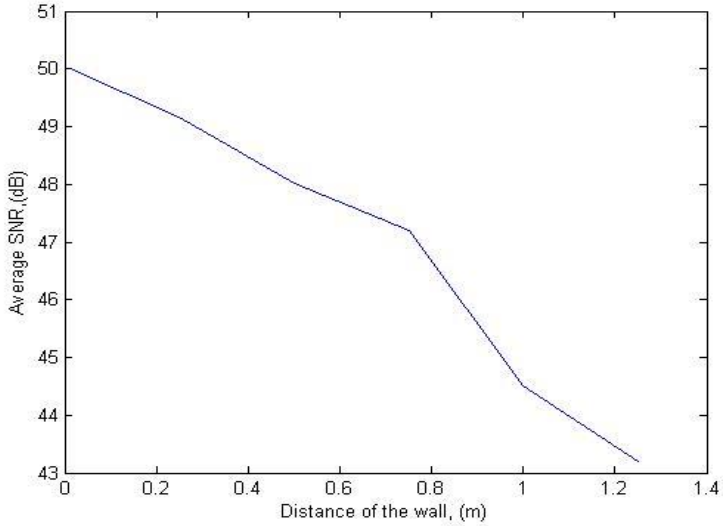


**Figure 5.4: Average SNR as a function of LED panel distance from a plastic wall (Berlin, winter, cloudy sky).**

The average SNR close to the wall (0.01 m) is ~ 57 dB and ~ 50 dB for plaster and plastic walls (Figure 5.3 and Figure 5.4). The average SNR performance degrades to ~ 51 dB and ~ 49 dB when the panels are 3 steps (0.75 m distance) and ~44 dB and ~ 42 dB for 4 steps (1 m distance) away from the wall. In other words, system performance degrades by 22% when the position is more than 0.75 m from the wall; the degradation is only 2 % and 3.5% at distances of 0.25 m and 0.5 m.

Thus there is a conflict in that for best communications system performance LED panels should be close to the wall but conversely for best illumination, should be positioned in the centre of the room. Results are in agreement with [176] which indicated that for best SNR, LEDs should be placed close to the wall as a consequence of inter cell interference. The analysis considered only LOS components in optimising LED placement and cell area design. The analysis here considers NLOS components and placement of the LED panels close to the wall minimises the path loss due to wall reflections especially at poor surface reflectivity (e.g. plastic wall). Placement of the LED panels close to the wall (Figure 5.2(b)) can provide better performance from the communication perspective. However, design guidelines that meet both the lighting and communication requirements are necessary; balanced LED layouts that optimise system performance and fulfil the lighting requirements are discussed later in the Chapter.

### 5.2.2 LED panel layout

LED layout optimization is executed in terms of the average SNR, BER and data rate in the presence of the sunlight over the year under different metrological conditions. The optimum LED layout aims to provide a high QoS for all users in the room whilst fulfilling lighting standards [175].

### 5.2.2.1 Simulation methodology

Performance is analysed over four seasons in representative environments using Monte Carlo simulations. Figure 5.5: describes the methodology to determine optimum placement. The optimisation is constrained by two main requirements; maximising the average SNR across the room at an acceptable lighting illumination (according to EN12464-1standard [100]).

The characterisation considers a range of LED panel placements across a room of any size. A Matlab routine provides the SNR variation across the room within the lighting constraint. However the global optimum provided by this route is not sufficiently robust and results from these nonlinear equations are tested and confirmed [176] through Monte Carlo simulation. The evaluation consumes significant computational time of up to 72 hours/simulation [169].

It is worth noting that a number of optimisation approaches exist. For example, genetic algorithms and pattern search [177, 178] may provide a global optimum for the nonlinear optimisation considering the stated constrains; however those algorithms are sensitive to initial conditions. Further, results from those algorithms yield a global optimum and need extensive verification to ensure that the results are the optimum for the spectrum of conditions and constrains [124, 176, 179].

Although the methodology for the present analysis is specifically developed to consider different design aspects for systems that emulate real scenarios, results have been tested for different constrains to validate the approach. The methodology adopted aims to find the optimum placement of the LED panels in any room size based on an extensive search of placements that provide the highest SNR whilst at the same time meets the illumination constrains. All possible placements of the panels in the room are considered; then all calculated SNRs are searched to identify the optimum placement. A validation function ensures that there are no repeated LED placement coordinates in the results database. The process of verifying the results is presented later in the Chapter.

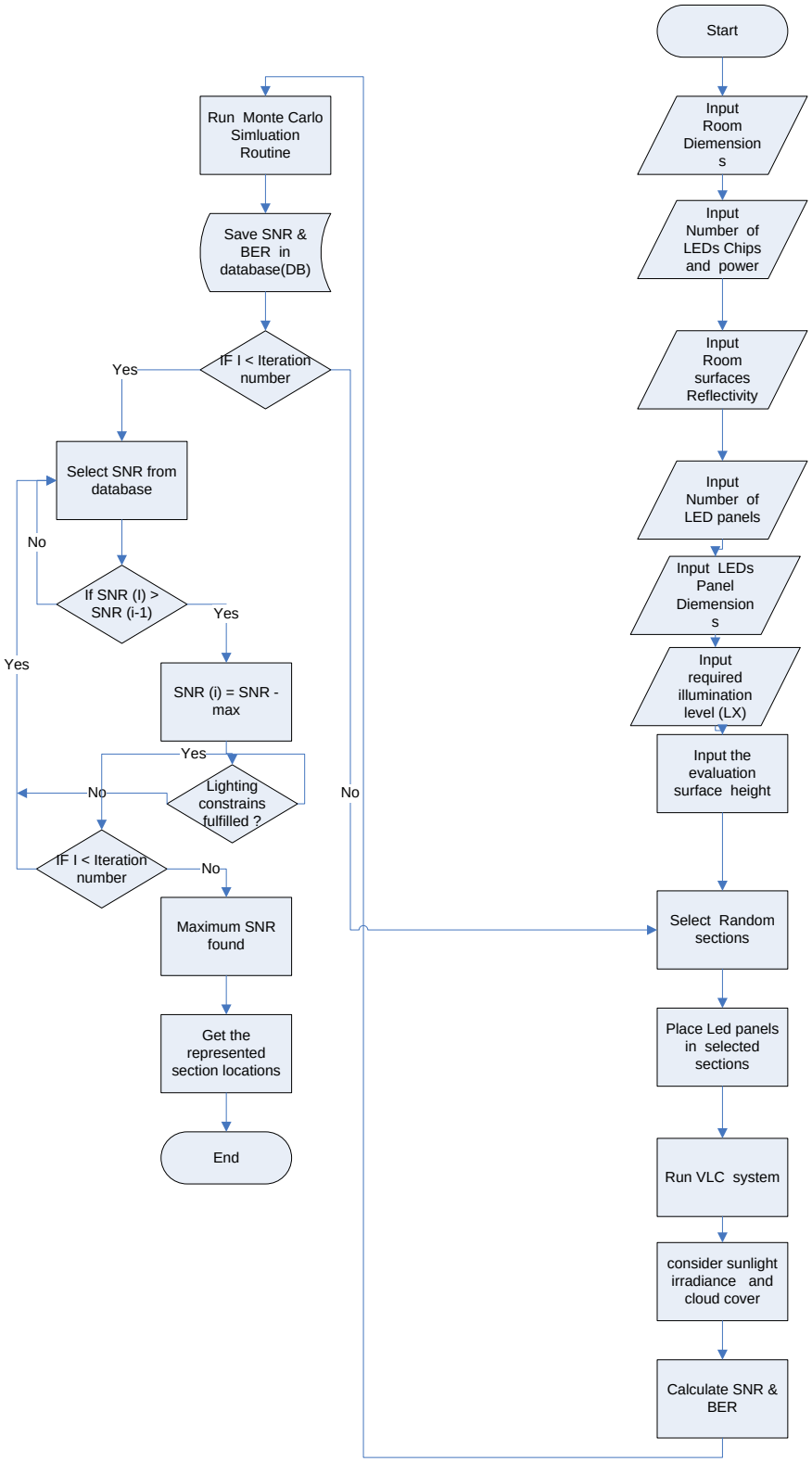


**Figure 5.5: LED layout optimisation methodology.**

The aim is to determine the LED layout that optimises communication performance and minimises the variance of SNR over the room to maintain an acceptable QoS for all users within the room. A user interface is developed to ease the execution of the evaluation (Figure 5.6).

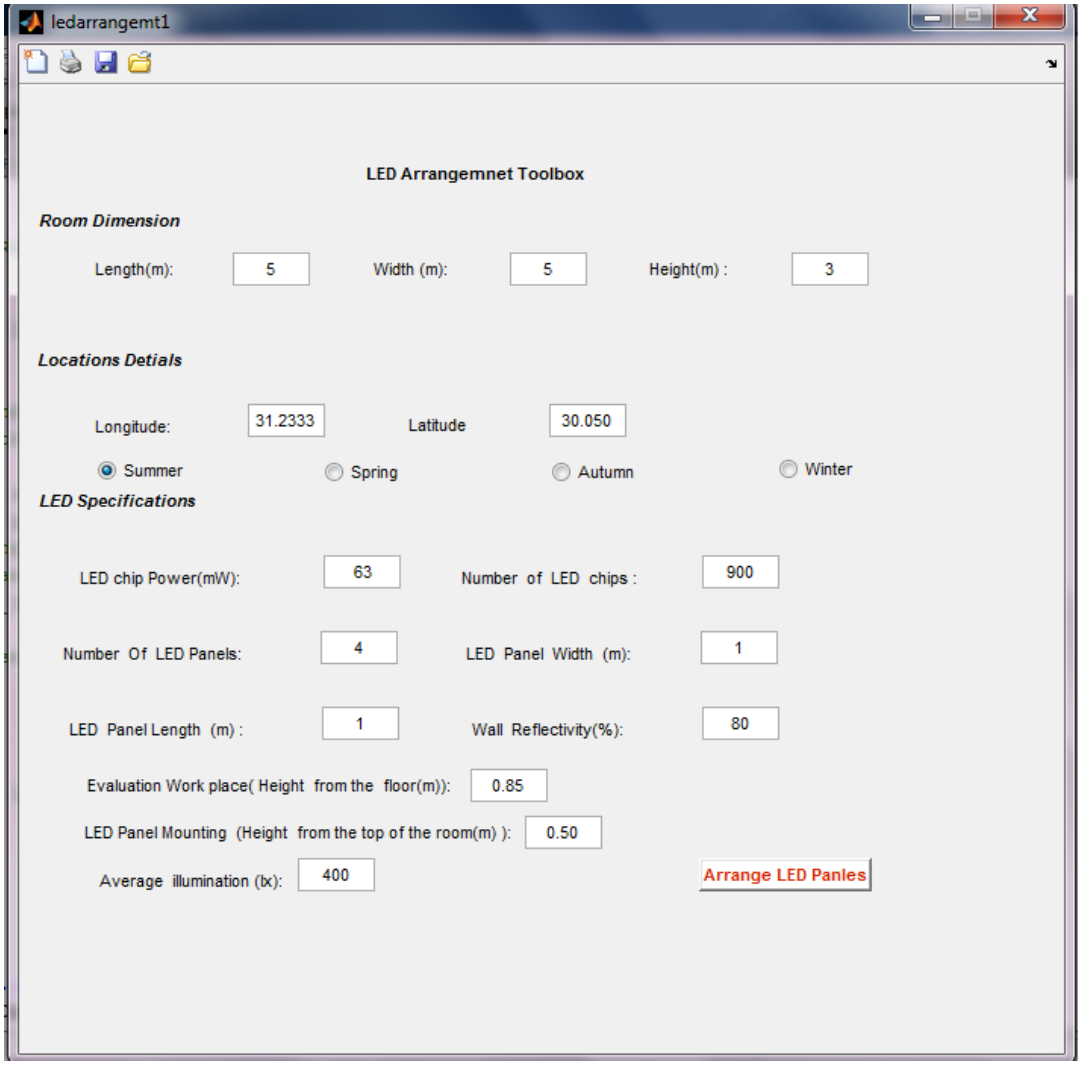


**Figure 5.6(a): User interface - input.**

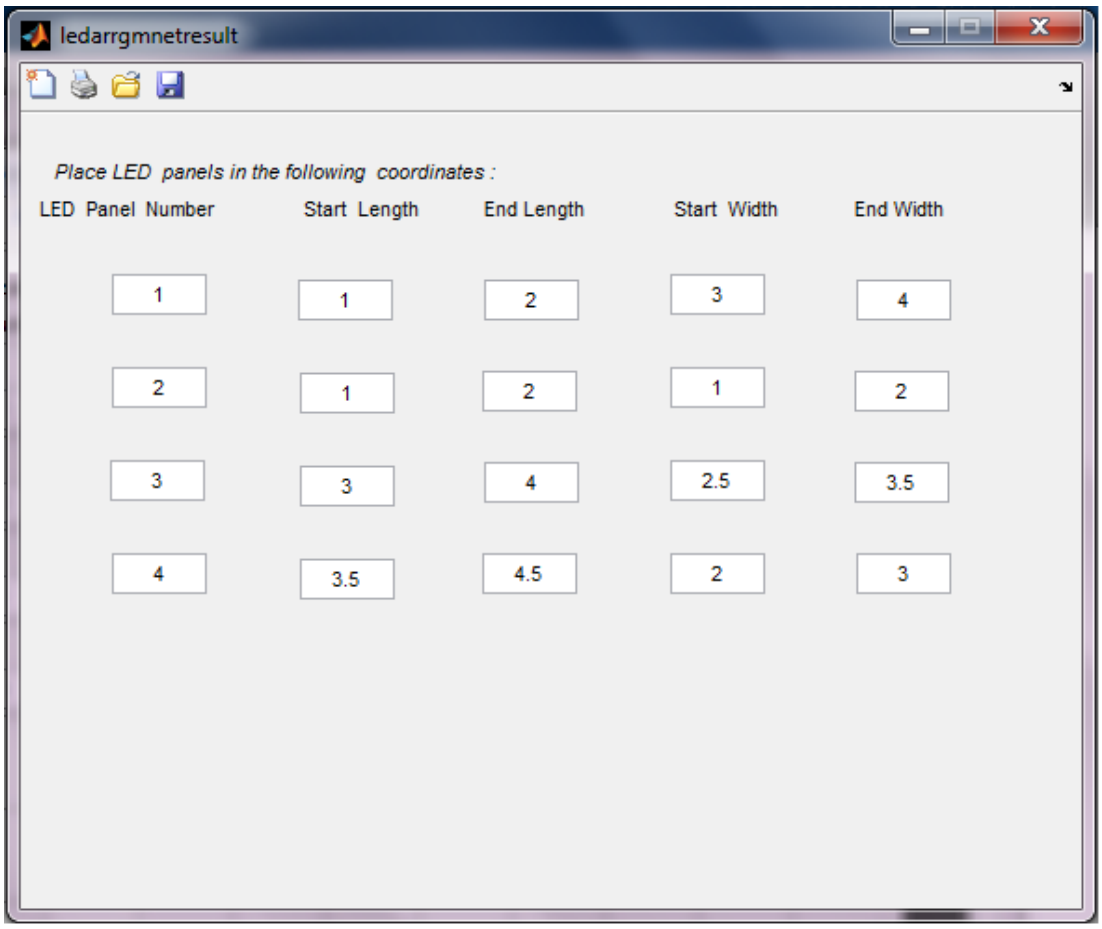


**Figure 5.6(b). User inteface - results.**

The analysis is carried out for a 1 Mbit/s data rate and 0.54 $^{A}/_{W}$ photodiode Responsivity. Simulation parameters are largely the same as in Chapter 4 (Table 5.1) except some modifications are made to enable a meaningful comparison between the results from the adopted methodology and other research work [51].

**Table 5.1: Simulation parameters.**

| System parameter | Value |
|---|---|
| **Photodiode Responsivity** | 0.54 $A/W$ |
| **Data rate ($R_b$)** | 1 Mbit/s |
| **$A_{pd}$( Receiver area)** | 3 $cm^2$ |
| **FOV** | 120 degree |
| **FWHM angle** | 9 degrees |
| **Number of LEDs** | 900 |
| **LED chip Power** | 63 mW |
| **Number of LED Panels** | 4 |
| **Distance between LED chips** | 7 cm |

It is assumed that all LEDs transmit at the same data rate in the same direction and all reflectors are considered as Lambertian. Ceilings are at 0.5 m distance from the top of the room and receivers are at a height of 0.85 m form the floor. Forty nine receivers are uniformly distributed over the coverage area. Any interference between LEDs is neglected. All simulation parameters are derived from commercial off-the-shelf components.

### 5.2.2.2 SNR Performance

The evaluation is carried out over the year for two representative locations, Berlin and Cairo. Summer and winter seasons are considered only; results for the rest of the year are assumed to lie between these extremes. Indicative performance can be derived from the results for autumn and spring presented in Chapter 4.

#### 5.2.2.2.1 Summer

Four LED panels provide the specified illumination level in the range 300 lx - 800 lx as governed by the European standards for indoor workplace lighting EN12464-1 [175]

The average SNR (Figure 5.7 and Figure 5.8) over the room for a Cairo summer - clear sky where the noise owing to sunlight irradiance is at maximum - is in the range of ~ 86 dB -53 dB, ~81 dB - 50 dB for plaster and plastic walls respectively.

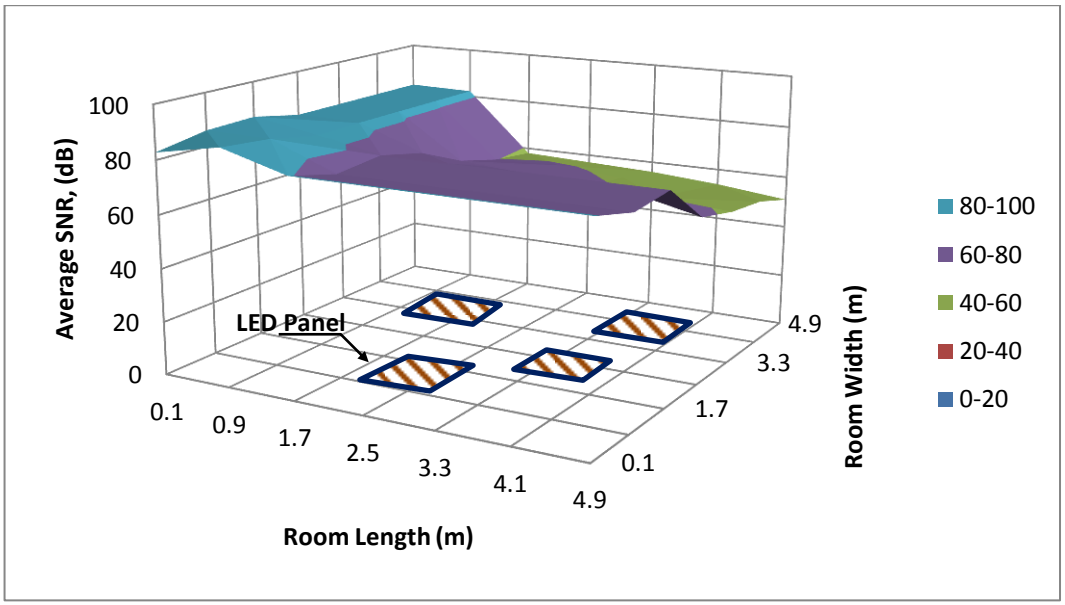


**Figure 5.7: Average SNR for a Cairo summer, clear sky and plaster wall.**

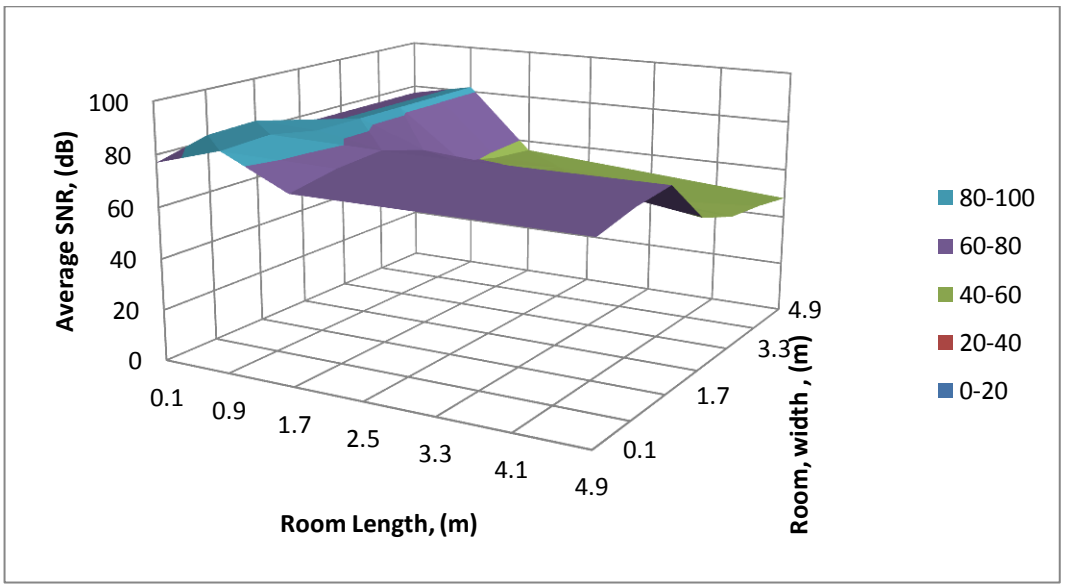


**Figure 5.8: Average SNR for a Cairo summer, clear sky and plastic wall.**

The average SNR increases by 15% when the proposed LED layout is compared to the results of [51] under the same simulation conditions. The maximum average SNR for both LED layouts in [51] is 73 dB and under the same scenario, the SNR improves by ∼15% and ∼10% for plaster and plastic walls. The minimum average SNR is 53 dB in a corner of the room.

Moreover, the luminance level for office environments is stipulated to be 400 lx on average (equal to ∼ 60 dB SNR) over 50 % of the room whilst the remainder of the room should not fall below 100 lx on average; the lighting constraint is fulfilled by the proposed LED layout. Hence the LED layout provides optimised system performance in the presence of sunlight and fulfils the lighting illumination standards.

#### 5.2.2.2.2 Winter

In the winter season, sunlight irradiance is at a minimum, as encountered in Berlin owing to a high percentage of cloud coverage. The average SNR for a Berlin winter lies in the range of ∼ 87 dB - 63 dB and ∼ 82 dB - 54 dB for plaster and plastic walls (Figure 5.9 and Figure 5.10). The SNR improves by ∼17% compared to the results of [51]. As expected, the SNR decreases to ∼ 53 dB for plastic walls due to poorer surface reflectivity. The SNR within the room follows the variation of sunlight irradiance and cloud cover over the year.

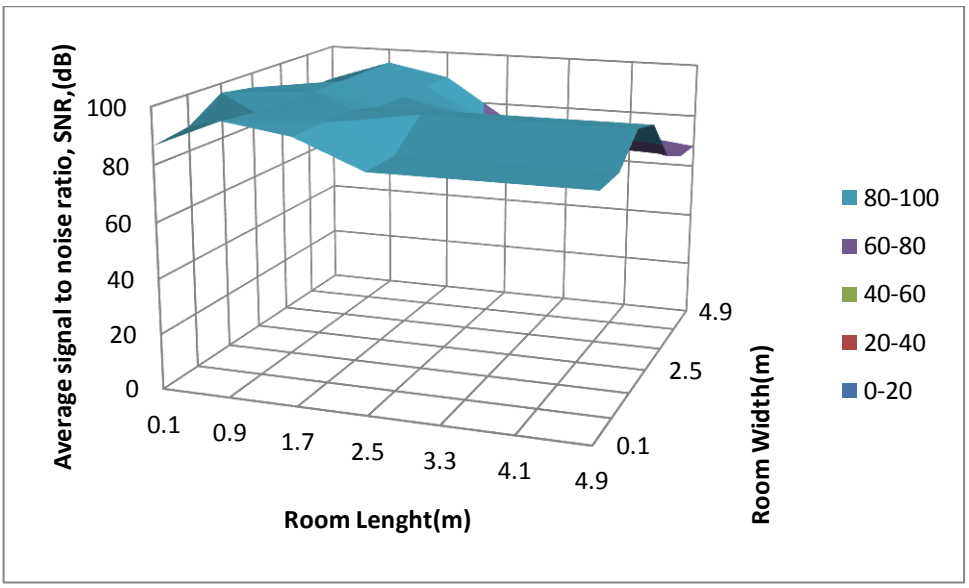


**Figure 5.9: Average SNR for a Berlin winter, cloud sky and plaster walls**.

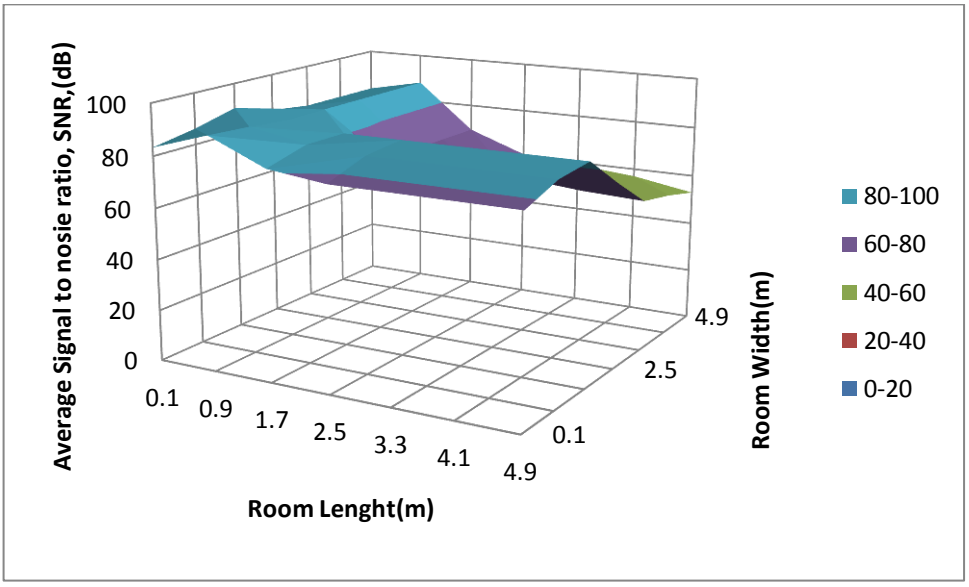


**Figure 5.10: Average SNR for a Berlin winter, cloud sky and plastic walls.**

A comparison of performance as a function of metrological conditions - as represented by Cairo and Berlin - is presented in Figure 5.11 (plaster walls) and Figure 5.12 (plastic walls).

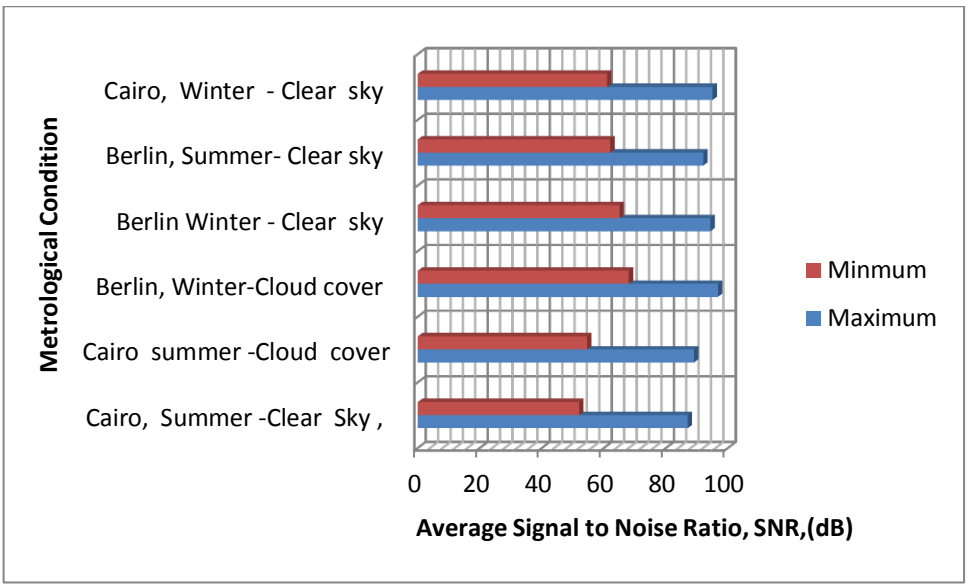


**Figure 5.11: Average SNR for Cairo and Berlin over the year for plaster walls**.

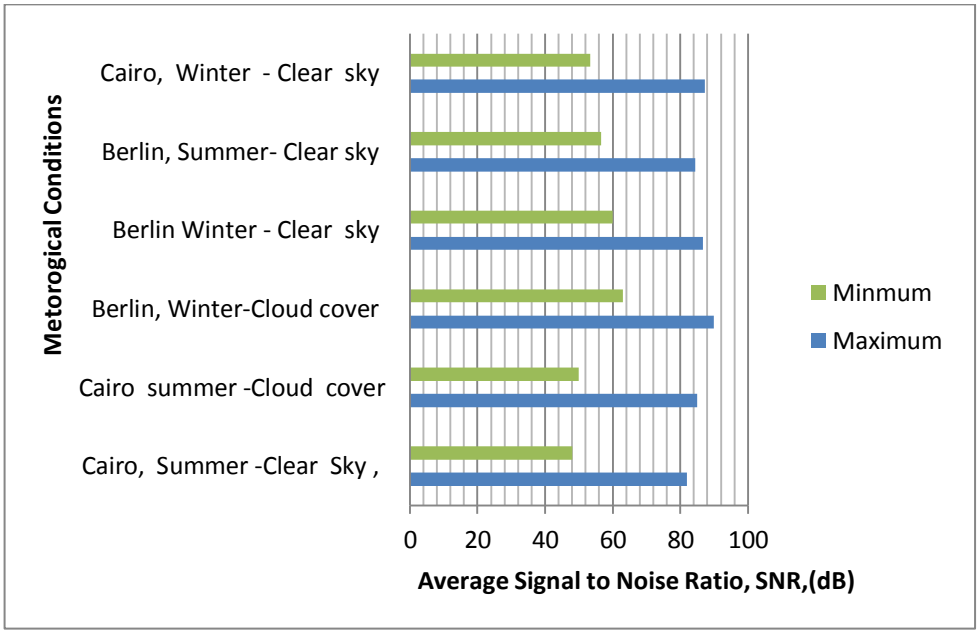


**Figure 5.12: Average SNR for Cairo and Berlin over the year for plastic walls.**

Figure 5.11 and Figure 5.12 summarise the maximum and minimum average SNR for the proposed LED layout. The layout provides an enhancement of system performance compared to the results in [51]; the maximum SNR lies in the range of

~ 96 dB – 68 dB achieved as expected, in Germany for a winter day with significant cloud coverage and plaster walls. The SNR in Cairo is in the range of ~ 87 dB - 52 dB, 89 dB - 54 dB, 95 dB - 61 dB for summer clear sky, summer cloudy sky and winter clear sky respectively. For Berlin, the SNR is in the range of ~ 94 dB - 64 dB and ~92 dB - 62 dB for winter clear sky and summer clear sky respectively. Again, the lighting illumination requirement [175] is fulfilled under all metrological conditions.

The proposed LED layout provides better performance for the same room size, number of LED chip, LED spacing, LED panel dimensions under the same simulation system parameters as in [51]. An enhancement of up to 17% and 10% is achieved compared to results of [51] for plaster and plastic walls. Moreover, the proposed LED layout provides better system performance with a lower number of LEDs than Komine *et al* [25] viz. the former used 1400 LED chips as opposed to the 900 chips in the present study. The same system performance is achieved with a ~ 35% reduction in the number of LED chips illuminating the same size of room directly attributed to an optimised layout and the higher intensity of chips employed [25]. The central luminous intensity of chip employed in [25] was 0.73 cd (20 mW transmitted power) and the employed chip (63 mW transmitted power) has maximum luminous intensity of 9.5 cd.

#### 5.2.2.2.3. Results Validation

The results are verified through two routes; a sensitivity analysis through evaluating the SNR as a function of placement and executing the simulation many times (five times) to validate the repeatability of results. In addition, the parameters and LED placement of reported research [51] is used as input to the adopted methodology to verify results. A 900 LED chip panel is assumed in a 5 m × 5 m × 3 m room and receivers are placed at a horizontal plane. The vertical distance between LED panels and receivers is 1.65 m and LED panels placement are as depicted in Figure 5.13.

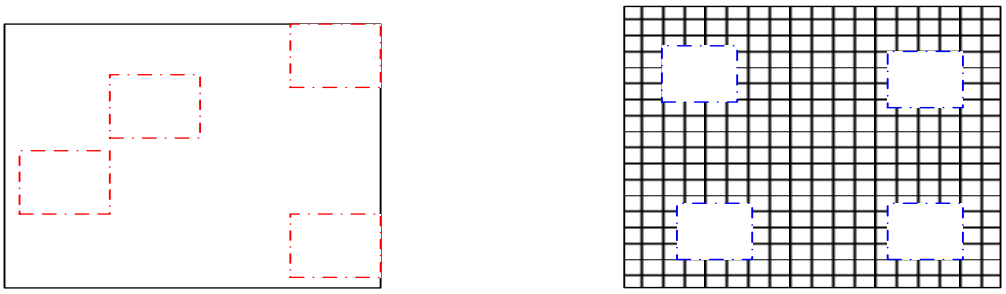

**(a)** **(b)**

**Figure 5.13: LED placement trials.**

The two layouts in Figure 5.13(a) and Figure 5.13(b) are used to verify results whilst fulfilling the stipulated constrains. Testing for a Cairo summer, clear sky scenario reveals that the SNR varies in the range of ~78 dB to ~48 dB when LED panels are at placement position A; at placement position B, the SNR varies in the range of ~68 dB to ~57 dB. The SNR is inferior for both placements in comparison to the optimum performance as captured in Figure 5.7. Multiple simulations runs with different seeds yield consistent results. Moreover, LED panels are moved inward gradually in 0.2 m steps for the Berlin winter scenario to further validate that the LED placement is the optimum; it was found that the SNR varies in the range of ~81.5 dB to ~53 dB in the first step and in the range of ~76 dB to ~44 dB at the second step for plaster walls. In summary, the three methods utilised for validation corroborate consistency in the results.

### 5.2.2.3 Bit Error Rate (BER)

The BER is evaluated using the same LED layout and simulation parameters for the two representative locations over the year in order to map the boundaries of system performance over different metrological conditions.

#### 5.2.2.3.1 Summer

During the summer season, sunlight irradiance is at its highest intensity and thus the BER falls within the range $10^{-21}$ to $10^{-12}$ for plastic walls (Figure 5.14).

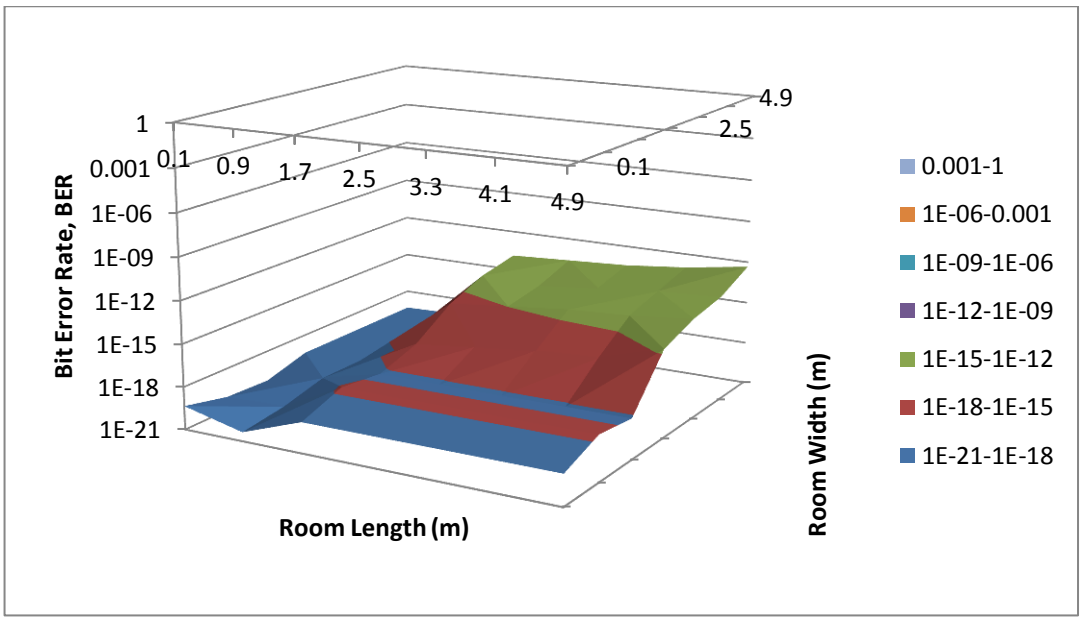


**Figure 5.14: BER performance for a Cairo summer, clear sky and plaster wall.**

The BER decreases to the range of $10^{-20}$ to $10^{-11}$ for plastic walls owing to reduced surface reflectivity (Figure 5.15). As expected the lowest BER corresponds to the sunlight irradiance at the highest level. It is worth noting that;

- LED layout placement is chosen to maximise the SNR
- the room is equipped by 900 LED chips to provide acceptable lighting levels ensuring all users are able to read/write across the space
- the lighting requirement is a key factor in attainable performance. The 400 lx illumination decreed by standards must service 50% of the room area (minimum)

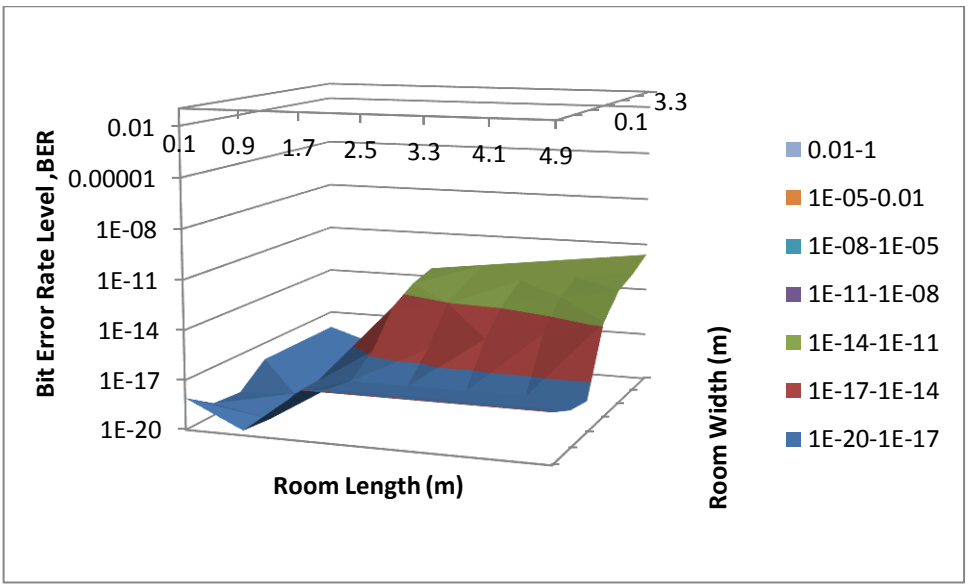


**Figure 5.15: BER performance for a Cairo summer, clear sky and plastic wall.**

### 5.2.2.3.2 Winter

The sunlight irradiance in a winter season is weak especially when cloud coverage is significant. As expected, the BER improves compared to results for the same system configuration during summer. The BER lies in the range of $10^{-23}$ to $10^{-15}$ (Figure 5.16) across most of the room for plaster walls.

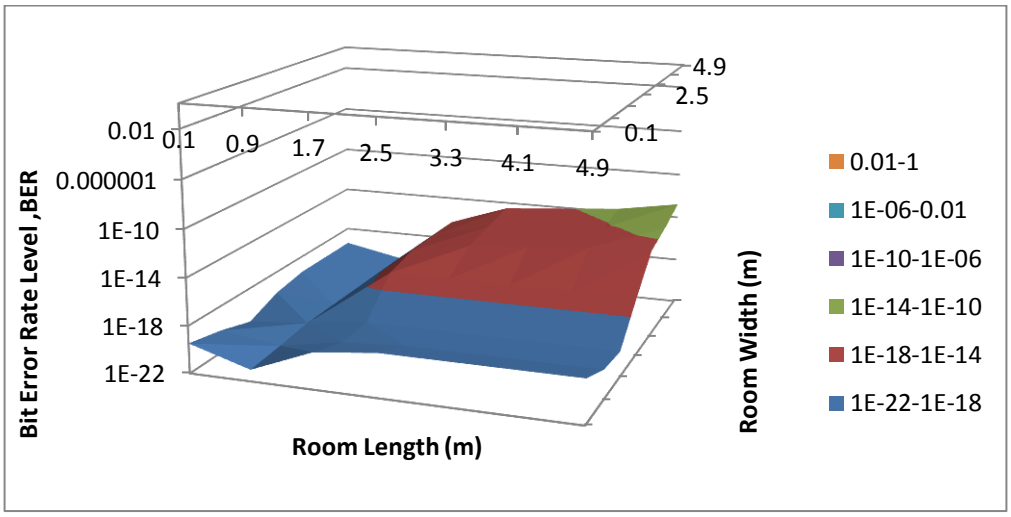


**Figure 5.16: BER performance in Berlin winter, cloud cover and plastic wall.**

The BER is in the range of $10^{-22}$ to $10^{-13}$ (Figure 5.17) for plastic walls. System performance degrades at higher data rates due to ISI and sunlight irradiance.

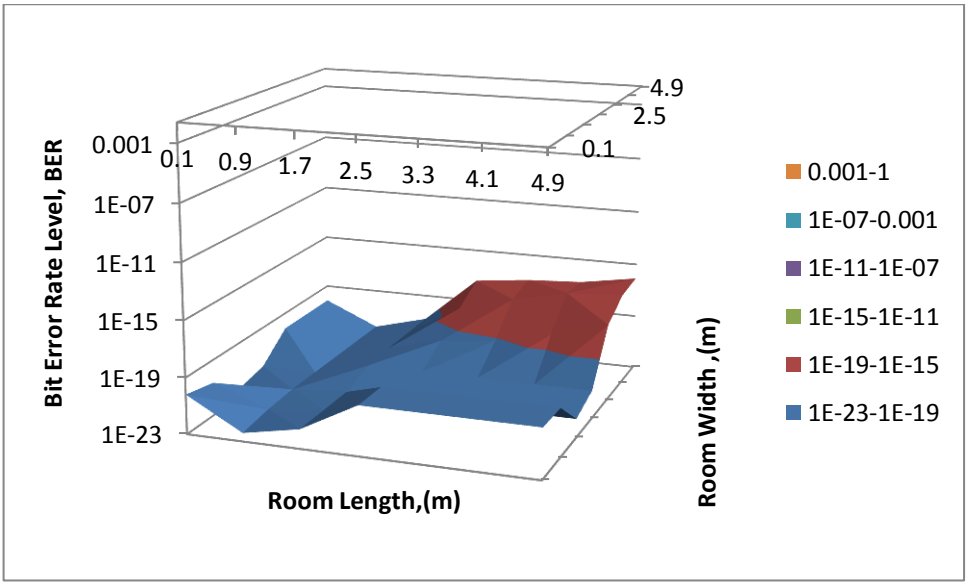


**Figure 5.17: BER performance in Berlin winter, cloud cover and plaster walls.**

### 5.2.2.4 Data Rate

The attainable data rate is one of the key metrics that distinguish system performance; thus the performance of the system is evaluated as a function of data rate through the arithmetic mean of the BER across the room. The scenarios considered are as above - winter (cloudy sky) and summer (clear sky) - and the results are presented in Figure 5.18, Figure 5.19, Figure 5.20 and Figure 5.21.

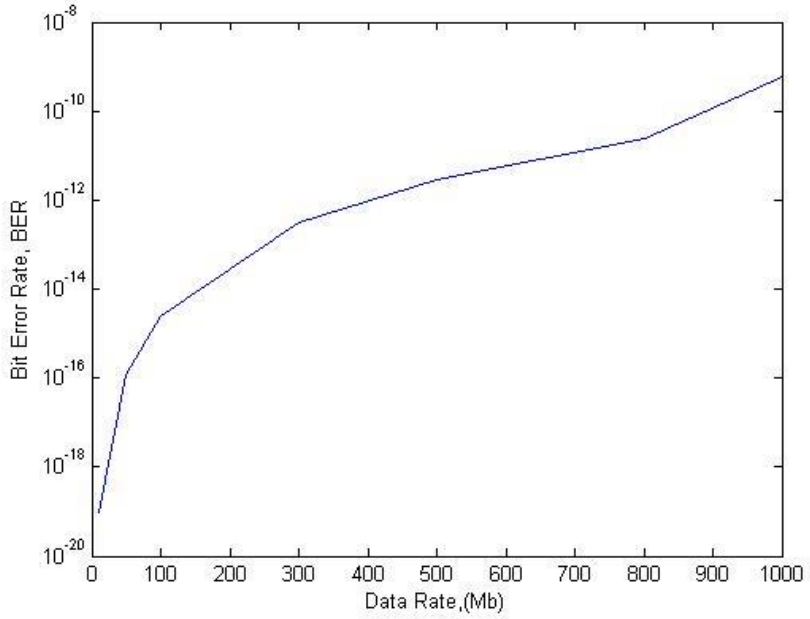


**Figure 5.18: BER as a function of data rate for a Berlin winter, cloudy sky and plaster wall.**

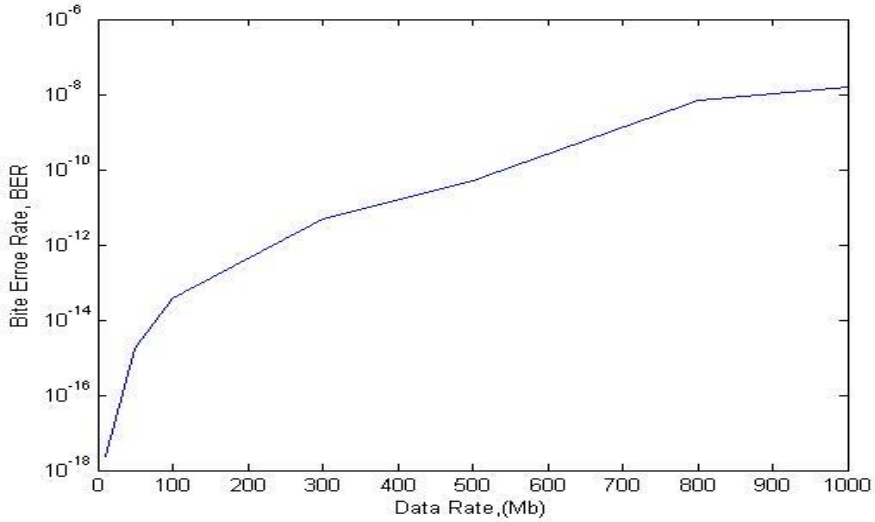


**Figure 5.19: BER as a function of data rate for a Cairo summer, clear sky and plaster wall.**

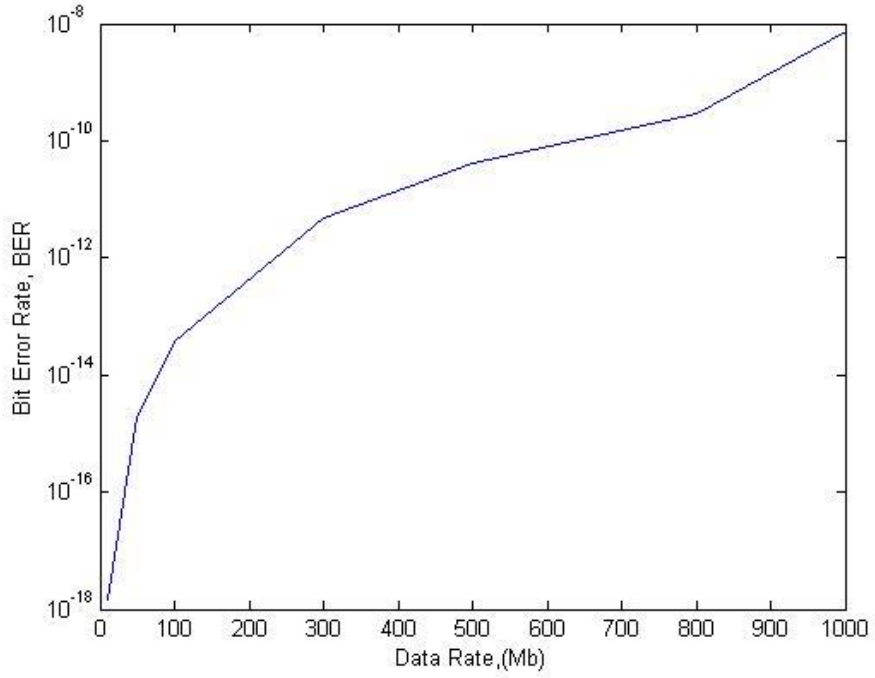


**Figure 5.20: BER as a function of data rate for a Berlin winter, cloudy sky and plastic wall.**

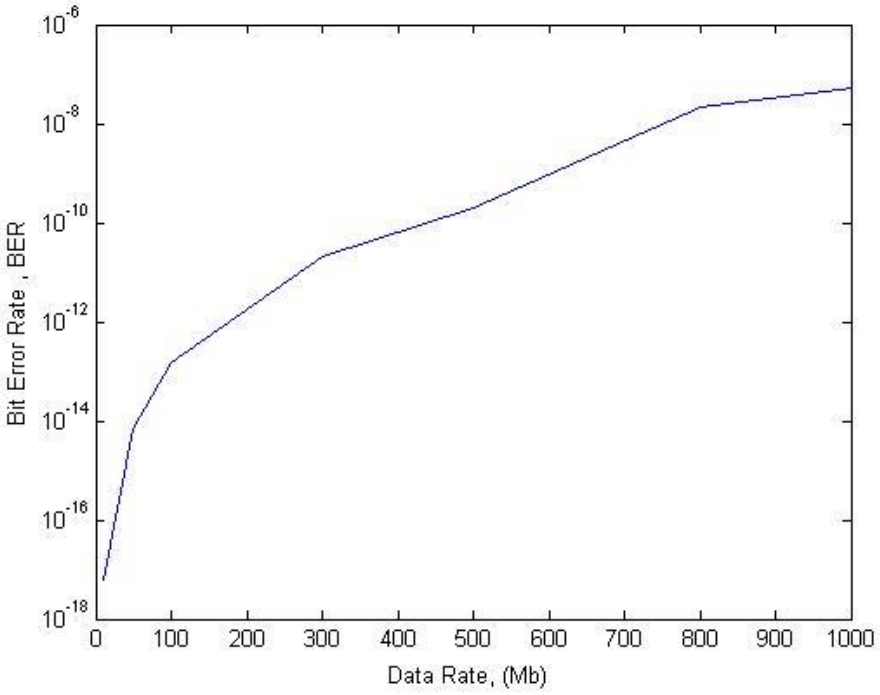


**Figure 5.21: BER as a function of data rate for a Cairo summer, clear sky and plastic wall.**

The BER varies between $10^{-18}$ to $10^{-9}$ and $10^{-17}$ to $10^{-8}$ during winter and summer for plaster walls; for plastic walls, the BER falls to between $10^{-18}$ to $10^{-8}$ and $10^{-17}$ to $10^{-6}$ for the two metrological conditions.

The BER is enhanced compared to the results of analysis in Chapter 4 due to a number of factors; higher LED luminance, greater number of LED chips (900 LEDs as opposed to 400 LEDs in earlier analyses), receivers are placed on desks (at 0.85 m height) not on the floor and LED layout is different.

### 5.2.3 SNR

In order to investigate the performance for large office rooms comprising a significant number of windows, receivers are placed on a horizontal plane (at 0.85 m height) represented as 'red circles' in Figure 5.17. The methodology detailed in Section 5.2.2.1 is adopted to determine the optimum LED layout for maximum SNR with the lowest variation across the room whilst meeting the room lighting standard. The symmetric LED layout provides balanced illumination for all users over the room and in turn facilitates the implementation of the VLC overlay.

The simulation assumes that 25 LED panels (Philips Core View [180]) emitting a total of 47 W are deployed for such a big room to meet the lighting standard. LED panels are mounted on the ceiling distributed symmetrically (Figure 5.1). Photodiode receivers (represented in red circles) are placed on the desk at a height of 0.85 m from the floor and the simulation parameters are as summarised in Table 5.2.

**Table 5.2: Simulation parameters for a 12 m × 12 m × 3 m room.**

| System Parameter | Value |
|---|---|
| **Photodiode Responsivity** | 0.54 $A/W$ |
| **Data Rate ($R_b$)** | 1 Mbit/s |
| **$A_{pd}$** | 3 $cm^2$ |
| **FOV** | 120 degrees |
| **FWHM** | 9 degrees |
| **Initial LED Luminaire Efficiency** | 72 lm/W |
| **LED Panel Power** | 47 W |
| **Number of LED Panels** | 25 |
| **Distance between LED Chips** | 3 cm |

The distance between neighbouring LED chips in each panel is set to 3cm following [176]. In order to meet the standard, the illumination is greater than 400 lx. A symmetrical layout with LED panel in the centre minimises the variation of system performance across the room whilst providing balanced lighting and quality of experience. The room is assumed to be clutter-free and the analysis is therefore confined to a new or renovated space. The proposed LED layout is depicted in Figure 5.22.

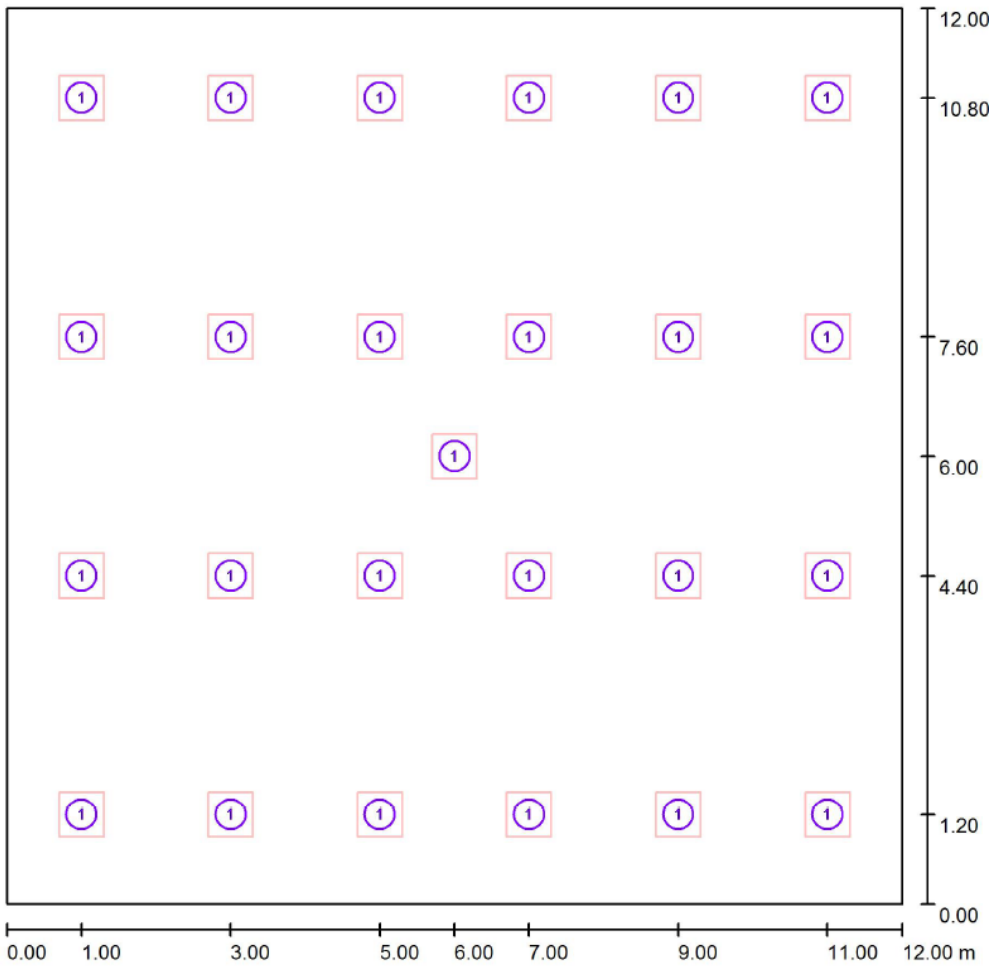


**Figure 5.22: LED layout in a 12m ×12m×3m room.**

### 5.2.3.1. Room Lighting

Illumination within the room is the primary, essential function of the system and in this case, a minimum of 400 lx is required for read and write across the room. Figure 5.23(a) shows the illumination distribution isolines across the room. For the room under evaluation and for the proposed LED layout to provide sufficient illumination for workspace, a minimum illumination of 420 lx is required in order to meet the lighting standard [175]. The ‘squares’ are the projection LED panels locations on the ceiling (Figure 5.23(b)).

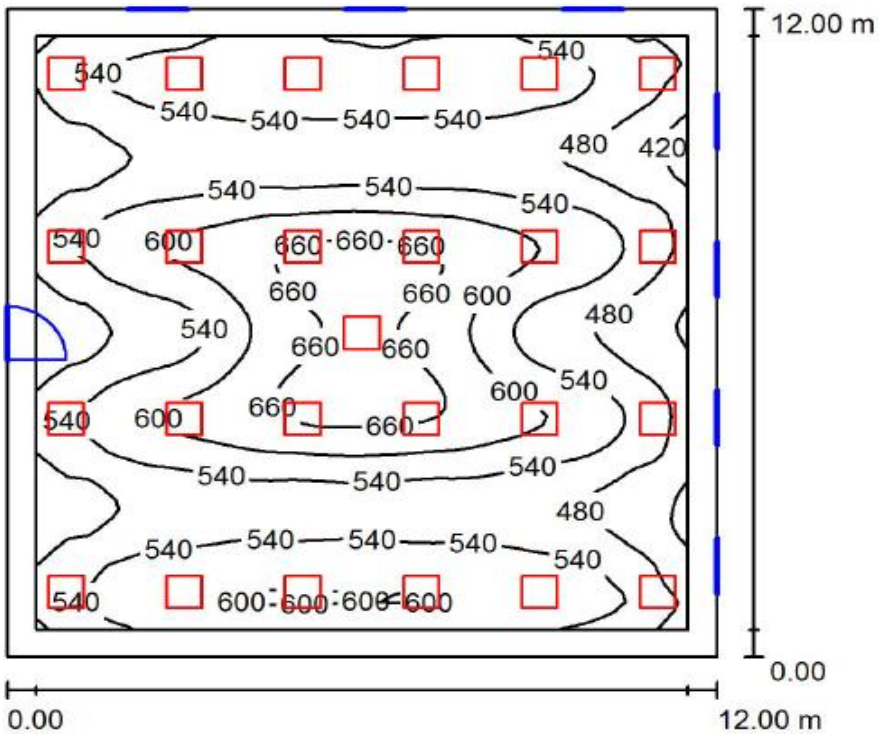


**Figure 5.23(a): Illumination isolines across a 12m×12m×3m room.**

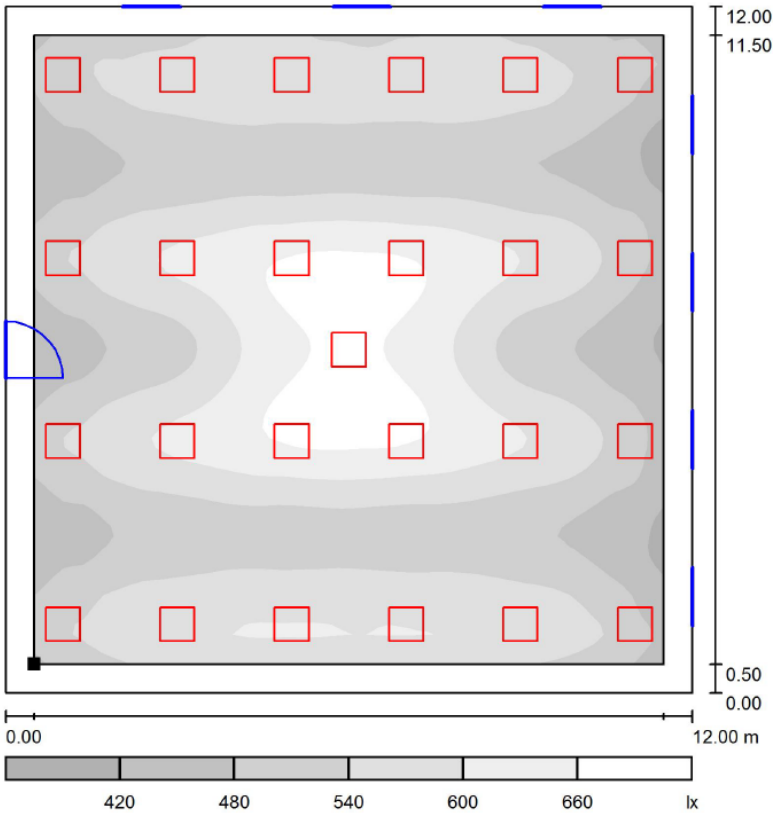


**Figure 5.23(b): Illumination grey scale across a 12m×12m×3m room.**

### 5.2.3.2. SNR

The SNR is evaluated following the methodology used for a standard room. A symmetric LED layout is assumed and 81 receivers (photodiodes) are uniformly distributed over the working desk area.

The average SNR is in the range of ~94 dB - ~75 dB and ~ 89dB - ~ 64 dB during a Cairo summer, clear sky for plaster (Figure 5.24) and plastic walls; and varies in the range ~98 dB - ~79 dB and ~92dB - ~68 dB during a Berlin winter, cloud cover for plaster (Figure 5.25) and plastic walls respectively.

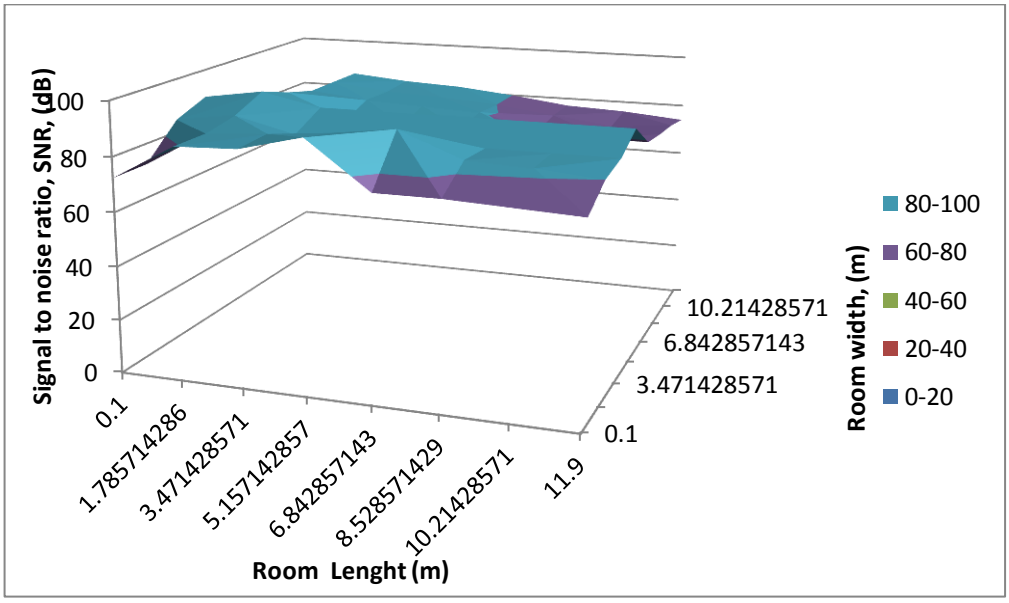


**Figure 5.24: Average SNR for a Cairo summer, clear sky and plaster wall (12 m × 12 m × 3 m room).**

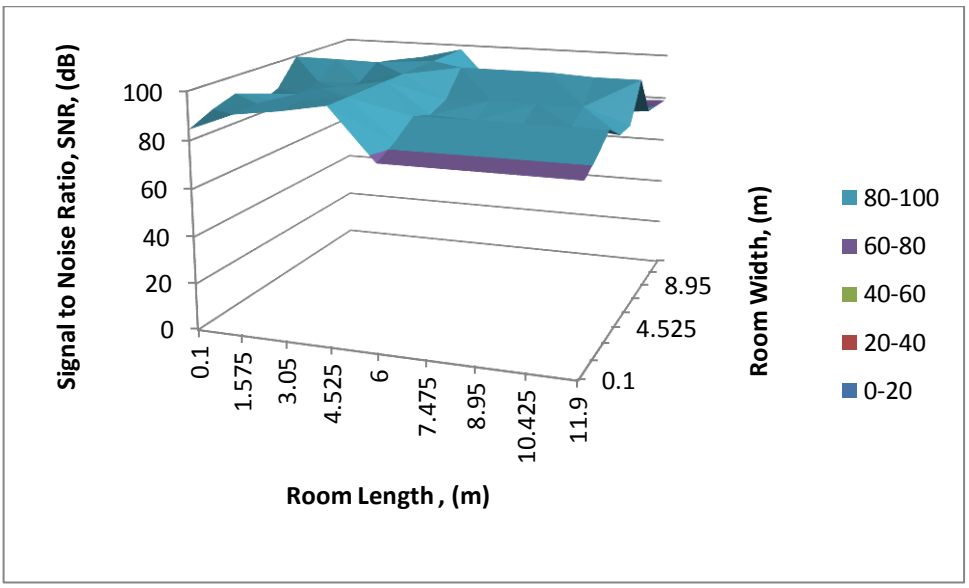


**Figure 5.25: Average SNR for a Berlin winter, cloudy sky and plaster wall (12 m × 12 m × 3 m room).**

The SNR variation across the room is more significant compared to the results for the smaller, 5 m × 5 m × 3 m room. Due to the added constraint of minimising the SNR deviation across the room, [176] concluded that LED panel locations close to the wall provide better communication system performance however at the expense of compromised illumination and vice versa. Here the methodology provides a balance from both the lighting and communications systems perspectives

The LED layout design aims to optimise system performance with three main constrains;

- SNR maximisation
- fulfilment of illumination standard for the room; according to the indoor illumination standard [175], at least 50% of the room must be illuminated at the minimum level of 400 lx
- SNR variation across the room is minimised

The proposed LED layout provides many competitive advantages compared to other reported results in the area. The optimisation can be applied to different room size

[75, 76], considers the impact of sunlight irradiance, cloud cover and metrological condition hitherto not investigated rigorously. The approach treats two often competing goals to provision standard lighting overlaid with high data rate connections [74]. LOS and NLOS paths up to the fifth reflection are also considered [75, 83, 176] as well as representative wall surfaces.

The characterisation informs VLC system design guidelines for any room size utilising commercial off-the-shelf components not limited by the number of LED constellations and placements [51].

## 5.3. Field-of-View (FOV)

A high QoS is one the main customer requirements for any wireless communication system. In the case of VLC systems, FOV is one of the main parameters of the receiver specification that aids in the optimisation of system performance under different operational scenarios and metrological conditions.

The characterise the impact of FOV, a VLC system is evaluated within an empty 6 m × 6 m × 3 m room comprising 8 LED panels on the ceiling directed towards 49 photodiode receivers distributed uniformly in the floor. All LEDs have a 60 degree half -transmitting power profile and all other system parameters are as stated in Table 5.3. The LED is assumed to be the OSRAM LCW W5AM [181], LOS and NLOS paths and average surface reflectivity ~0.8 (plaster wall) are considered in the evaluation.

**Table 5.3: Simulation parameters for FOV analysis.**

| System parameter | Value |
|---|---|
| Photodiode Responsivity | 0.54 $A/W$ |
| Data Rate ($R_b$) | 100 Kbit/s |
| Physical Photodiode Area $A_{pd}$ | 1 $cm^2$ |
| FOV | 120 degrees |
| FWHM | 9 degrees |
| Initial LED Luminaire Efficiency | 76 Lm/W |
| Drive Current | 50 mA |
| Number of LED Panels | 8 |
| Distance between LED Chips | 5 cm |

System performance is simulated as a function of FOV in 5 degrees steps. The average SNR as a function of FOV for a Cairo, clear sky condition for a 6 m × 6 m × 3 m room is shown in Figure 5.26 and an office of 12 m × 12 m × 3 m size in Figure 5.27. A small increase in receiver FOV has no significant impact on performance. The relative change in performance with each step is incremental, ~1.5% of the average SNR within the room. The average SNR increase up to a FOV nearly equal to double the transmittance half angle is negligible; however the average SNR is improved by 36% when the FOV is at ~165 degrees (Figure 5.26). The relatively intense LED illumination required for lighting the room has a strong beneficial impact on system performance even with the significant noise level owing to sunlight during the summer and an extremely wide FOV, especially if the receiver is away from the window or door. The recommendation is to use as wide a FOV as possible.

The results for the larger room (12 m × 12 m × 3 m) with the same number of LEDs (Figure5.27) indicate that the relative increase of the average SNR is ~3.3% for each 5 degree FOV increment. For an extremely wide FOV (165 degrees), the performance increases by ~55% relative to the narrow FOV value of 65 degrees (equivalent to the half power transmittance LED angle).

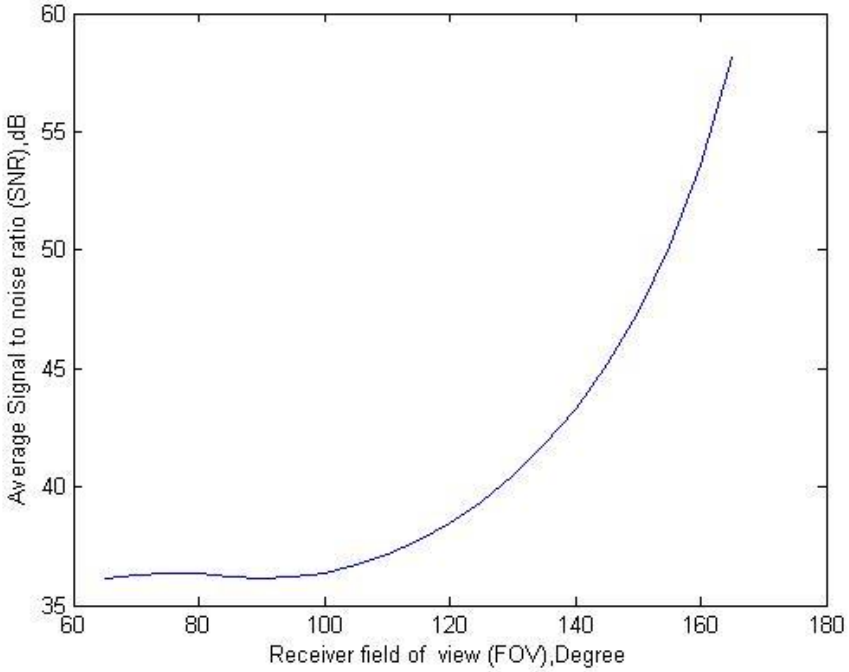


**Figure 5.26: Average SNR as a function of FOV in a 6 m × 6 m × 3 m room for Cairo, clear sky.**

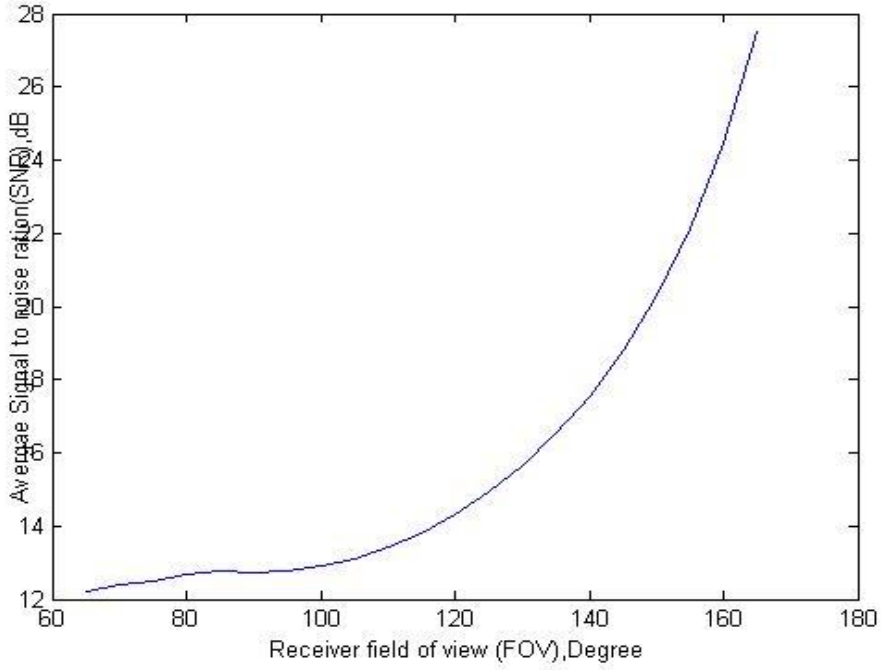


**Figure 5.27: Average SNR as a function of FOV in a 12 m × 12 m × 3 m room for Cairo, clear sky.**

Small increments of the FOV do not yield significant beneficial impact on system performance; however, any small decrement of the FOV to below the half power transmittance LED angle leads to system degradation. In environments with low sunlight irradiance, the recommendation is the set the FOV to an extremely wide setting to provide improved QoS and the receiver should be placed at a certain distance away from the window or door (source of sunlight irradiance), a factor discussed later in this Chapter.

## 5.4 Lights 'on'

VLC transmits information only when the primary function of lighting is active. Recent evolutions have incorporated intelligence into the lighting system in terms of energising the illumination only if the room is occupied, in so doing preserving energy. Furthermore lighting is often switched off if sufficient daylight is available. Thus for connectivity the illumination must be kept 'switched-on' and therefore the energy consumed for communication purposes is a 'not for free' penalty to the gains achieved in moving to solid state lighting.

Thus in general terms, the illumination is turned on no matter the level of natural light as long as there are users inside the room and in some scenarios, the illumination may be on to maintain the communication link even if there are no user inside the room. Relatively recent research [115] has proposed hybrid system implementations using the visible light band in tandem with IR links or a mix between VLC and current Wi-Fi links. However, those proposals are not applicable in environments sensitive to RF interference. In this context, this section investigates the trade-off between energy consumption and system performance in the presence of the sunlight.

A 6 m × 6 m × 3 m room equipped with 4 LED panels (Phillips Core View [180]) each emitting a total power 47 W and receivers uniformly distributed at horizontal plane at 0.85 m from the floor in considered (Figure 5.28). The aim is to determine the total number of LED chips that can provide acceptable system performance.

In the previous section, the average SNR is optimised through the most appropriate layout of panels taking into consideration the lighting standard. In this case, the lighting constraint is neglected as the evaluation centres on the case where natural sunlight illumination is sufficient for user needs and/or there are no users in the room. In both cases the lower the number of LED panels employed, the better the energy consumption, especially relevant to geographies that enjoy sunshine throughout most of the year, suffer from energy shortfalls and follow roadmaps to adopt energy efficient principles.

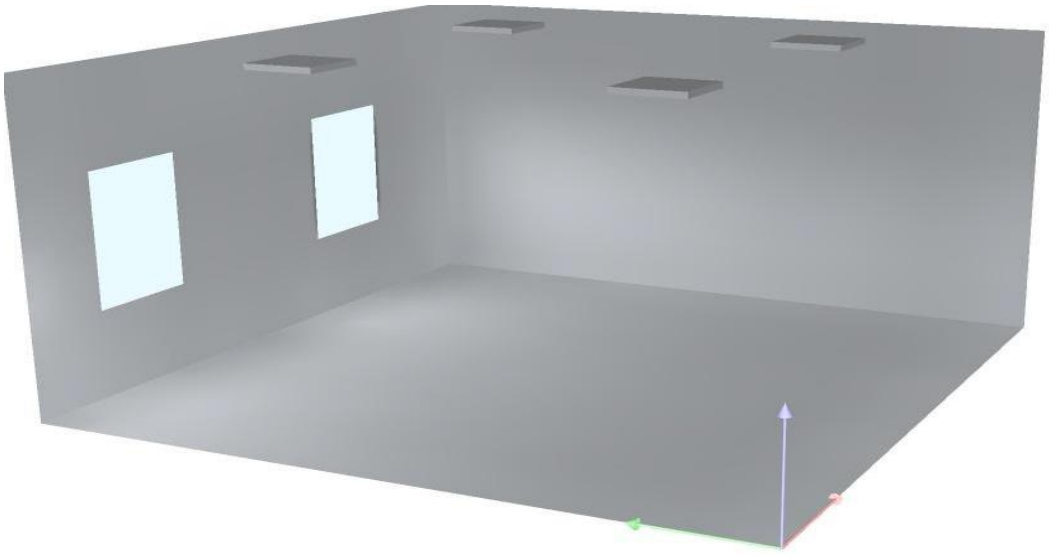

**Figure 5.28: Room under evaluation.**

Any building design must consider window area and an adopted requirement is to incorporate at least 10% of the area for windows [163] for natural light. The distance between receiver location and the source of natural light is thus considered to optimise system performance as a function of receiver location within the room.

### 5.4.1 Distance from a Window

The evaluation is conducted for a Cairo summer day, clear sky at noon when sunlight irradiance is at maximum intensity. Figure 5.29 shows the isolines across the room at

a 0.85 m height. Results indicate that sunlight intensity decays away from the window in the direction of the room centre. The mapping of intensity starts at a distance of 0.5 m from the wall in 0.25 m steps.

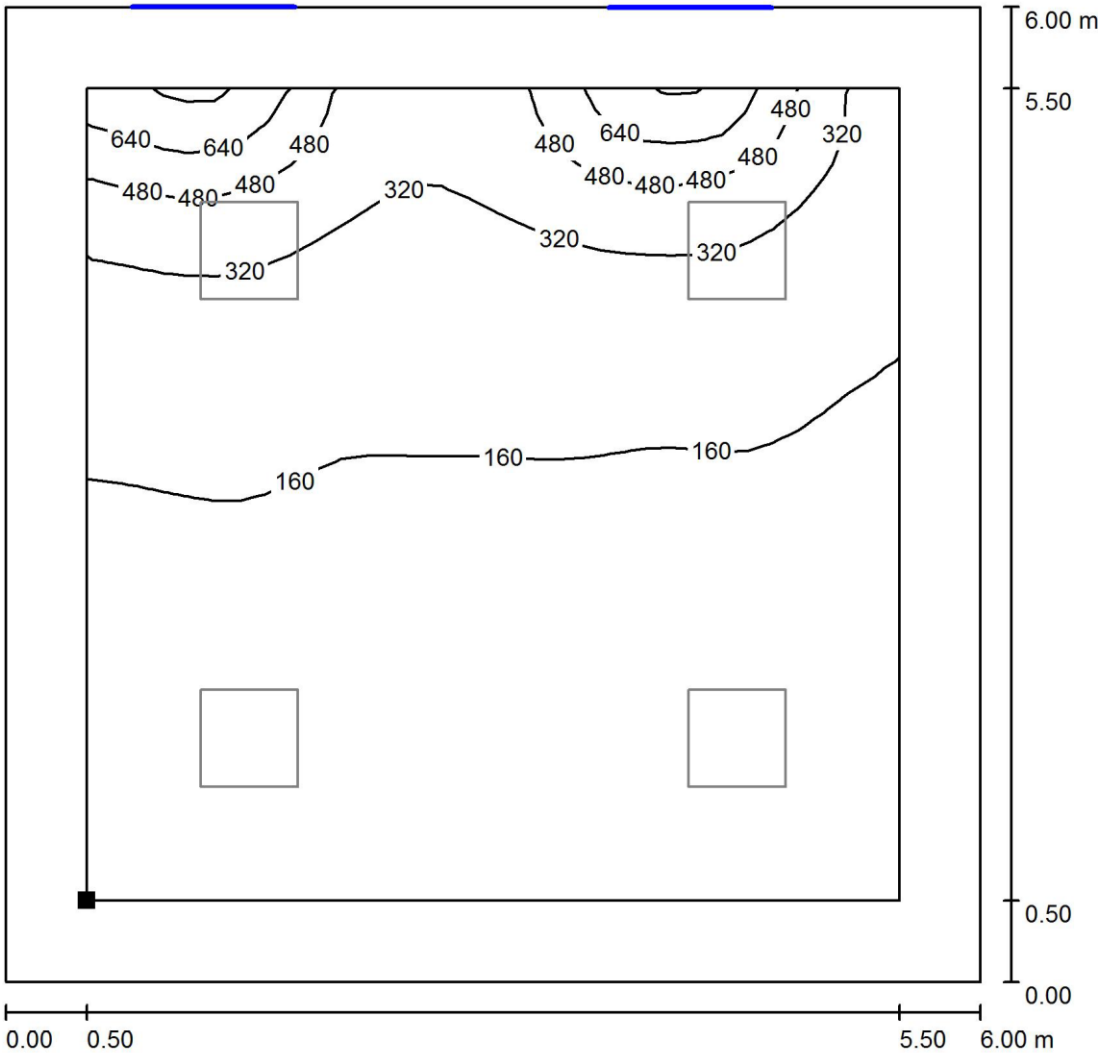


**Figure 5.29: Isolines for a daylight scenario for a Cairo summer.**

The simulation is conducted using Dialux software [182], showing that daylight reduces in intensity by 25% for each step. At a distance 1.25 m from the window, sunlight irradiance reduces by 50% compared to the irradiance at distance 0.5 m; irradiance reduces by 25% at a distance 0.5 m from the window. From the above mapping, the recommendation is to place receivers at a 1.25 m distance from the

window. Furthermore, receivers at a distance less than 1 m to the window should be set to a narrow FOV and directed towards the centre of the room if maximum value is to be derived from LOS paths.

### 5.4.2 SNR as a function of the Number of Transmitters

The SNR performance is evaluated as a function of the number of LED, neglecting the lighting constraint. In addition the assumption is that there are no users inside the room, there is sufficient daylight illumination and users do not to switch off the lighting. The goal is to minimise the number of LEDs that need to be energised to maintain an acceptable communication link and in so doing minimise energy consumption. A user interface is developed to simplify the execution of the evaluation (Figure.5.30).

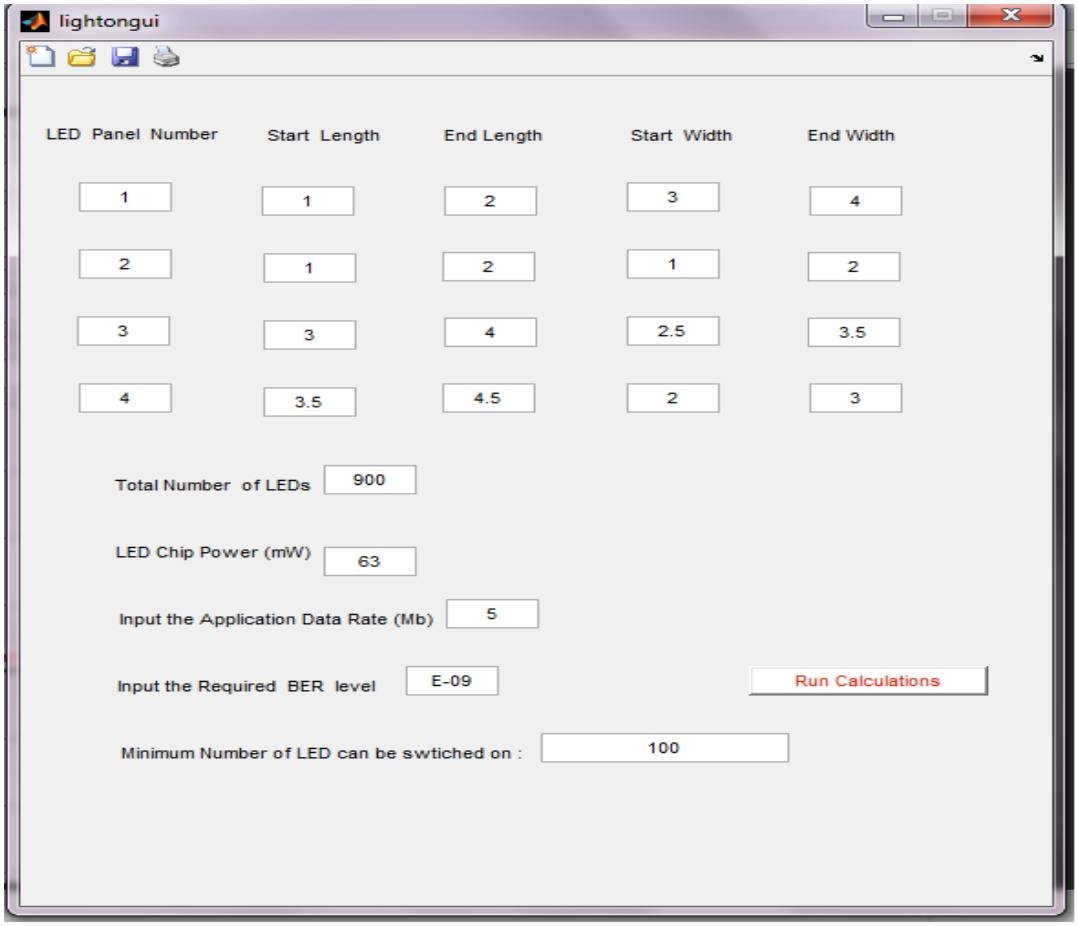


**Figure 5.30: User interface - lights 'on'.**

The evaluation is conducted for the system specification detailed in Section 5.2.2.2 at a 1 Mbit/s data rate for the two extreme environmental conditions.

### 5.4.2.1. Summer

The analysis during summer time corresponds to high levels of sunlight irradiance. The impact of the sunlight on performance is relaxed compared to previous scenarios owing to the distance to the window as discussed in Section 5.4.1. The arithmetic mean of the average SNR over all receivers distributed over the coverage area is calculated as a function of the total number of LEDs in the room. The average SNR is ~27 dB,~30 dB, ~31 dB, ~33 dB and ~36 dB for a plaster wall as the number of LED chips rises from 36, 64, 100, 144 to 196 (Figure 5.31).

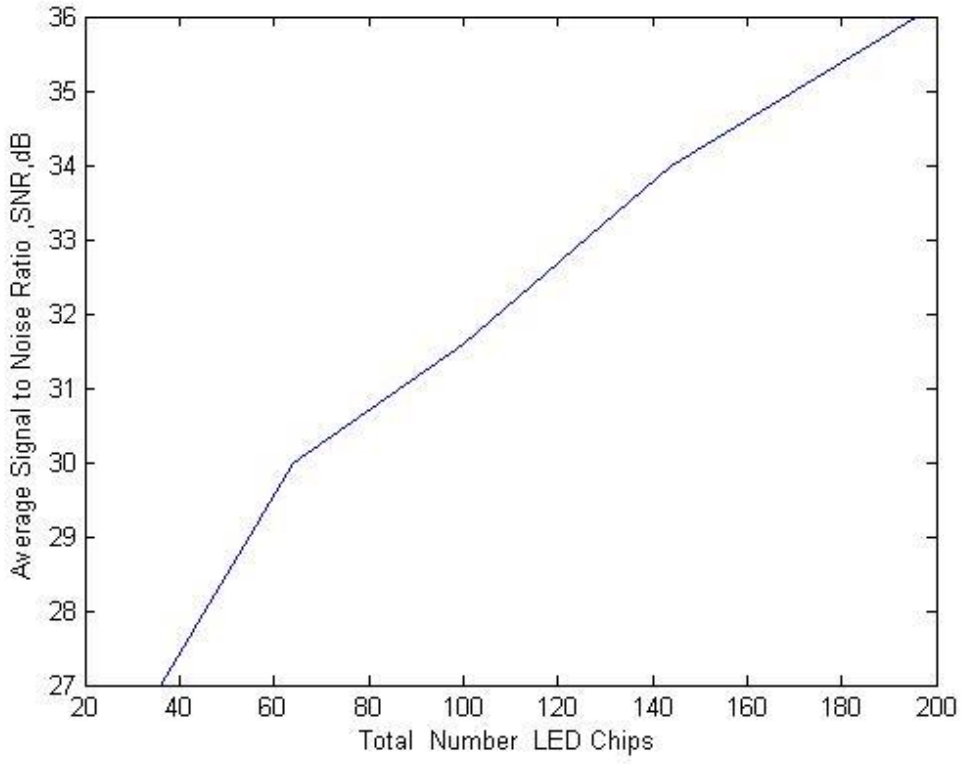


**Figure 5.31: Average SNR as a function of the number of LED chips for a Cairo summer.**

The average SNR is evaluated at a 1Mbit/s data rate and an acceptable BER ($10^{-9}$) is obtained for 196 LED chips. In the other words, it is possible to provide acceptable SNR, BER performance at this specified data with 21% of the total number of chips (in this case 900 LEDs) (Section5.2.2.2) in all scenarios whether users occupy the room or not; thus a 79% reduction in the energy consumption results.

### 5.4.2.2. Winter

For a Berlin winter, the average SNR is ~30 dB, ~33.5 dB, ~35.8 dB, ~38 dB and ~40 dB for a plaster wall as the number of LED chips rises from 36, 64, 100, 144 to 196 (Figure 5.32). The average SNR is better than for the Cairo summer case. Now an acceptable $10^{-9}$ BER can be achieved with only 11% of the total number of LED chips used in the scenario described in Section 5.2.2.2. Thus a 1 Mbit/s data rate communication link can be operated at a 89% energy saving compared to when all LED chips (900 LEDs) are energised.

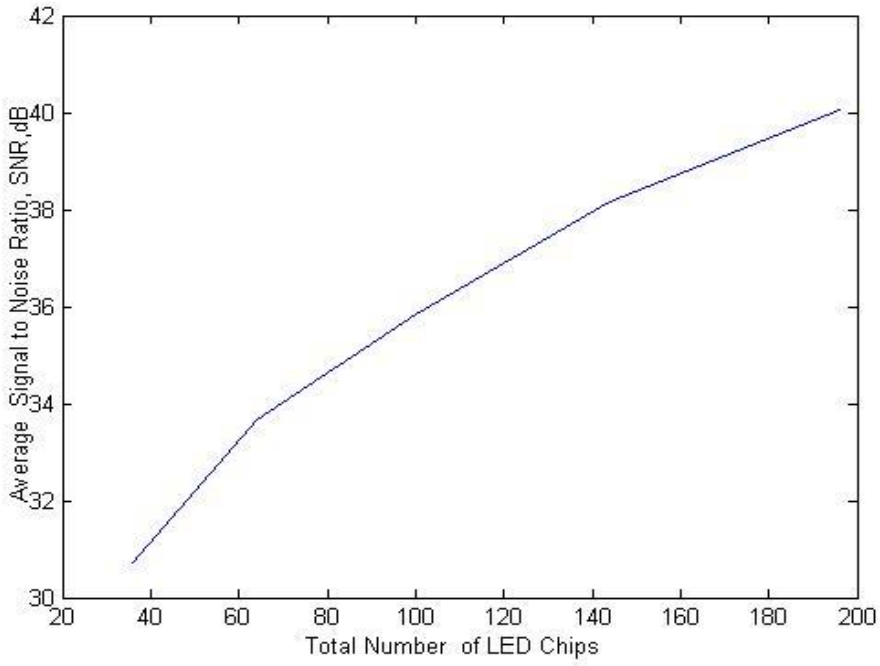


**Figure 5.32: Average SNR as a function of the number of LED chips for a Berlin winter.**

As expected, the illumination coverage of the room is reduced compared to the case when all LEDs are activated. Thus the communication link offers an acceptable QoS to a limited number of users across the room, achieved by controlling the number of LED chips energised in each panel. Feedback control to the driver circuit can be implemented preferentially powering LEDs based on the location of the user terminals in the room. This functionality can be embedded within the higher network layers and represents an extension of the research discussed under the Future Work section of Chapter 6.

### 5.4.2.3. Data Rate

An evaluation of bounds to the attainable data rate as a function of the percentage of LED chips that are energised is executed. The BER is also evaluated at different data rates under different metrological conditions. For a Berlin winter, the BER is in the range from $\sim 10^{-8}$ to $\sim 10^{-4}$ (Figure 5.33) when 11 % (100 LED chips) of all chips are activated at data rates of 5 Mbit/ and 100 Mbit/s respectively. For a Cairo summer, the BER degrades to lie between $10^{-7}$ to $10^{-3}$ at data rates of 5 Mbit/s and 100 Mbit/s (Figure 5.34). The BER in summer is evaluated at 20 % of the total number of LED chips. The evaluation for both cases is conducted for plaster walls.

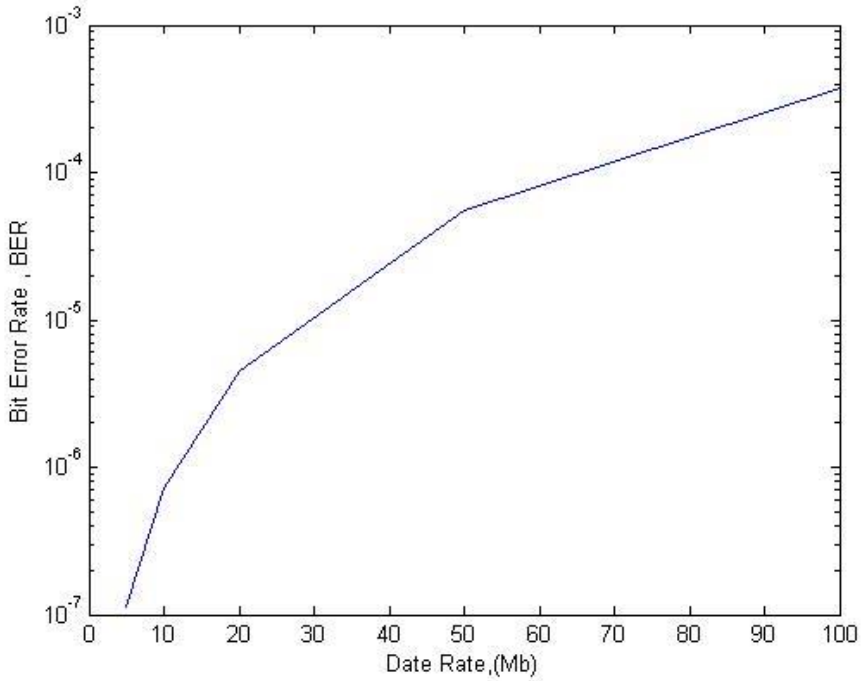


**Figure 5.33: BER as a function of data rate for a Cairo summer, clear sky.**

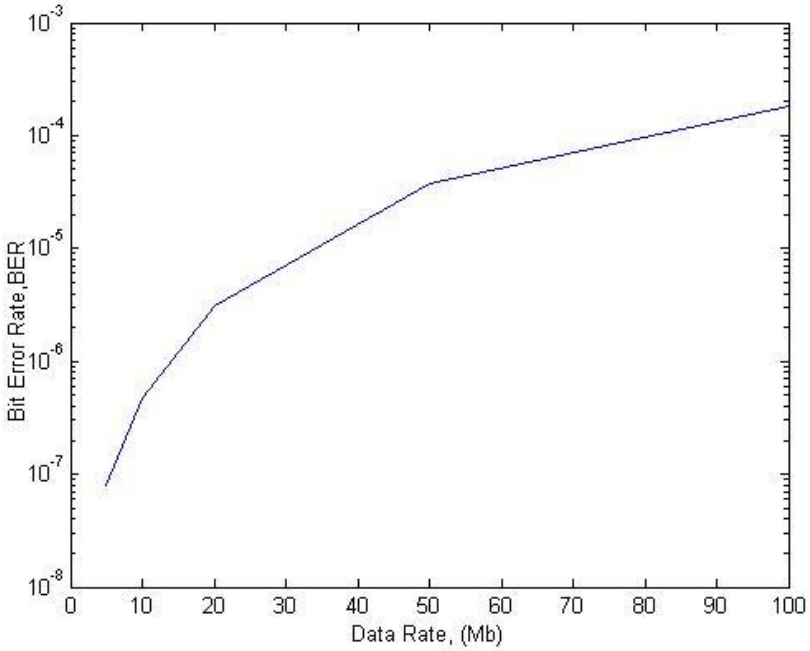


**Figure 5.34: BER as a function of data rate for a Berlin winter, cloudy sky.**

The achieved BER (Berlin) is two orders of magnitude better ($10^{-9}$) compared to the results of Borogovac *et al.* [117] where a $10^{-6}$ BER was achieved using 52 LED chips emitting at a higher power (0.87 W) than the LEDs used in the present evaluation (63 mW).

The evaluation framework is flexible, can be applied at any room size, LED panel specification under a range of metrological conditions while the work of [117] was carried out for a fixed room size and the analysis did not consider shot noise owing to sunlight nor the impact of cloud coverage. Moreover, the applied methodology treats both LOS and NLOS paths up to the fifth reflection, in so doing reducing the probability of shadowing inside the room; [117] consider LOS components only. The framework also has the flexibility to evaluate the impact of location and time whilst most reported research is confined to a fixed location without the impact of sunlight and cloud cover over the year.

## 5.5. Conclusions

LED layout is investigated in order to optimise VLC system performance and fulfil the lighting constraint governed by standards. Research to date has reported on LED layout design in rooms; however few analyses considered the optimisation process from a mathematical perspective, did not consider meeting lighting standards and did not utilise commercially available LED panels. Moreover, evaluations were confined to a specific room size, did not consider the impact of sunlight irradiance and cloud coverage and were limited to LOS components only.

The framework developed is aimed at generating design guidelines for system developers that are applicable to any room size, wall reflectivity, and illumination level, any location worldwide with consideration of both LOS and NLOS components and the impact owing to sunlight irradiance. A comparison of reported LED layout optimisation methodologies with the approach adopted in the research is summarised in Table 5.4.

**Table 5.4: A comparison of the optimisation of LED layout methodologies.**

| Methodology / Criteria | Proposed | Ding *et.al.* [74] | Azizan *et.al.* [75] | Wang *et.al* [83] |
|---|---|---|---|---|
| **Flexible Room Size** | Yes | Limited to fixed room size | Limited to fixed room size | Limited to fixed room size |
| **Impact of Sunlight Irradiance** | Yes | AWGN | AWGN | AWGN |
| **Cloud Cover Impact** | Yes, consideration of cloud cover at different representative locations over clear and cloudy skies | No consideration for metrological conditions | No consideration for metrological conditions | No consideration for metrological conditions |
| **Flexible LED Specification** | Yes | No | No | No |
| **Lighting Constraint** | Yes | Not considered | No | No |
| **SNR Maximisation** | Yes | Yes | Yes | Yes |
| **Minimisation of SNR variation across the room** | Yes | No | Yes | No |
| **Flexible Applications/ Locations** | Yes | Not considered | Not considered | Not considered |
| **Different Surfaces** | Yes | No, LOS components only | No, LOS components only | No, LOS components only |

Results are verified by a sensitivity analysis through two routes; variation in LED panel placement and comparison with reported results. Two room sizes, 5 m × 5 m × 3 m room and a 12 m × 12 m × 3 m room and the results of [52] are considered for comparison. The proposed layout provides an improved SNR, a 15% and 17%

enhancement compared to results of [51] for a Cairo summer and Berlin winter respectively. The results achieved are for the same number of LED chips and simulation parameters. The design provides better system performance with a concomitant improvement in energy consumption. Also the lighting constraint under all metrological conditions over the year has been fulfilled.

The analysis is extended to evaluate system performance over different metrological conditions for different surfaces (Table 5.5).

**Table 5.5: SNR performance over the year.**

| Average SNR / Metrological Condition | Maxi. at plaster wall surface (dB) | Mini. at plaster wall surface (dB) | Max. at plastic wall surface (dB) | Mini. plastic wall surface (dB) |
|---|---|---|---|---|
| **Cairo, Summer – Clear Sky** | 87 | 52 | 82 | 48 |
| **Cairo summer – Cloud cover** | 89 | 54.5 | 85 | 50 |
| **Berlin, Winter- Cloud cover** | 96.7 | 68 | 90 | 63 |
| **Berlin Winter – Clear sky** | 94.3 | 65 | 86.7 | 60 |
| **Berlin, Summer- Clear sky** | 92 | 62 | 84.5 | 56.54 |
| **Cairo, Winter – Clear sky** | 95 | 61 | 87.3 | 53.34 |

BER at a 1 Mbit/s data rate is in the range of $\sim 10^{-21}$ to $\sim 10^{-12}$ for a Cairo summer and in the range of $\sim 10^{-22}$ to $\sim 10^{-13}$ for a Berlin winter. The BER is excellent inherently owing to the high illumination level required for office rooms by the standard (minimum 400 lx). System performance is also evaluated as a function of

data rate. A 900 Mbit/s data rate at a $10^{-9}$ and $10^{-8}$ BER can be achieved for a Berlin winter and Cairo summer for plaster walls. For plastic walls, the BER degrades to $10^{-8}$ and $10^{-6}$ under the same metrological conditions and data rate. The solution minimises the variation of system performance across the room; excellent system performance is achieved from both a lighting and communication perspective for a large office room 12 m × 12 m × 3 m.

The evaluation is further extended to provide ain-depth analysis of the impact on system performance as a function of the LED panel distance from a wall, distance to the window and receiver FOV. System performance degrades by 22% when the LED panel is more than 0.75 m from the wall; it degrades by 2 % and 3.5% at a distance 0.25 m and 0.5 m from the wall. Thus a trade-off in LED panel location has been identified; on the one hand the LED panel should be placed close to the wall from the communication system perspective whilst on the other hand, LED panels should be placed near the centre of the room to provide acceptable illumination to all users across the room. A balanced solution has been defined that fulfils both the lighting and communication system needs for a 12 m × 12 m × 3 m room. The recommendation is that LED panels be placed at the centre to minimise variations of the signal across the room.

The performance analysis considered the distance to a source of natural light, in this case assumed to be windows. At a distance 1.25 m form the window, the daylight irradiance falls by 50% compared to irradiance at a distance 0.5 m from the window. The recommendation is that receivers should be placed at a 1.25 m distance from the window for this scenario.

All system developers are now obligated to optimise system performance at the lowest energy consumption possible in order to implement efficient energy management strategies around the world. However the conflict in this case is that in order for the communications to operate, the lights should be switched on continuously which introduces an energy consumption overhead. A methodology has been developed to optimise the performance of the system based on the control of the

number of LED chips energised to achieve a specified data rate for the application. The average SNR is evaluated to be ~30 dB, ~33.5 dB, ~35.8 dB, ~38 dB and ~40 dB as the number of LED chips rises from 36, 64, 100, 144 and 196 respectively for a plaster wall.

A $10^{-9}$ BER can be achieved when 11% (100 LEDs) of the total numbers of LED chips are energised. Thus a 1Mbit/s data rate is achieved at $10^{-9}$ BER for a Berlin winter with 89% energy saving compared to the case when all LED chips (900 LEDs) are activated. Furthermore the BER falls in the range $\sim 10^{-8}$ to $\sim 10^{-4}$ at this LED utilisation level as the data rate increases from 5 Mbit/s to 100 Mbit/s. For a Cairo summer, the BER performance degrades to $10^{-7}$ to $10^{-3}$ at 5 Mbit/s and 100 Mbit/ data rate respectively. In conclusion, the system developer can select the number of LED chips to energise according to the application and/or the priority of the data to be transmitted.

# Chapter 6

# Conclusions and Future Work

## 6.1 Summary

The research centres on the design of the VLC systems in the presence of sunlight irradiance. The aim is through systematic evaluation of system performance, to develop design and operational guidelines for VLC system deployments under different metrological conditions to meet the requirements of advanced multimedia wireless service provision.

The dissertation presents the background to the evolution of wireless communication systems outlining the drive for VLC system development. A summary of VLC system competitive advantages is highlighted through comparison with current wireless communication systems, the main driver being the increasing use of the RF spectrum by current network solutions.

Although VLC systems provide many competitive advantages such as license free, high data rate, highly available, energy efficient and environmental friendly operation, some challenges remain and form the seeds of the research;

- Illumination on; VLC systems operation is overlaid on an already deployed solid state illumination infrastructure and in some scenarios where natural sunlight irradiance is sufficient for lighting, there is no need for the lights to be on potentially compromising the communication link. In this context, a solution to overcome the issue at minimum energy consumption and to maintain an acceptable system performance is challenging.

- Sunlight irradiance; as 47 % of sunlight irradiance falls within the visible light frequency band of the spectrum, natural light incident on the receiver impacts on system performance. Sunlight impinging on photodiode receivers generates shot noise; thus both direct and indirect levels of natural light as a function of network location must be considered in determining VLC system performance. To date, no rigours analysis of the impact of natural light under different metrological conditions on system performance has been undertaken; reported research treats the shot noise owing to sunlight as Additive Gaussian White noise for simplicity. However, changes in the meteorological conditions reflecting varying operational environments is an important factor in evaluating system performance hitherto not characterised.
- Uplink: VLC can establish both uplink and downlinks through separation in time, code or wavelength but operation in bidirectional mode as in RF systems leads to crosstalk. Conventional approaches such as Time Division Duplexing (TDD) and Wavelength Division Duplexing (WDM) can be applied to solve the implementation need. Latterly hybrid system approaches have been proposed to derive the benefits of both VLC and WiFi/or IR links at the same time. Eye safety limits must be maintained and in addition, hybrid system solutions are not valid for environments where RF interference is a barrier.
- Line–of-Sight (LOS) and Non-Line-of-Sight (NLOS); although LOS paths represent the strongest interference signal, for a fuller understanding of attainable performance it is beneficial to consider indirect signal paths with a view to understanding the effect of shadowing. LOS and NLOS components are considered in the characterisation in tandem with varying surface reflectivity for indoor environments.

## 6.2 System Evaluation

It is assumed that sunlight irradiance impinges on receivers through direct and indirect paths both modulated by cloud coverage. All paths generate shot noise that affects the link budget. Shot noise is dependent on the intensity of sunlight falling within the receiver Field-of-View (FOV) over the day. Natural light intensity has

been measured using a cosine corrected light sensor which captures irradiance levels through a 180 degrees hemisphere and can be categorised in five main classes defined by the level of irradiance; the five main categories; natural light class, clear night-full moon, winter day-overcast sky, summer day-overcast sky, winter day-clear sky and summer day-clear sky.

The SNR and BER performance are evaluated as a function of natural light classes. Moreover, the evaluation considers both LOS and NLOS components; the magnitude of the signal degrades gradually with every reflection and dramatically after the third reflection especially in large room (15 m × 15 m × 3 m) with low reflectivity surface . The evaluation is extended to determine the performance with NLOS components over a range of surface reflectivities viz. plaster wall, plastic wall, floor, ceiling surfaces. Plaster walls yield the best performance and are thus recommended in system implementation.

The evaluation of the VLC system performance over a range of natural light classes shows that the lowest SNR and BER are for summer days with clear sky when sunlight irradiance is at a maximum and the highest SNR and BER are for clear nights with a full moon. A summary of the evaluation is presented in Figure 6.1 where 1, 2, 3, 4, 5 are the natural light classes defined in Table 6.1. The shot noise owing to sunlight becomes the dominant source of noise for summer days.

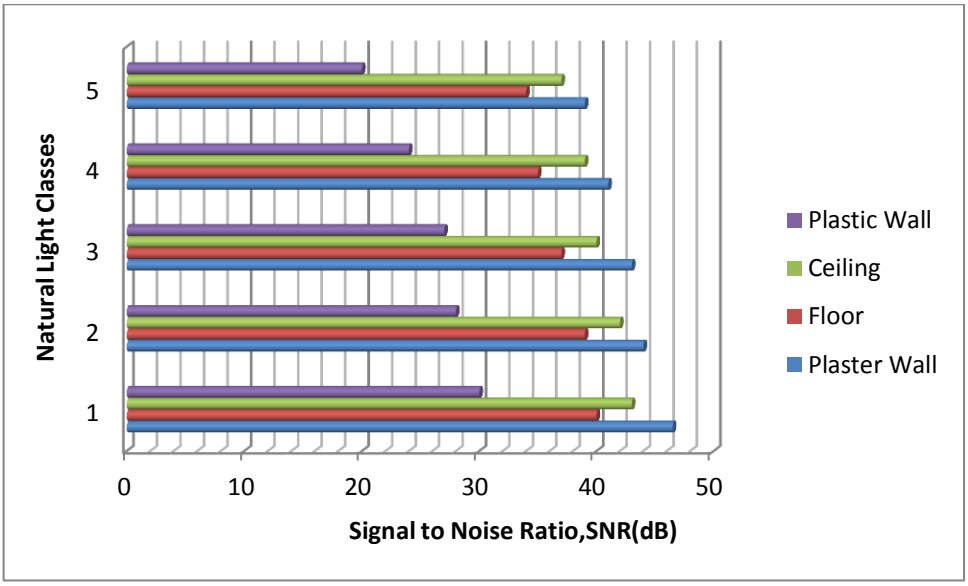


**Figure 6.1; The average system SNR as a function of natural light classes.**

In order to provide a more in depth evaluation of system characteristics, the analyses are extended to include both types of sunlight irradiance (direct and indirect) over the year under different metrological conditions. Sunlight irradiance is modelled over the year for three representative locations; Glasgow-Scotland, Berlin-Germany and Cairo-Egypt. The model uses the location's longitude, latitude, time of day and day of the year to generate the level of irradiance over the year; clear sky sunlight irradiance is estimated on an hourly basis over the year of 2011 for different representative locations.

The evaluation also considers a range of surfaces. Attainable BER from $10^{-6}$ to $10^{-12}$ are achieved at a 100 kbit/s data rate over the majority of operational scenarios using hourly estimations (8760 hours) of sunlight irradiance. The lowest SNR (and BER) occur for summer days in Cairo where sunlight intensity is at maximum and the highest SNR is achieved in Glasgow for winter. Attainable SNRs of ~36 dB and ~13.5 dB are achievable for Glasgow–winter (plaster wall) and Cairo-summer (plastic wall) respectively.

The evaluation is extended to consider diffuse sunlight irradiance; the impact of sunlight irradiance is further enhanced through consideration of cloud coverage throughout the year. The assessment is conducted using a combination of Matlab software and Monte Carlo simulations for a number of operational scenarios. Monte Carlo simulations are characterised by long simulation times to convergence and consume significant computational resources. A high performance computer facility is employed to execute on the evaluation for such complex system scenarios.

The evaluation targets two extreme scenarios embodied by the meteorological conditions prevailing in Cairo and Berlin and based on worldwide cloud coverage statistics. A comparative analysis of the SNR and BER for the system is conducted over the year on an hourly basis. The attainable SNR ranges from ~ 13.5 dB to ~ 39.5 dB for a Cairo summer, clear sky day (minimum) and for a Berlin winter cloudy (maximum) sky day. Table 6.1 and Table 6.2 summarise the comparative performance of systems at these locations for clear and cloudy skies. The BER lies in the range from $10^{-13}$ to $10^{-10}$ at the specified data rate (100 kbit/s) for plaster and plastic walls. A maximum data rate of 10 Mbit/s and 50 Mbit/s at a $10^{-9}$ BER for a summer clear sky (Cairo) and winter cloudy sky (Berlin) (plaster walls) is attainable.

**Table 6.1: Average system SNR; for Cairo and Berlin, clear skies.**

| Season | Plastic wall (dB) | | Ceiling surface (dB) | | Floor surface (dB) | | Plaster wall (dB) | |
|---|---|---|---|---|---|---|---|---|
| | **Cairo** | **Berlin** | **Cairo** | **Berlin** | **Cairo** | **Berlin** | **Cairo** | **Berlin** |
| **Winter** | ~ 17 | ~ 20 | ~ 29.5 | ~ 31 | ~ 34 | ~36 | ~ 36 | ~ *37.5* |
| **Autumn** | ~17.5 | ~ 19 | ~ 29 | *~30* | ~32.5 | ~33.5 | ~33 | *~34.5* |
| **Spring** | ~17.5 | ~ 18.5 | ~ 27.5 | ~ 29 | ~31.5 | ~33 | ~33.5 | ~ 35 |
| **Summer** | ~13.5 | ~ 17 | ~ 25.5 | ~ 27 | ~ 30 | ~32.5 | ~33 | ~35.5 |

Plaster walls (high reflectivity) are recommended for locations subject to high levels of sunlight to mitigate the impact of irradiance; plastic wall should be avoided.

**Table 6.2: Average system SNR; for Cairo and Berlin, cloudy skies.**

| Season | Plastic wall (dB) | | Ceiling (dB) | | Floor (dB) | | Plaster wall (dB) | |
|---|---|---|---|---|---|---|---|---|
| | **Cairo** | **Berlin** | **Cairo** | **Berlin** | **Cairo** | **Berlin** | **Cairo** | **Berlin** |
| **Winter** | ~ 19 | ~21.5 | ~ 32 | ~ 34 | ~ 35.5 | ~38 | ~38 | ~ 39.5 |
| **Autumn** | ~ 20 | ~20.5 | ~ 31.5 | ~ *32.5* | ~34 | ~ 35 | ~ 36.5 | ~38 |
| **Spring** | ~18.5 | ~ 19 | ~ 30 | ~ 31.5 | ~33.5 | ~ 34.5 | ~ 36 | ~ 37.5 |
| **Summer** | ~ 15.5 | ~18 | ~28 | ~ 29.5 | ~ 32.5 | ~ 34 | ~ 34 | ~ 37 |

The evaluation of system BER is presented as a function of data rates in order to reveal system performance boundaries and hence in turn, define viable applications for all metrological conditions. Table 6.3 summarise the comparative BER performance of the system as a function of data rate at the representative locations for clear and cloudy skies.

**Table 6.3: Average system BER as a function of data rate for Cairo and Berlin over the year.**

| Data Rate (Mbit/s) | BER (dB) | |
|---|---|---|
| | Winter- cloudy sky (Berlin) | Summer - clear sky (Cairo) |
| **1** | $1.7945e^{-14}$ | $1.0431e^{-13}$ |
| **5** | $2.2277\ e^{-11}$ | $1.3073e^{-10}$ |
| **10** | $4.8551\ e^{-10}$ | $2.8673e^{-09}$ |
| **20** | $1.0708\ e^{-08}$ | $6.3803e^{-08}$ |
| **50** | $6.5691\ e^{-07}$ | $3.9884e^{-06}$ |
| **100** | $1.5283\ e^{-06}$ | $9.5236e^{-05}$ |
| **200** | $3.7487\ e^{-04}$ | $1.5\ e^{-03}$ |
| **500** | $3.25\ e^{-02}$ | $4.82\ e^{-02}$ |

Moreover, a comparative analysis of the BER is conducted for cases when the sunlight irradiance estimation is considered from empirical models and when the shot noise owing to natural light is treated as Gaussian [41]. The results show that the data rate limits for a $10^{-6}$ BER are 65 Mbit/s and 120 Mbit/s in Cairo and Berlin respectively compared to 200 Mbit/s reported at the same BER for the same system configuration but when shot noise is assumed Gaussian. The result for the same system configuration (when shot noise is treated as Gaussian) differs by ~ 40% in the best scenario (Berlin) from the VLC system performance perspective. Normally the window size represent 10% of the room area, the system evaluation considered different window sizes in the room. The SNR performance degrades by 26% and 36% when the window area was 50% and 90% of the total room area respectively compared to the case when the window area is 10% of the room area. Moreover results indicate that system designers should consider placing receivers at a distance more than 0.75 m from the window to mitigate the impact of sunlight on system performance.

LED panel placement on the ceiling of a room has been optimised based on the best attainable system performance. The analysis is initiated by determining the optimum location in relation to the distance to the wall. Four LED panels are initially placed close to the wall and moved in 0.25m step away from the wall simultaneously in both directions. The SNR degrades consistently across the room as the LED panels move away from the wall. System performance degrades by 22% at a distance of 0.75 m from the wall, by 2 % and 3.5% at distances 0.25 m and 0.5 m from the wall. The closer the LED panels are to the wall, the better the performance. However it must be noted that the analysis is driven by the communications requirements; from an illumination perspective poorer lighting results.

The illumination and communication system requirements are contradictory. A balanced solution maintains acceptable communication system performance and provides an illumination level that meets standards. Results indicate that in order to partially meet both requirements, that the LED panel be placed at a 0.5 m distance from the wall; the difference in SNR is small compared to the case when the LED panels are closer to the wall and at the same location, the illumination level provided meets the standards for the room size.

The level of shot noise is dependent on the relative intensity of direct and indirect sunlight irradiance from (say) the window impinging within the photodiode Field-of-View (FOV). An evaluation of VLC system performance as a function of distance from the window is carried out at 0.25 m steps to determine optimum location. Natural light irradiance degrades by 50% at a distance 1.25 m from the window compared to a distance of 0.5 m. The recommendation is to place the panel at a 1.25 m distance from the window to minimise the impact on performance.

The receiver FOV determines the level of signal captured. Thus the SNR is evaluated as a function of receiver FOV for different room sizes under different metrological

conditions over the year. The SNR performance is evaluated with respect to FOV in 5 degree steps; however a 5 degree step change in receiver FOV has little impact on the SNR ~1.5%, 3.3% for 5 m × 5 m × 3 m and 12 m × 12 m × 3 m room respectively. As expected when the FOV is less than the incident angle, the system fails. Furthermore, the average SNR increases by 36% and 55% for 5 m × 5 m × 3 m and 12 m × 12 m × 3 m room when the FOV is more than double the incident angle. The impact of other fluorescent lighting near the receiver also represents a strong source of noise and may compromise the improvement; the evaluation of this scenario is out with the research scope.

In order to further optimise system performance the optimum LED panel locations are determined. Past research was limited to determining optimum panel placement for a single standard office room only, testing one or two LED constellations lacking a flexible assessment of LED arrangements. More importantly the analysis did not consider the constraint of meeting the illumination standard, the primary function of any lighting deployment. Furthermore the optimisation relied purely on mathematical formulations without consideration of LED panel specifications currently on the market and was only valid for a particular room size. Results were obtained considering LOS components only.

Here a more extensive optimisation is executed to determine optimum LED panel placements that both maximise system performance and fulfil the illumination standards. The methodology can be applied to any room size, any LED panel size and specification, any surface reflectivity, any receiver height, any illumination level and any LED panel output power levels. The framework is a design tool for VLC system developers helping to inform on potential implementation options.

The SNR and BER are evaluated over different metrological conditions using a range of LED panels for a 5 m × 5 m × 3 m room for plaster and plastic walls. The SNR

improves by 15% and 17% compared to the results of [51] for a Cairo summer and Berlin winter. The results are for the same number of LED chips under the same simulation parameters. The required performance can be achieved with a lower number of LEDs which in turn also brings savings in energy consumption with beneficial impact on the carbon footprint. The SNR and BER are evaluated over the year under different metrological conditions for specified LED panel placements; Table 6.4 summarises the SNR evaluation.

**Table 6.4: Comparison of the average SNR over the year at selected scenarios.**

| Average SNR / Metrological Condition | Maximum at plaster wall surface (dB) | Minimum at plaster wall surface (dB) | Maximum at plastic wall surface (dB) | Minimum plastic wall surface (dB) |
|---|---|---|---|---|
| **Cairo, Summer - Clear Sky** | 87 | 52 | 82 | 48 |
| **Cairo Summer - Cloud cover** | 89 | 54.5 | 85 | 50 |
| **Berlin, Winter- Cloud cover** | 96.7 | 68 | 90 | 63 |
| **Berlin Winter - Clear sky** | 94.3 | 65 | 86.7 | 60 |
| **Berlin, Summer- Clear sky** | 92 | 62 | 84.5 | 56.54 |
| **Cairo, Winter - Clear sky** | 95 | 61 | 87.3 | 53.34 |

The BER is in the range of $\sim 10^{-21}$ to $\sim 10^{-12}$ for a Cairo summer, clear sky and in the range of $\sim 10^{-22}$ to $\sim 10^{-13}$ for a Berlin winter, cloudy sky at a 1 Mbit/s data rate. As

expected the BER is excellent due to the high level of illumination as required by the standard for an office room (minimum 400 lx) and the optimum LED placement. Results also show that any application can operate over different metrological conditions for this LED placement.

System performance is evaluated as a function of data rate. A BER of $10^{-9}$ and $10^{-8}$ is achieved for a winter cloudy sky (Berlin) and summer clear sky (Cairo) for plaster walls at a 900 Mbit/s data rate. For a plastic wall the BER degrades to $10^{-8}$ and $10^{-6}$ at the same data rate and metrological conditions. The performance is tested for different locations and results are verified.

QoS is one of the main metrics any wireless communication system seeks to maintain in delivering a service to users. In this context, the evaluation is adapted to not only consider system and illumination performance but also to minimise the fluctuation of the SNR across the room, in so doing provisioning consistent performance for all users. The evaluation targets a large room (12 m × 12 m × 3 m) and excellent system performance is achieved from both lighting and communication perspectives.

The average SNR is in the range of ∼94 dB - ∼75 dB and ∼ 89dB - ∼ 64 dB for a Cairo summer clear sky and varies in the range ∼98 dB - ∼79 dB and ∼92dB - ∼68 dB for a Berlin winter, cloud cover for plaster and plastic walls respectively. A minimum illumination of 420 lx is achieved, meeting the lighting standard.

The illumination has to be on to maintain the communication link. As energy consumption is one of main design parameters in modern communication system designs, this restriction poses significant operational challenges. Here the ”illumination on” issue is addressed through the control of the number of LED chips that are energised when there are either no users occupying the room and/or the lighting level is sufficient from natural light. The analysis determines the optimum

LED placement and the number of LED chips energised to provide a specified BER and data rate. Users can input the data rate and BER required by the application and the tool calculates the number of LED chips to be energised i.e. the SNR is evaluated as a function of the number of the LED chips. The average SNR is ~ 30 dB, ~ 33.5 dB, ~ 35.8 dB, ~ 38 dB and ~ 40 dB as the total number of LEDs rises from 36, 64, 100, 144 and 196 respectively for plaster walls.

A $10^{-9}$ BER is achieved for 11% of the total number of LED chips viz. at a 1 Mbit/s data rate the link operates at $10^{-9}$ BER with 89% energy saving compared to the case of all LED chips activated. For a winter cloudy sky day in Berlin, the BER ranges from $\sim 10^{-8}$ to $\sim 10^{-4}$ as the data rate grows from 5 Mbit/s to 100 Mbit/s. For a summer, clear sky day in Cairo, the BER falls to $10^{-7}$ to $10^{-3}$ as the data rate ranges from 5 Mbit/s to 100 Mbit/s. The BER in summer is evaluated at 20 % of total number of LED chip utilisation for plaster walls.

## 6.3 Conclusions

In conclusion, the dissertation discusses the impact of sunlight irradiance on the performance of VLC systems. The evaluation not only consider LOS component but also through ray tracing NLOS components (up to fifth reflection) are considered to treat shadowing within the indoor environment. Furthermore the research is extended to consider the impact of cloud coverage on system performance over representative location. A comparative analysis of system performance for a range of surfaces routinely found within indoor environments is also carried out over the year. The extensive evaluation provides design guidelines for the system deployments over different operational scenarios and locations.

The dissertation provides additional design guidelines for the implementation and operation of the VLC system that enhance the QoS provisioned in terms of the receivers placement, relative distance to the wall so as to optimise the performance

from both the lighting and communication perspectives, to mitigate the impact of the sunlight and optimise receiver field of view for different room sizes.

A design tool for optimum LED placement within indoor environments has been developed for any room size and technical specification. The tool is flexible and aids in the design of LED placement across a room ensuring optimum performance for all users distributed throughout the room whilst fulfilling the illumination standards and minimising the variation in system performance across the room.

A potential solution to the "illumination on" operational challenge is developed and evaluated to provide robust system performance whilst minimising system energy consumption.

## 6.4 Future work

The development of the VLC systems inspired applications are still in their infancy and many research challenges remain. In respect of the communication systems, the application of cellular concept in VLC system designs is a rich vein of future research. The challenges associated with an 'attocell' network concepts are relevant and evaluation of the impact of sunlight irradiance on the end–to-end connectivity is a worthy research area. Concepts that mitigate the impact of shadowing and blockage of paths in indoor environments through the design of the cell represent significant challenges. Interference avoidance and mitigation algorithms to maintain the robustness of system availability and reliability under different operational scenarios is in general very challenging.

Investigation of different modulation techniques for VLC systems subject to sunlight irradiance that provide improvement in performance whilst reducing energy consumption is a worthwhile area. This investigation can be extended to consider the

role of VLC technologies for wireless sensor network applications in outdoor environments, self-powered through natural light.

The establishment of adaptive VLC communication links is an extension to the work detailed in Chapter 5. Adaptive approaches are able to control the selective powering of the LED panel based on the location of receivers. There are also many research challenges for VLC systems in the area of security uplink, coding and extension of system applications are all areas of research worthy of consideration.

# Bibliography


1. Elgala, H., R. Mesleh, and H. Haas, *Indoor optical wireless communication: potential and state-of-the-art.* IEEE Communications Magazine 2011. 49(9): p. 56-62.
2. Burchardt, H., et al., *VLC: Beyond Point-to-Point Communication.* pureVLC Ltd., Nov, 2013.
3. Haas, H., *Wireless data from every light bulb.* TED Global, Edinburgh, 2011.
4. Haas, H. *visible light commuincations : why VLC* 2013 [cited 2014 3-1-2014].
5. Pure, V., *Visible Light Communication: An introductory guide.* online] www. purevlc. net, 2012.
6. Hranilovic, S., *Wireless optical communication systems*2005: Springer.
7. Research, G., *Visible Light Communication (VLC) — A Potential Solution to the Global Wireless Spectrum Shortage*, 2011, GBI Research.
8. Zheng, Y. and M. Zhang. *Visible light communications-recent progresses and future outlooks*. in *Photonics and Optoelectronic (SOPO), 2010 Symposium on*. 2010. IEEE.
9. Grobe, L., et al., *High-speed visible light communication systems.* Communications Magazine, IEEE, 2013. 51(12): p. 60-66.
10. Haruyama, S., *Visible light communications: Recent activities in Japan.* Smart Spaces: A Smart Lighting ERC Industry—Academia Day at BU Photonics Center, Boston University (Feb. 8, 2011)(49 pages), 2011.
11. Grobe, L., et al., *High-speed visible light communication systems.* IEEE Communications Magazine, 2013. 51(12): p. 60-66.
12. Borah, D.K., et al., *A review of communication-oriented optical wireless systems.* EURASIP Journal on Wireless Communications and Networking, 2012. 2012(1): p. 1-28.
13. *Historia del control remoto*, in *Nexos: Sociedad, Ciencia, Literatura*2013. p. 7.
14. Nintendo. 1971 [cited 2014 15-1]; Available from: http://www.retrothing.com/2011/09/nintendo-light-telephone-their-craziest-product-ever.html.
15. VLC, P. *Differences Between Radio & Visible Light Communications ,A technical guid*. 2012 [cited 2013 1-12-2013]; Available from: http://www.purevlc.com/pureVLC_RadioTech_v1.0.pdf.
16. Bell, A.G., *The photophone.* Science, 1880. 1(11): p. 130-1.
17. Haruyama, S. *Progress of visible light communication*. in *Optical Fiber Communication (OFC), collocated National Fiber Optic Engineers Conference, 2010 Conference on (OFC/NFOEC)*. 2010. IEEE.
18. Tsonev, D., S. Videv, and H. Haas. *Light fidelity (Li-Fi): towards all-optical networking*. in *SPIE OPTO*. 2013. International Society for Optics and Photonics.

19. Bhalerao, M., S. Sonavane, and V. Kumar, *A SURVEY OF WIRELESS COMMUNICATION USING VISIBLE LIGHT*. International Journal of Advances in Engineering & Technology, 2012. 5(2).
20. George, J.J., et al., *A Survey on Visible Light Communication.* International Journal Of Engineering And Computer Science, 2014. 3(2): p. 3905-3908.
21. Khandal, D. and S. Jain, *Li-Fi (Light Fidelity): The Future Technology in Wireless Communication.*
22. Commission, I.E., *IEC 60825-1,«.* Safety of Laser Products—Part, 2001. 1.
23. Tsonev, D., S. Videv, and H. Haas, *Light Fidelity (Li-Fi): Towards All-Optical Networking.*
24. Sathiya.T , E.D., S.Raja, *Visible Light Communication for Wireless Data Transmission.* International Journal of Innovative Research in Electrical, Electronics , Instrumentation and Control Engineering, 2014. 2(2): p. 5.
25. Komine, T. and M. Nakagawa, *Fundamental analysis for visible-light communication system using LED lights.* IEEE Trans. on Consum. Electron., 2004. 50(1): p. 100-107.
26. Langer, K.-D. and J. Grubor. *Recent developments in optical wireless communications using infrared and visible light*. in *Transparent Optical Networks, 2007. ICTON'07. 9th International Conference on*. 2007. IEEE.
27. Lee, C.G., *Advanced Trends in Wireless Communications*, D.M. Khatib, Editor 2011. p. 327-338.
28. Duffie, J.A. and W.A. Beckman, *Solar engineering of thermal processes*2013: John Wiley & Sons.
29. OMEGA. *OMEGA project* 2012 [cited 2012 5-9-2012]; Available from: http://www.ict-omega.eu/.
30. Alavi, S.E., A.S.M. Supa'at, and S.M. Idrus. *Integrated system of visible free space optic with PLC*. in *Communications (MICC), 2009 IEEE 9th Malaysia International Conference on*. 2009. IEEE.
31. O'brien, D., et al. *Visible light communications: Challenges and possibilities*. in *IEEE 19th International Symposium onPersonal, Indoor and Mobile Radio Communications, 2008. PIMRC 2008. .* 2008. IEEE.
32. Kitano, S., S. Haruyama, and M. Nakagawa. *LED road illumination communications system*. in *Vehicular Technology Conference, 2003. VTC 2003-Fall. 2003 IEEE 58th*. 2003. IEEE.
33. Visible Light Communications Consortium. 2013 10-2-2013 [cited 2013 10-2-2013]; Available from: http://www.vlcc.net.
34. WWRF. 2012 [cited 2011 16-5-2011]; Available from: http://www.wwrf.ch/.
35. Hoa Le, M., et al. *Indoor Gigabit optical wireless communications: Challenges and possibilities*. in *12th International Conference on Transparent Optical Networks (ICTON), 2010* 2010.
36. Yang, Y., et al. *Design of indoor wireless communication system using LEDs*. in *2009 Asia Communications and Photonics Conference and Exhibition (ACP), .* 2009. IEEE.
37. Vucic, J., et al., *White light wireless transmission at 200 Mb/s net data rate by use of discrete-multitone modulation.* IEEE Photonics Technology Letters, , 2009. 21(20): p. 1511-1513.
38. Grubor, J., et al., *Wireless high-speed data transmission with phosphorescent white-light LEDs.* ECOC 2007, 2007.

39. Zeng, L., et al., *Improvement of date rate by using equalization in an indoor visible light communication system.* 2008.
40. Zeng, L., et al. *Equalisation for high-speed Visible Light Communications using white-LEDs.* in *Communication Systems, Networks and Digital Signal Processing, 2008. CNSDSP 2008. 6th International Symposium on*. 2008. IEEE.
41. Komine, T., et al., *Adaptive equalization system for visible light wireless communication utilizing multiple white LED lighting equipment.* Wireless Communications, IEEE Transactions on, 2009. 8(6): p. 2892-2900.
42. Komine, T., et al. *Adaptive equalization for indoor visible-light wireless communication systems*. in *2005 Asia-Pacific Conference on Communications*, . 2005. IEEE.
43. Komine, T., et al., *Adaptive equalization system for visible light wireless communication utilizing multiple white LED lighting equipment.* IEEE Transactions on Wireless Communications, , 2009. 8(6): p. 2892-2900.
44. Hoa, L.-M., et al., *100-Mb/s NRZ Visible Light Communications Using a Postequalized White LED.* IEEE Photonics Technology Letters, 2009. 21(15): p. 1063-1065.
45. Afgani, M.Z., et al. *Visible light communication using OFDM*. in *2nd International Conference on Testbeds and Research Infrastructures for the Development of Networks and Communities, 2006. TRIDENTCOM 2006.* . 2006. IEEE.
46. Lopez-Hernandez, F., et al. *Low-cost diffuse wireless optical communication system based on white LED*. in *Consumer Electronics, 2006. ISCE'06. 2006 IEEE Tenth International Symposium on*. 2006. IEEE.
47. Noshad, M. and M. Brandt-Pearce, *Can Visible Light Communications Provide Gb/s Service?* arXiv preprint arXiv:1308.3217, 2013.
48. Tanaka, Y., et al. *Indoor visible communication utilizing plural white LEDs as lighting*. in *12th IEEE International Symposium on Personal, Indoor and Mobile Radio Communications, 2001* 2001. IEEE.
49. Zhang, X., et al. *Optimal power allocation in spatial modulation OFDM for visible light communications*. in *b IEEE 75th Vehicular Technology Conference (VTC Spring), 2012*. 2012. IEEE.
50. Komine, T. and M. Nakagawa. *Performance evaluation of visible-light wireless communication system using white LED lightings*. in *Computers and Communications, 2004. Proceedings. ISCC 2004. Ninth International Symposium on*. 2004. IEEE.
51. Grubor, J., et al., *Broadband information broadcasting using LED-based interior lighting.* Journal of Lightwave Technology, 2008. 26(24): p. 3883-3892.
52. Grubor, J., et al. *Bandwidth-efficient indoor optical wireless communications with white light-emitting diodes*. in *6th International Symposium on Communication Systems, Networks and Digital Signal Processing, 2008. CNSDSP 2008.* . 2008. IEEE.
53. Ramirez-Iniguez, R., S.M. Idrus, and Z. Sun, *Optical wireless communications: IR for wireless connectivity*2008: CRC Press.

54. Elgala, H., R. Mesleh, and H. Haas, *Indoor broadcasting via white LEDs and OFDM.* IEEE Transactions on Consumer Electronics, 2009. 55(3): p. 1127-1134.
55. Elgala, H., R. Mesleh, and H. Haas. *Practical considerations for indoor wireless optical system implementation using OFDM*. in *Telecommunications, 2009. ConTEL 2009. 10th International Conference on*. 2009. IEEE.
56. Elgala, H., et al. *OFDM visible light wireless communication based on white LEDs*. in *IEEE 65th Vehicular Technology Conference, 2007. VTC2007-Spring.* . 2007. IEEE.
57. Li, Y., N. Seshadri, and S. Ariyavisitakul, *Channel estimation for OFDM systems with transmitter diversity in mobile wireless channels.* Selected Areas in Communications, IEEE Journal on, 1999. 17(3): p. 461-471.
58. Elgala, H., R. Mesleh, and H. Haas, *An LED model for intensity-modulated optical communication systems.* IEEE Photonics Technology Letters, 2010. 22(11): p. 835-837.
59. Mesleh, R., H. Elgala, and H. Haas, *LED nonlinearity mitigation techniques in optical wireless OFDM communication systems.* IEEE/OSA Journal of Optical Communications and Networking 2012. 4(11): p. 865-875.
60. Langer, K.-D., et al. *Optical wireless communications for broadband access in home area networks*. in *Transparent Optical Networks, 2008. ICTON 2008. 10th Anniversary International Conference on*. 2008. IEEE.
61. Langer, K.-D., et al. *Advances and prospects in high-speed information broadcast using phosphorescent white-light LEDs*. in *11th International Conference on Transparent Optical Networks, 2009. ICTON'09.* . 2009. IEEE.
62. González, O., *Multiple-Input Multiple-Output (MIMO) Optical Wireless Communications.* 2012.
63. Zeng, L., et al., *High data rate multiple input multiple output (MIMO) optical wireless communications using white LED lighting.* Selected Areas in Communications, IEEE Journal on, 2009. 27(9): p. 1654-1662.
64. Fan, K., et al. *The effect of reflection on indoor visible-light communication system utilizing white LEDs*. in *Wireless Personal Multimedia Communications, 2002. The 5th International Symposium on*. 2002. IEEE.
65. Jivkova, S., B. Hristov, and M. Kavehrad, *Power-efficient multispot-diffuse multiple-input-multiple-output approach to broad-band optical wireless communications.* IEEE Transactions on Vehicular Technology 2004. 53(3): p. 882-889.
66. O'Brien, D.C., et al. *Multiple input multiple output systems for optical wireless: challenges and possibilities*. in *SPIE Optics+ Photonics*. 2006. International Society for Optics and Photonics.
67. Jivkova, S. and M. Kavehrad. *Shadowing and blockage in indoor optical wireless communications*. in *Global Telecommunications Conference, 2003. GLOBECOM'03. IEEE*. 2003. IEEE.
68. Lee, I., M. Sim, and F. Kung, *Performance enhancement of outdoor visible-light communication system using selective combining receiver.* IET optoelectronics, 2009. 3(1): p. 30-39.

69. Cornelius, C.M. and J.P. Dowling, *Modification of Planck blackbody radiation by photonic band-gap structures.* Physical Review A, 1999. 59(6): p. 4736.
70. Gagliardi, R. and S. Karp, *Optical Communications,(John Wiley & Sons)*, 1995, Inc.
71. Bird, R.E. and C. Riordan, *Simple solar spectral model for direct and diffuse irradiance on horizontal and tilted planes at the earth's surface for cloudless atmospheres.* Journal of Climate and Applied Meteorology, 1986. 25(1): p. 87-97.
72. Sugiyama, H., S. Haruyama, and M. Nakagawa. *Brightness control methods for illumination and visible-light communication systems*. in *Wireless and Mobile Communications, 2007. ICWMC'07. Third International Conference on*. 2007. IEEE.
73. Ntogari, G., et al., *Combining Illumination Dimming Based on Pulse-Width Modulation With Visible-Light Communications Based on Discrete Multitone.* Journal of Optical Communications and Networking, 2011. 3(1): p. 56-65.
74. Ding, D., X. Ke, and L. Xu. *An optimal lights layout scheme for visible-light communication system*. in *Proceedings of the 18th International Conference on Electronic Measurement and Instruments, ICEMI'2007*. 2007.
75. Azizan, L.-H., M.S. Ab-Rahman, and K. Jumiran. *Analytical approach on SNR performance of visible light communication for modern lighting layout*. in *Innovation Management and Technology Research (ICIMTR), 2012 International Conference on*. 2012. IEEE.
76. Nguyen, H., et al. *A MATLAB-based simulation program for indoor visible light communication system*. in *7th International Symposium on Communication Systems Networks and Digital Signal Processing (CSNDSP), 2010*. 2010. IEEE.
77. Nguyen, H.Q., et al., *Effect of LED emission cross-section in indoor visible light communication systems.* EURASIP Journal on Wireless Communications and Networking, 2012. 2012(1): p. 1-11.
78. Do, T.-H. and M. Yoo. *Received power and SNR optimization for visible light communication system*. in *Fourth International Conference on Ubiquitous and Future Networks (ICUFN), 2012* 2012. IEEE.
79. Zitzler, E. and L. Thiele, *Multiobjective evolutionary algorithms: a comparative case study and the strength Pareto approach.* IEEE Transactions on Evolutionary Computation, 1999. 3(4): p. 257-271.
80. Zitzler, E., M. Laumanns, and L. Thiele, *SPEA2: Improving the strength Pareto evolutionary algorithm*, 2001, Eidgenössische Technische Hochschule Zürich (ETH), Institut für Technische Informatik und Kommunikationsnetze (TIK).
81. Jiayuan, W., K. Zhe, and Z. Nianyu. *Research on indoor visible light communication system employing white LED lightings*. in *IET International Conference on Communication Technology and Application (ICCTA 2011),*. 2011.
82. Lo, S., *Visible Light Communications.* IEEE Transactions on Consumer Electronics, 2004. 50(1).

83. Wang, J., Z. Kang, and N. Zou, *Research on indoor visible light communication system employing white LED lightings.* 2011.
84. Tronghop, D., et al. *Modeling and analysis of the wireless channel formed by LED angle in visible light communication*. in *International Conference on Information Networking (ICOIN), 2012*. 2012. IEEE.
85. Choi, J.H., S.W. Koo, and J.Y. Kim. *Performance analysis of optimum line coding for high speed data communication in VLC system*. in *9th International Symposium on Communications and Information Technology, 2009. ISCIT 2009.* . 2009. IEEE.
86. Prokais, J.G., *Digital Communications, 2001, 202-207*, McGraw Hill, New York.
87. Yi, Y., K. Lee, and K. Lee. *Performance analysis of indoor visible lighting communication using spread codes*. in *9th International Symposium on Communications and Information Technology, 2009. ISCIT 2009.* . 2009. IEEE.
88. Yi, Y., C. Li, and K. Lee, *Optimum Spread Code Applied in Indoor Visible Light Data Transmission for Optical Multipath Dispersion Reduction.* IETE Technical Review, 2013. 30(3): p. 233-239.
89. Mase, S., et al. *Error correcting scheme for road-to-vehicle visible light communication using LED array*. in *11th International IEEE Conference on Intelligent Transportation Systems, 2008. ITSC 2008.* . 2008. IEEE.
90. Arai, S., et al. *Experimental on hierarchical transmission scheme for visible light communication using led traffic light and high-speed camera*. in *Vehicular Technology Conference, 2007. VTC-2007 Fall. 2007 IEEE 66th*. 2007. IEEE.
91. Wong, D.W.K. and G. Chen, *Optical design and multipath analysis for broadband optical wireless in an aircraft passenger cabin application.* Vehicular Technology, IEEE Transactions on, 2008. 57(6): p. 3598-3606.
92. Hong, H., Y. Ren, and C. Wang. *Information illuminating system for healthcare institution*. in *Bioinformatics and Biomedical Engineering, 2008. ICBBE 2008. The 2nd International Conference on*. 2008. IEEE.
93. Haruyama, S. *Progress of visible light communication*. in *Conference on (OFC/NFOEC) Optical Fiber Communication (OFC), collocated National Fiber Optic Engineers Conference, 2010* 2010. IEEE.
94. Pang, G., et al. *LED traffic light as a communications device*. in *Intelligent Transportation Systems, 1999. Proceedings. 1999 IEEE/IEEJ/JSAI International Conference on*. 1999. IEEE.
95. Wada, M., et al. *Road-to-vehicle communication using LED traffic light*. in *Intelligent Vehicles Symposium, 2005. Proceedings. IEEE*. 2005. IEEE.
96. Hara, T., et al. *A new receiving system of visible light communication for ITS*. in *IEEE Intelligent Vehicles Symposium, 2007*. 2007. IEEE.
97. Kumar, N., L.N. Alves, and R.L. Aguiar. *Design and analysis of the basic parameters for traffic information transmission using VLC*. in *1st International Conference on Wireless Communication, Vehicular Technology, Information Theory and Aerospace & Electronic Systems Technology, 2009. Wireless VITAE 2009.* . 2009. IEEE.
98. Bouchet, O., et al. *Hybrid wireless optics (HWO): Building the next-generation home network*. in *6th International Symposium on Communication*

*Systems, Networks and Digital Signal Processing, 2008. CNSDSP 2008.* . 2008. IEEE.

99. Kotake, H.H., S. Nakagawa, and K. M Seki. *BER characteristic of ground-to-train communication system using free-space optics technology*. 2007. Transparent Optical Networks, 2007. ICTON'07. 9th International Conference on.
100. IEC. *International Electrotechnical Commission -Safety of laser products - Part 1: Equipment classification and requirements*. 2014 [cited 2014 15-8-2014]; Available from: http://webstore.iec.ch/Webstore/webstore.nsf/ArtNum_PK/49687!opendocument&preview=1.
101. Dimitrov, S., et al., *On the SIR of a cellular infrared optical wireless system for an aircraft.* Selected Areas in Communications, IEEE Journal on, 2009. 27(9): p. 1623-1638.
102. Omiyi, P., H. Haas, and G. Auer, *Analysis of TDD cellular interference mitigation using busy-bursts.* Wireless Communications, IEEE Transactions on, 2007. 6(7): p. 2721-2731.
103. Haas, H. and S. McLaughlin, *Next generation mobile access technologies: Implementing TDD*2007: Cambridge University Press.
104. Boyle, J., *Wireless technologies and patient safety in hospitals.* Telemedicine Journal & e-Health, 2006. 12(3): p. 373-382.
105. Le Minh, H., et al., *High-speed visible light communications using multiple-resonant equalization.* IEEE Photonics Technology Letters 2008. 20(14): p. 1243-1245.
106. Hanzo, L., et al., *Wireless myths, realities, and futures: from 3G/4G to optical and quantum wireless.* Proceedings of the IEEE, 2012. 100(Special Centennial Issue): p. 1853-1888.
107. Ramirez, R., S.M. Idrus, and Z. Sun, *Optical Wireless Communications: IR for Wireless Connectivity*, 2008, CRC press, Taylor & Francis.
108. Kato, K., et al., *High-efficiency waveguide InGaAs pin photodiode with bandwidth of over 40 GHz.* Photonics Technology Letters, IEEE, 1991. 3(5): p. 473-474.
109. Barron, C., et al., *Resonant-cavity-enhanced pin photodetector with 17 GHz bandwidth-efficiency product.* Electronics letters, 1994. 30(21): p. 1796-1797.
110. Tan, I.-H., et al., *120-GHz long-wavelength low-capacitance photodetector with an air-bridged coplanar metal waveguide.* Photonics Technology Letters, IEEE, 1995. 7(12): p. 1477-1479.
111. Shiba, K., et al., *10 Gbit/s asymmetric waveguide APD with high sensitivity of− 30 dBm.* Electronics letters, 2006. 42(20): p. 1177-1178.
112. Rajagopal, S., R.D. Roberts, and S.-K. Lim, *IEEE 802.15. 7 visible light communication: modulation schemes and dimming support.* Communications Magazine, IEEE, 2012. 50(3): p. 72-82.
113. Elgala, H., R. Mesleh, and H. Haas, *Indoor optical wireless communication: potential and state-of-the-art.* Communications Magazine, IEEE, 2011. 49(9): p. 56-62.
114. Kim, Y., et al. *Position estimation algorithm based on tracking of received light intensity for indoor visible light communication systems*. in *Ubiquitous*

*and Future Networks (ICUFN), 2011 Third International Conference on*. 2011. IEEE.
115. Rahaim, M.B., A.M. Vegni, and T.D. Little. *A hybrid Radio Frequency and broadcast Visible Light Communication system*. in *GLOBECOM Workshops*. 2011.
116. Fitzek, F.H. and M.D. Katz, *Cognitive wireless networks: concepts, methodologies and visions inspiring the age of enlightenment of wireless communications*2007: Springer.
117. Borogovac, T., et al. *"Lights-off" visible light communications*. in *GLOBECOM Workshops (GC Wkshps), 2011* 2011. IEEE.
118. Kwonhyung, L., P. Hyuncheol, and J.R. Barry, *Indoor Channel Characteristics for Visible Light Communications.* IEEE Communications Letters, IEEE, 2011. 15(2): p. 217-219.
119. Sheu, J.-K., et al., *White-light emission from near UV InGaN-GaN LED chip precoated with blue/green/red phosphors.* Photonics Technology Letters, IEEE, 2003. 15(1): p. 18-20.
120. Sidorovich, V.G. *Solar background effects in wireless optical communications*. in *ITCom 2002: The Convergence of Information Technologies and Communications*. 2002. International Society for Optics and Photonics.
121. Kahn, J.M. and J.R. Barry, *Wireless infrared communications.* Proceedings of the IEEE, 1997. 85(2): p. 265-298.
122. Garcia, J., et al., *Dimming of high-brightness LEDs by means of luminous flux thermal estimation.* Power Electronics, IEEE Transactions on, 2009. 24(4): p. 1107-1114.
123. Beczkowski, S. and S. Munk-Nielsen. *LED spectral and power characteristics under hybrid PWM/AM dimming strategy*. in *Energy Conversion Congress and Exposition (ECCE), 2010 IEEE*. 2010. IEEE.
124. Gancarz, J., H. Elgala, and T.D. Little, *Impact of lighting requirements on VLC systems.* Communications Magazine, IEEE, 2013. 51(12): p. 34-41.
125. Doshi, M. and R. Zane, *Control of solid-state lamps using a multiphase pulsewidth modulation technique.* Power Electronics, IEEE Transactions on, 2010. 25(7): p. 1894-1904.
126. Bai, B., Z. Xu, and Y. Fan. *Joint LED dimming and high capacity visible light communication by overlapping PPM*. in *19th Annual Conference of Wireless and Optical Communications (WOCC), 2010* 2010. IEEE.
127. Wolf, M., et al., *ICT-213311 OMEGA.*
128. Arredondo, B., et al., *Visible light communication system using an organic bulk heterojunction photodetector.* Sensors, 2013. 13(9): p. 12266-12276.
129. Kim, J.-H., et al. *Visible light communication at 20 Mb/s using illumination LEDs*. 2006.
130. Vučić, J., et al., *513 Mbit/s visible light communications link based on DMT-modulation of a white LED.* Journal of Lightwave Technology, 2010. 28(24): p. 3512-3518.
131. Gfeller, F.R. and U. Bapst, *Wireless in-house data communication via diffuse infrared radiation.* Proceedings of the IEEE, 1979. 67(11): p. 1474-1486.

132. Cui, K., et al. *Line-of-sight visible light communication system design and demonstration*. in *7th International Symposium on Communication Systems Networks and Digital Signal Processing (CSNDSP), 2010* 2010. IEEE.
133. Barry, J.R., et al., *Simulation of multipath impulse response for indoor wireless optical channels.* IEEE Journal on Selected Areas in Communications 1993. 11(3): p. 367-379.
134. Deqiang, D., K. Xizheng, and X. Linpeng. *An Optimal Lights Layout Scheme for Visible-Light Communication System*. in *8th International Conference on Electronic Measurement and Instruments, 2007. ICEMI'07.* . 2007. IEEE.
135. MathWorks, I., *MATLAB: the language of technical computing. Desktop tools and development environment, version 7*. Vol. 9. 2005: MathWorks.
136. Sarbazi, E., et al. *Indoor channel modelling and characterization for visible light communications*. in *Transparent Optical Networks (ICTON), 2014 16th International Conference on*. 2014. IEEE.
137. addressable LeDs, I., *cree® Xlamp® Xm-l color leds.*
138. Patel, M.R., *Wind and solar power systems: design, analysis, and operation*2005: CRC press.
139. Quaschning, V., *Understanding Renewable Energy Systems* Vol. 1. 2005: Earthscan.
140. Swartman, R. and O. Ogunlade, *Solar radiation estimates from common parameters.* Solar energy, 1967. 11(3): p. 170-172.
141. Sabbagh, J., A. Sayigh, and E. El-Salam, *Estimation of the total solar radiation from meteorological data.* Solar energy, 1977. 19(3): p. 307-311.
142. Besharat, F., A.A. Dehghan, and A.R. Faghih, *Empirical models for estimating global solar radiation: A review and case study.* Renewable and Sustainable Energy Reviews, 2013. 21: p. 798-821.
143. Angstrom, A., *Solar and terrestrial radiation. Report to the international commission for solar research on actinometric investigations of solar and atmospheric radiation.* Quarterly Journal of the Royal Meteorological Society, 1924. 50(210): p. 121-126.
144. Prescott, J., *Evaporation from a water surface in relation to solar radiation.* Transactions of the Royal Society of South Australia, 1940. 64(1940): p. 114-118.
145. Glover, J. and J. McCulloch, *The empirical relation between solar radiation and hours of sunshine.* Quarterly Journal of the Royal Meteorological Society, 1958. 84(360): p. 172-175.
146. Ögelman, H., A. Ecevit, and E. Tasdemiroğlu, *A new method for estimating solar radiation from bright sunshine data.* Solar energy, 1984. 33(6): p. 619-625.
147. Bahel, V., H. Bakhsh, and R. Srinivasan, *A correlation for estimation of global solar radiation.* Energy, 1987. 12(2): p. 131-135.
148. Gopinathan, K., *A simple method for predicting global solar radiation on a horizontal surface.* Solar & wind technology, 1988. 5(5): p. 581-583.
149. Elagib, N.A. and M.G. Mansell, *New approaches for estimating global solar radiation across Sudan.* Energy Conversion and Management, 2000. 41(5): p. 419-434.
150. Bakirci, K., *Correlations for Estimation of Solar Radiation on Horizontal Surfaces.* Journal of Energy Engineering, 2008. 134(4): p. 130-134.

151. Muzathik, A., et al., *Estimation of global solar irradiation on horizontal and inclined surfaces based on the horizontal measurements.* Energy, 2011. 36(2): p. 812-818.
152. Paltridge, G. and D. Proctor, *Monthly mean solar radiation statistics for Australia.* Solar energy, 1976. 18(3): p. 235-243.
153. Supit, I. and R. Van Kappel, *A simple method to estimate global radiation.* Solar energy, 1998. 63(3): p. 147-160.
154. Jones, P.A., *Cloud-Cover Distributions and Correlations.* Journal of Applied Meteorology, 1992. 31(7): p. 732-741.
155. Samimi, J., *Estimation of height-dependent solar irradiation and application to the solar climate of Iran.* Solar energy, 1994. 52(5): p. 401-409.
156. Badescu, V., *Correlations to estimate monthly mean daily solar global irradiation: application to Romania.* Energy, 1999. 24(10): p. 883-893.
157. Sabziparvar, A.A., *A simple formula for estimating global solar radiation in central arid deserts of Iran.* Renewable energy, 2008. 33(5): p. 1002-1010.
158. Allen, R.G., *Self-calibrating method for estimating solar radiation from air temperature.* Journal of Hydrologic Engineering, 1997. 2(2): p. 56-67.
159. Mahmood, R. and K.G. Hubbard, *Effect of time of temperature observation and estimation of daily solar radiation for the Northern Great Plains, USA.* Agronomy Journal, 2002. 94(4): p. 723-733.
160. Katiyar, A. and C. Pandey, *A Review of Solar Radiation Models—Part I.* Journal of Renewable Energy, 2012.
161. skyeninstruments. *Light measurement guidance notes*. 2012 [cited 2012 1-2-2012]; Available from: www.skyeninstruments.com.
162. Beshr, M., I. Andonovic, and M.H. Aly, *The Effect of Natural Light on the Performance of Visible Light Communication Systems}.*
163. Crosbie, M. and D. Watson, *Time-Saver Standards for Architectural Design: Technical Data for Professional Practice: Technical Data for Professional Practice*. Vol. 1. 2004: McGraw-Hill Prof Med/Tech.
164. Bindel, D. and J. Goodman, *Principles of Scientific Computing*, 2009, Manuscript.
165. Li, W., *Reliability assessment of electrical power systems using Monte Carlo methods*1994: Springer.
166. Jeruchim, M.C., P. Balaban, and K.S. Shanmugan, *Simulation of communication systems: modeling, methodology and techniques*2000: Springer.
167. Rubinstein, R.Y. and D.P. Kroese, *Simulation and the Monte Carlo method*. Vol. 707. 2011: John Wiley & Sons.
168. Rahaim, M.B., T. Borogovac, and J.B. Carruthers, *CandlES: communication and lighting emulation software*, in *Proceedings of the fifth ACM international workshop on Wireless network testbeds, experimental evaluation and characterization*2010, ACM: Chicago, Illinois, USA. p. 9-14.
169. Computing, H.P. *Academic and Research Computer Hosting Industry and Enterprise in the West of Scotland: ARCHIE-WeSt*. 2013 [cited 2013 10-12-2012]; Available from: http://www.archie-west.ac.uk/.
170. Xiang, Y., et al., *Human shadowing effect on indoor visible light communications channel characteristics.* Optical Engineering, 2014. 53(8): p. 086113-086113.

171. LXHL-LW6C-datasheet. *LXHL-LW6C*. 2012 [cited 2102; LED data sheet ]. Available from: http://www.datasheetarchive.com/LXHL-LW6C-datasheet.html.
172. Moreira, A.J., R.T. Valadas, and A. de Oliveira Duarte, *Optical interference produced by artificial light.* Wireless Networks, 1997. 3(2): p. 131-140.
173. Wu, D., et al. *Power distribution and Q-factor analysis of diffuse cellular indoor visible light communication systems*. in *16th European Conference on Networks and Optical Communications (NOC), 2011* 2011. IEEE.
174. Wang, Z., et al., *Performance of a novel LED lamp arrangement to reduce SNR fluctuation for multi-user visible light communication systems.* Optics express, 2012. 20(4): p. 4564-4573.
175. Standardization, E.C.f. and *EN 12464-1. Light and lighting – Lighting of work places – Part 1: Indoor work places.*, 2011, European Committee for Standardization Brusel. p. 56 p.
176. Stefan, I. and H. Haas. *Analysis of Optimal Placement of LED Arrays for Visible Light Communication*. in *Vehicular Technology Conference (VTC Spring), 2013 IEEE 77th*. 2013. IEEE.
177. Cheng, R. and M. Gen, *Genetic algorithms and engineering design.* New York, 1997.
178. Gen, M. and R. Cheng, *Genetic algorithms and engineering optimization*. Vol. 7. 2000: John Wiley & Sons.
179. Koziel, S. and X.-S. Yang, *Computational optimization, methods and algorithms*. Vol. 356. 2011: Springer.
180. Philips. *CoreView panel -RC160V LED34S/830 PSU W60L60 CLI- Data sheet*. 2012; Available from: http://www.ecat.lighting.philips.com/l/indoor-luminaires/recessed/coreview-panel/910503910029_eu/.
181. OSRAM. *OSRAM LCW W5AM data sheet*. 2012 [cited 2013 4- 6-2013]; Available from: http://www.osram-os.com/Graphics/XPic6/00087560_0.pdf/LCW%20W5AM.pdf.
182. DIAL, *Dialux software* 2012: DIAL GmbH, Lüdenscheid, Germany.

# Appendix I:

# Average SNR Performance for Cairo and Berlin over the Year

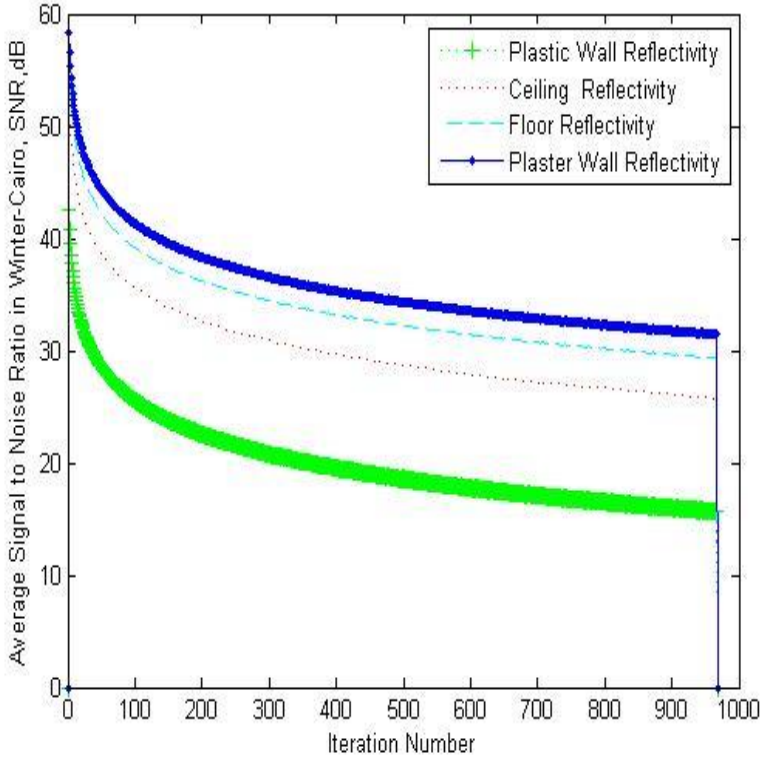


Figure V.1: The average system SNR for Cairo for winter, clear sky.

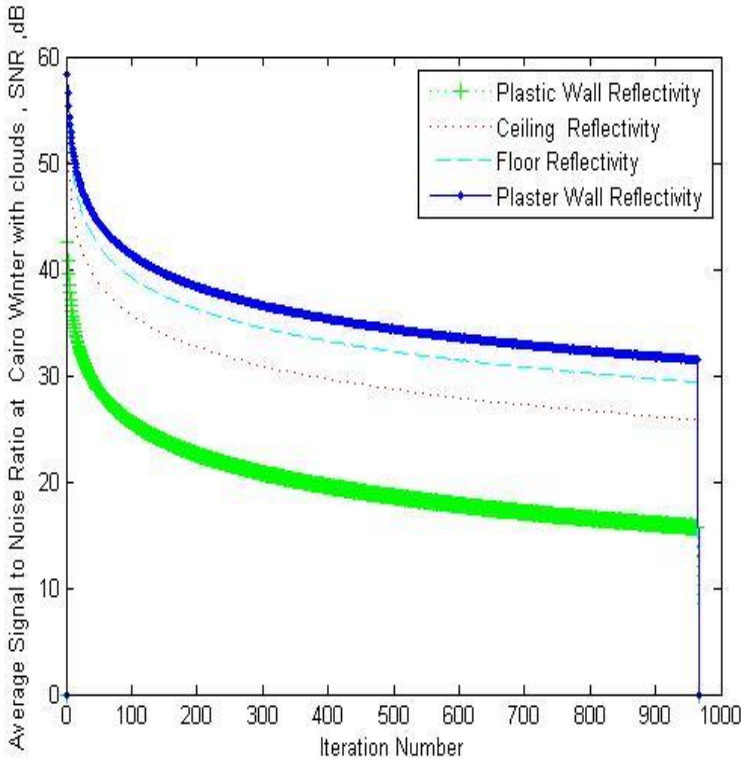


Figure V.2 : The average system SNR for Cairo for winter, cloud cover.

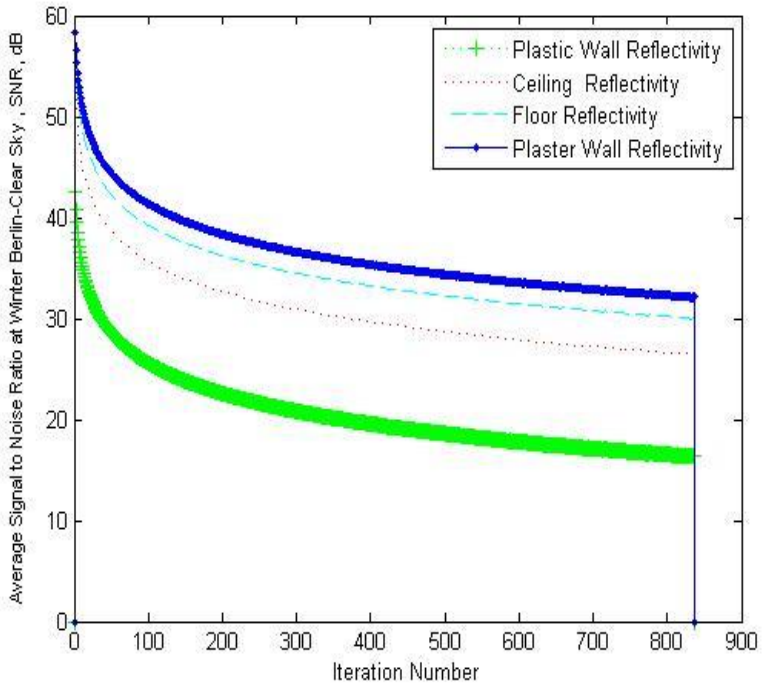


Figure V.3: The average system SNR for Berlin for winter, clear skies.

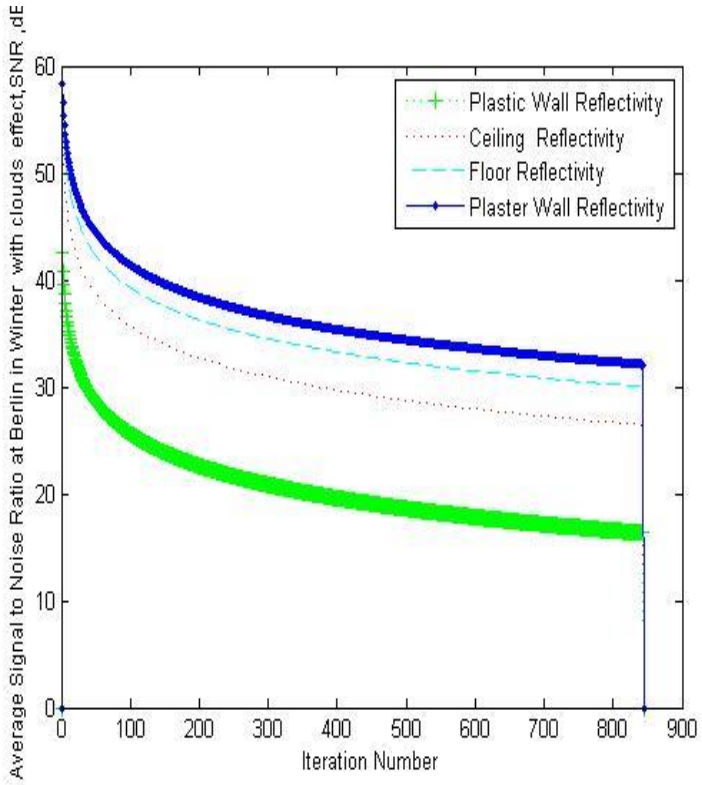


Figure V.4: The average system SNR for Berlin for winter, cloudy skies.

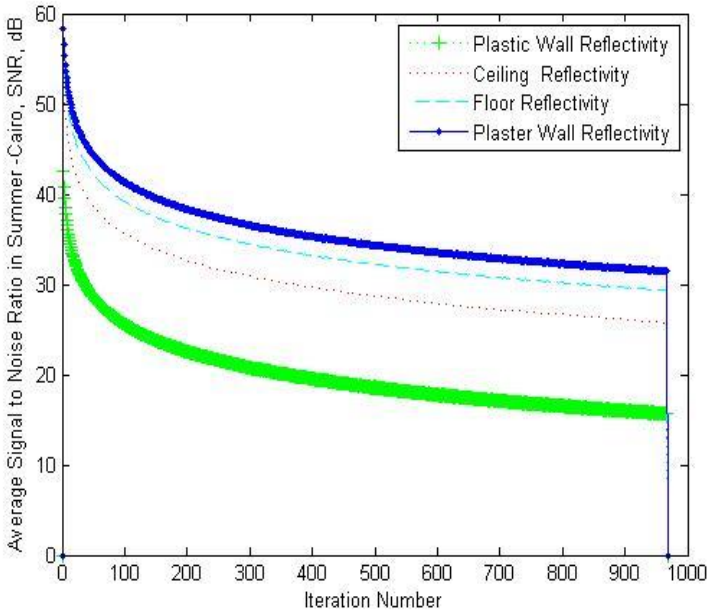


Figure V.5 : The average system SNR for Cairo for summer, clear sky.

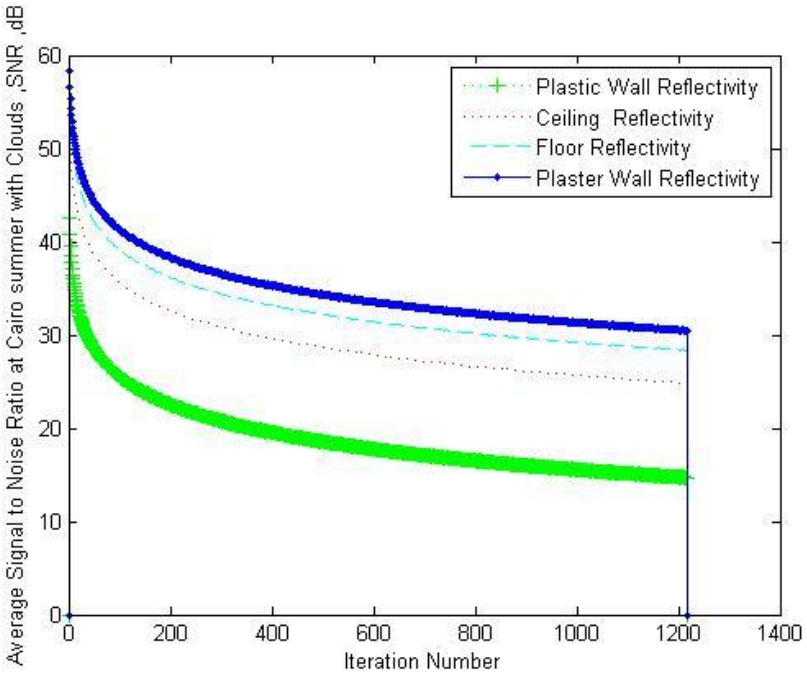


Figure V.6 : The average system SNR for Cairo for summer, cloudy sky.

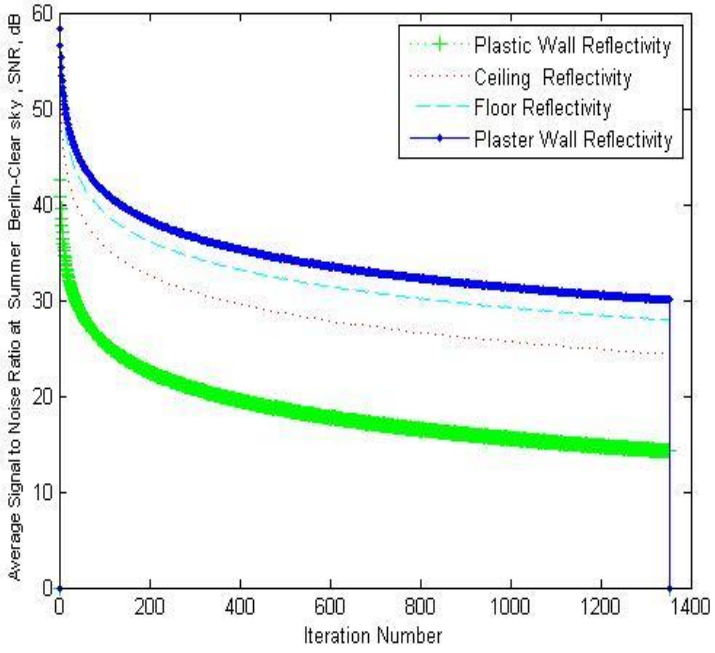


Figure V.7 : The average system SNR for Berlin for summer, clear sky.

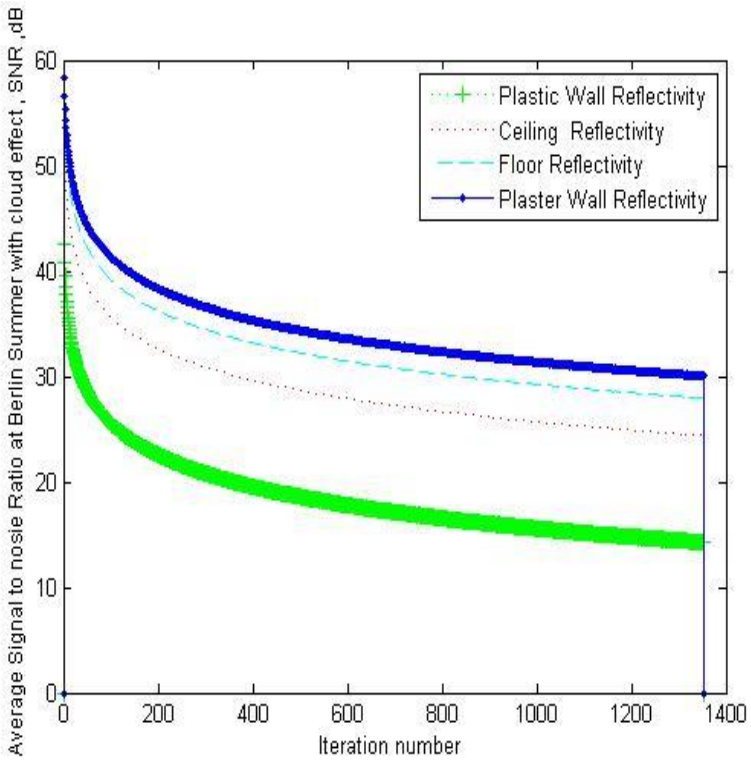


Figure V.8: The average system SNR for Berlin for summer, cloudy sky.

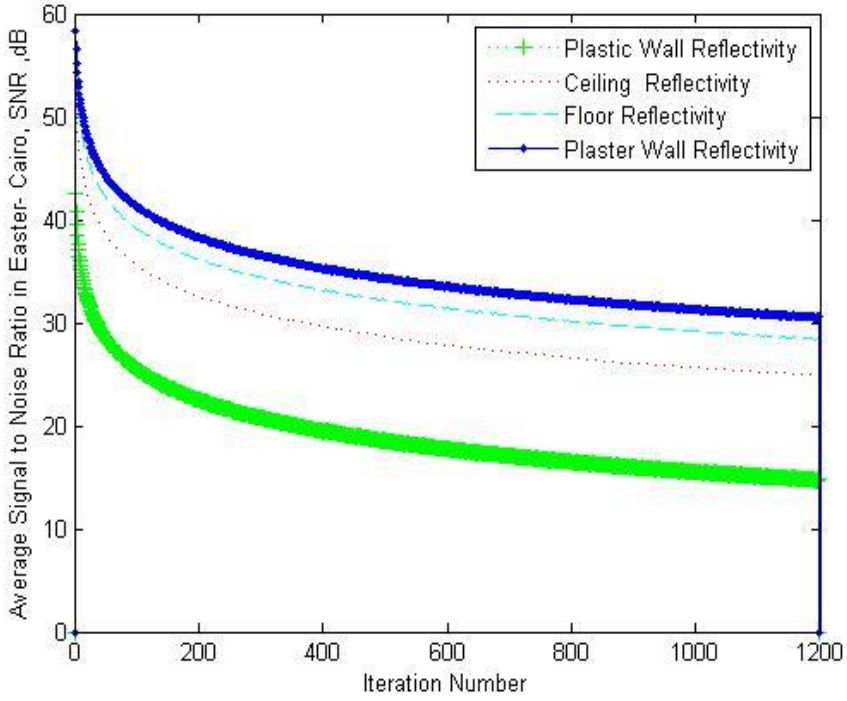


Figure V.9 : The average system SNR in Cairo for spring, clear sky.

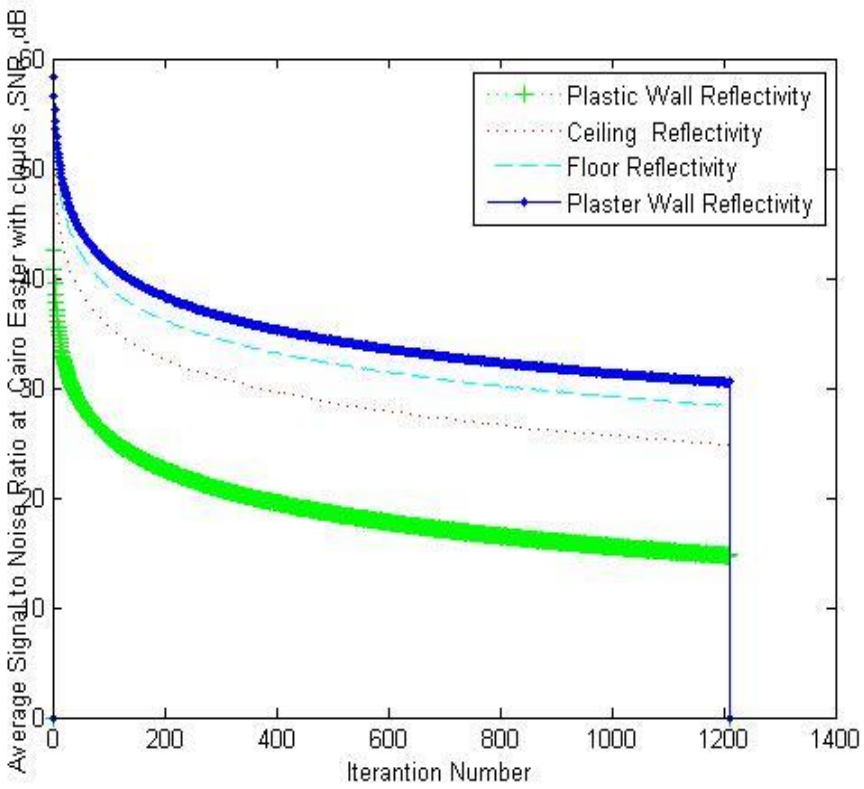


Figure V.10: The average system SNR in Cairo for spring, cloudy sky.

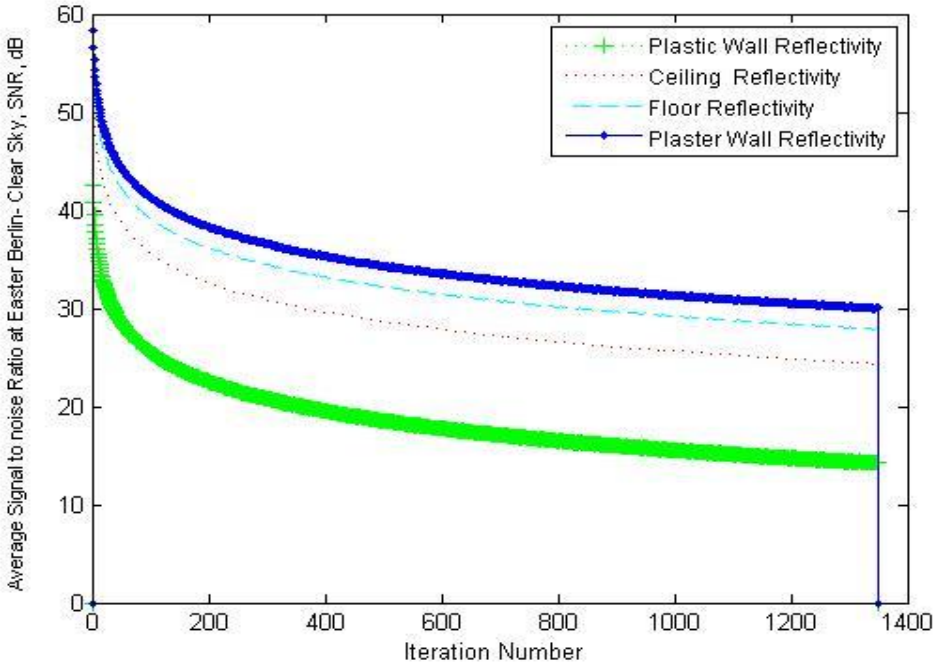


Figure V.11 :The average system SNR in Berlin for spring, clear sky.

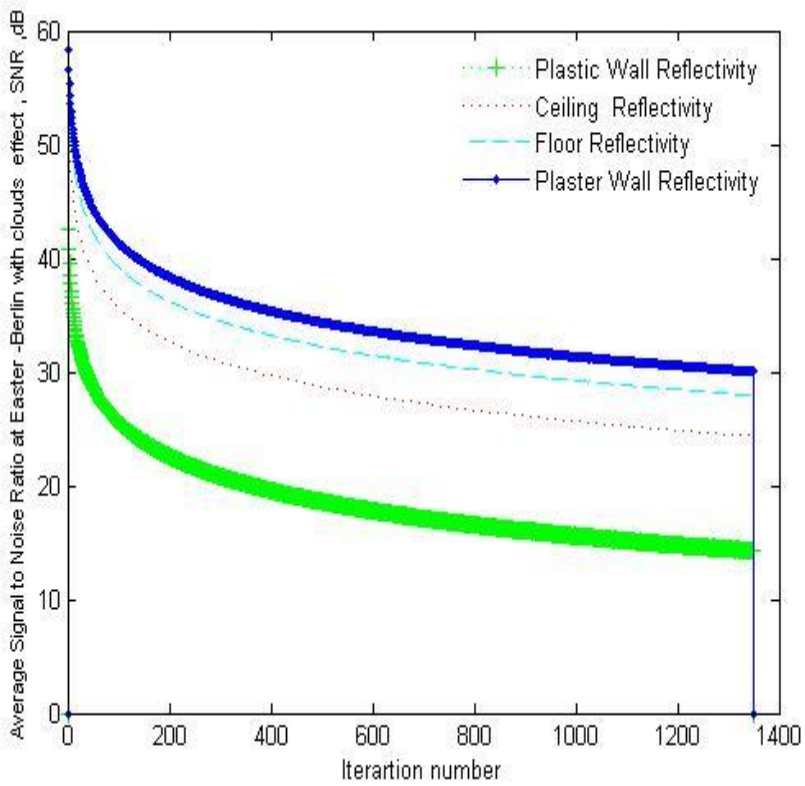


Figure V.12:The average system SNR for Berlin for spring, cloudy sky.

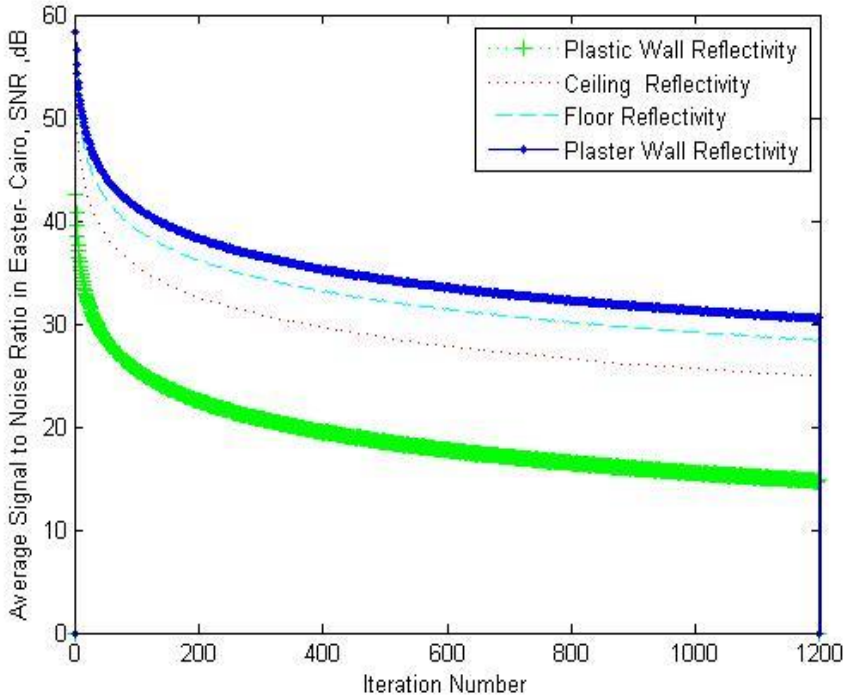


Figure V.13: The average system SNR in Cairo for spring, clear sky.

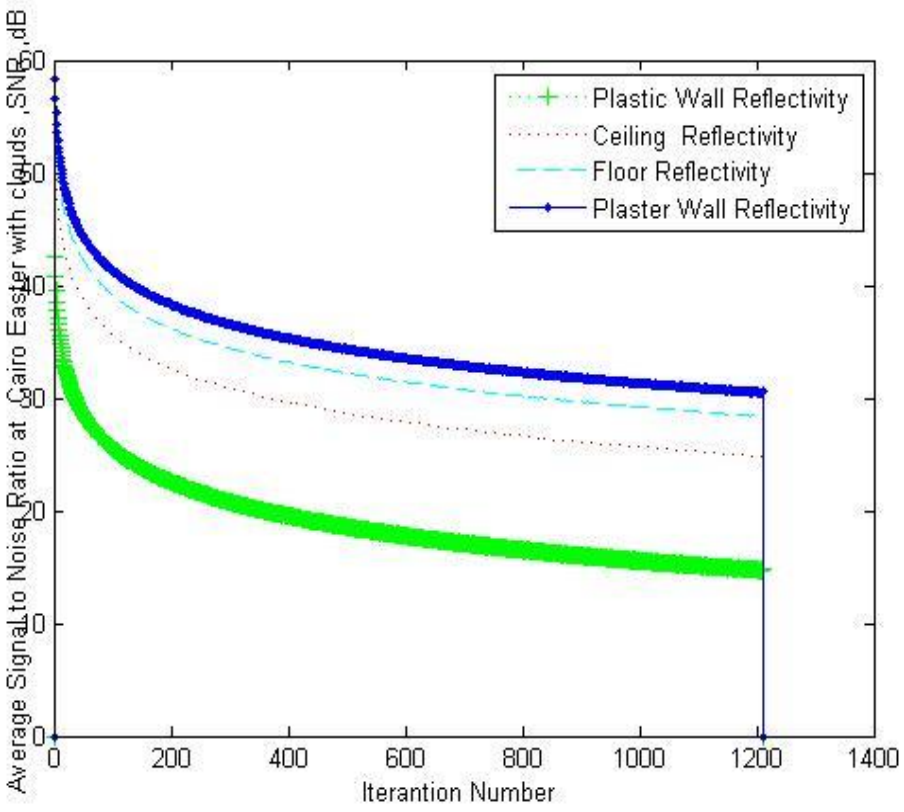


Figure V.14 : The average system SNR in Cairo for spring, cloudy sky.

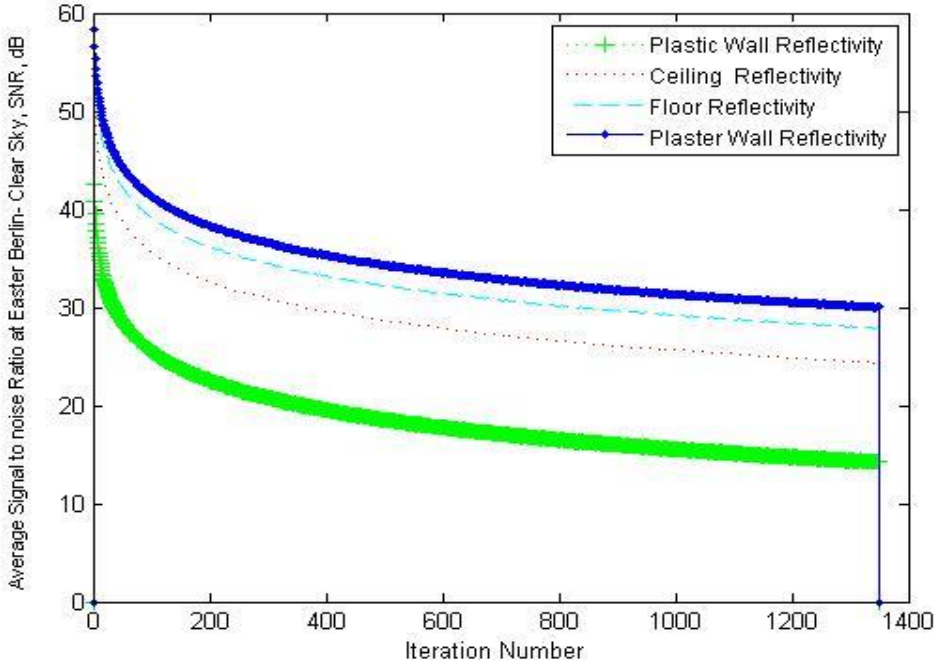


Figure V.15 :The average system SNR in Berlin for spring, clear sky.

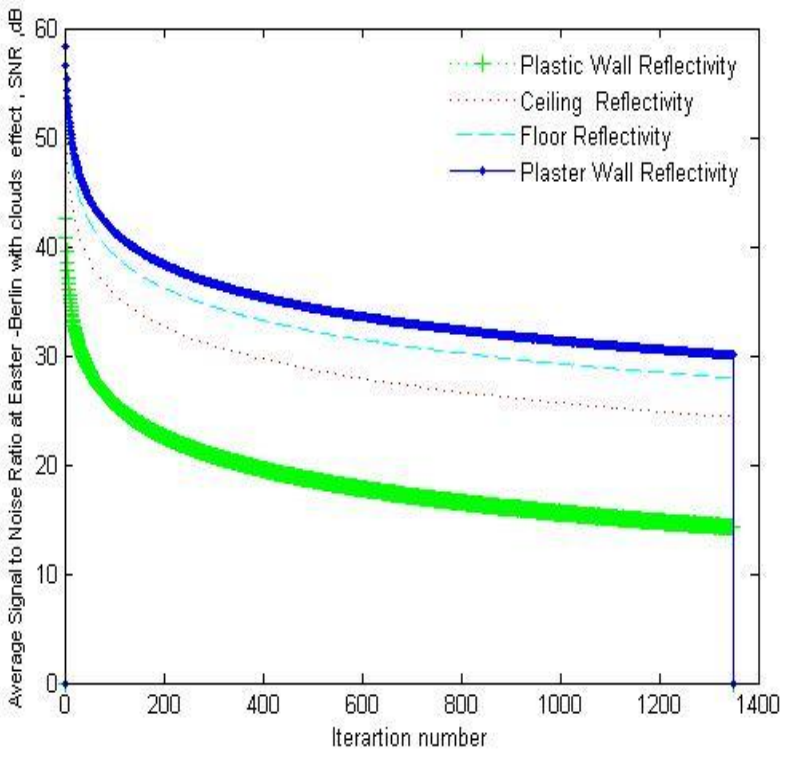


Figure V.16 :The average system SNR for Berlin for spring, cloudy sky.

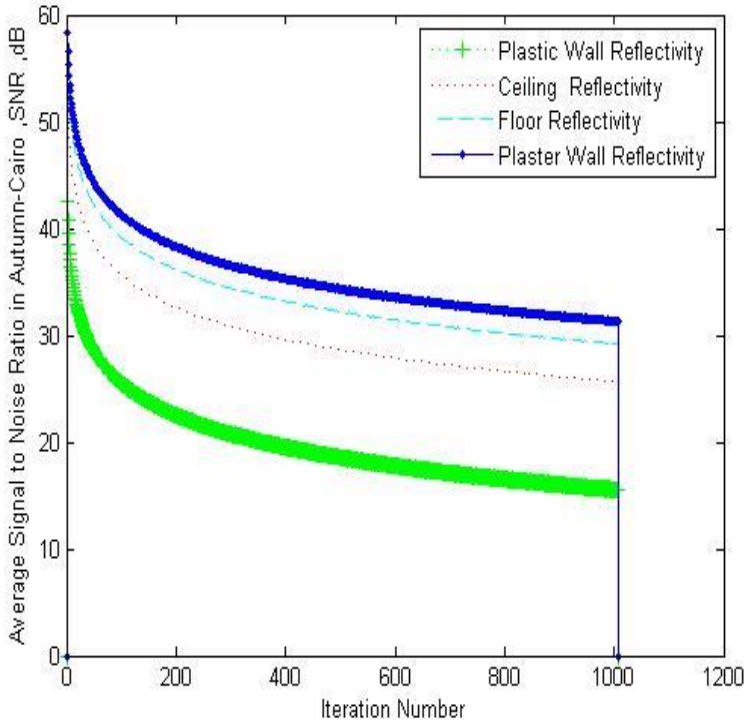


Figure V.17 : The average system SNR in Cairo for autumn, clear sky.

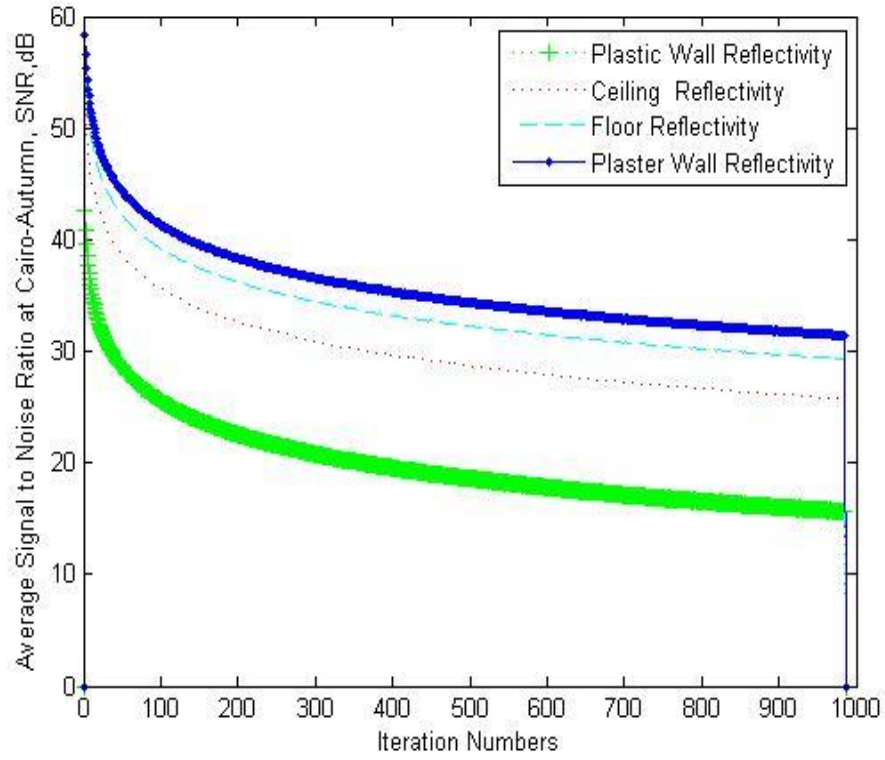


Figure V.18: The average system SNR for Cairo for autumn, cloudy sky.

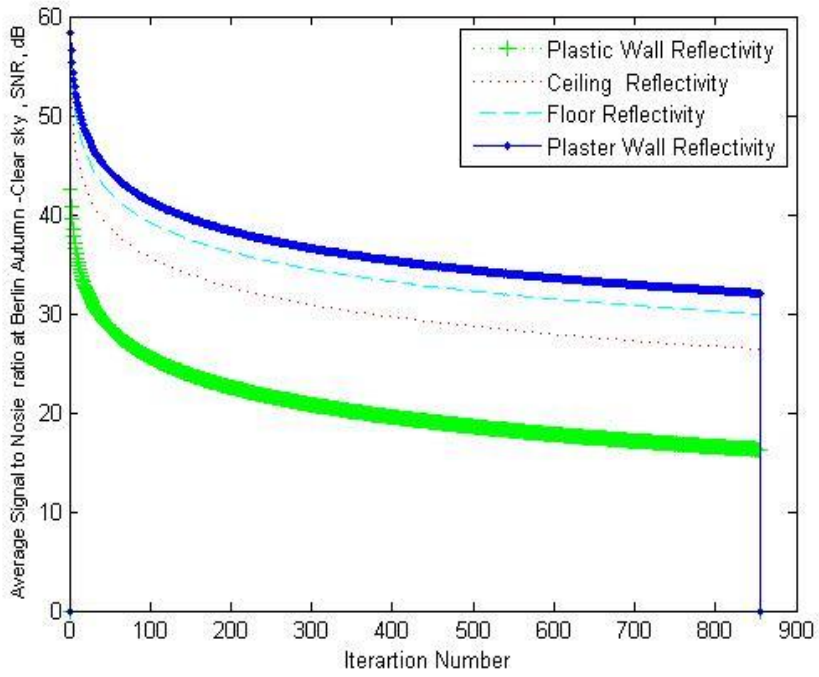


Figure V.19 : The average system SNR for Berlin for autumn, clear sky.

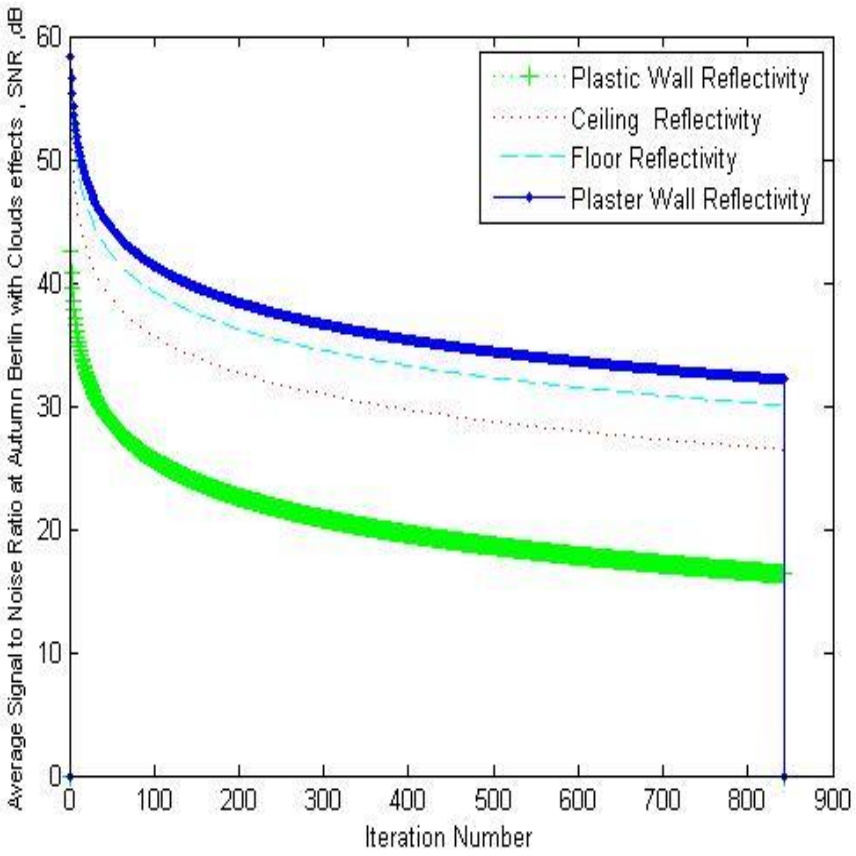


Figure V.20 : The average system SNR for Berlin for autumn, cloudy sky.